A-11089-MS

C.3

CIC-14 REPORT COLLECTION
REPRODUCTION
COPY

Los Alamos National Laboratory is operated by the University of California for the United States Department of Energy under contract W-7405-ENG-36.

# Computer Code Simulations of Explosions in Flow Networks and Comparison with Experiments

LOS ALAMOS NATL. LAB. LIBS.
3 9338 00323 1429

Los Alamos National Laboratory
Los Alamos, New Mexico 87545

An Affirmative Action/Equal Opportunity Employer

This work was supported by the US Department of Energy, Division of Operational and Environmental Safety.

Edited by M. C. Timmers, Group N-6
Prepared by L. M. Lawson, Group N-6

DISCLAIMER

This report was prepared as an account of work sponsored by an agency of the United States Government. Neither the United States Government nor any agency thereof, nor any of their employees, makes any warranty, express or implied, or assumes any legal liability or responsibility for the accuracy, completeness, or usefulness of any information, apparatus, product, or process disclosed, or represents that its use would not infringe privately owned rights. Reference herein to any specific commercial product, process, or service by trade name, trademark, manufacturer, or otherwise, does not necessarily constitute or imply its endorsement, recommendation, or favoring by the United States Government or any agency thereof. The views and opinions of authors expressed herein do not necessarily state or reflect those of the United States Government or any agency thereof.

LA-11089-MS

UC-38
Issued: October 1987

# Computer Code Simulations of Explosions in Flow Networks and Comparison with Experiments

W. S. Gregory
B. D. Nichols
J. A. Moore
P. R. Smith*
R. G. Steinke
R. D. Idzorek

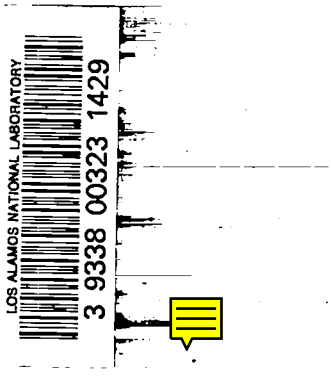


*Consultant at Los Alamos. New Mexico State University, Department of Mechanical Engineering, 159 Jett Hall, Las Cruces, NM 88003.

Los Alamos National Laboratory
Los Alamos, New Mexico 87545

TABLE OF CONTENTS


| | | Page |
|---|---|---|
| ABSTRACT | | 1 |
| I. | INTRODUCTION | 2 |
| II. | TEST EQUIPMENT | 2 |
| | A. Two-Dimensional Shock Transmission Set-Up. | 2 |
| | B. Shock-Tube Ventilation System Test Set-Up. | 4 |
| | C. Hydrogen/Air and Blasting Cap Ventilation System Test Set-Up | 4 |
| III. | COMPUTER CODE DESCRIPTIONS | 7 |
| | A. The EVENT84 Computer Code | 7 |
| | B. The NF85 Computer Code | 13 |
| IV. | COMPUTER CODE MODELING | 15 |
| | A. NF85 Shock Transmission Model. | 15 |
| | B. NF85 Shock-Tube Ventilation System Model | 15 |
| | C. EVENT84 Hydrogen/Air and Blasting Cap Explosion System Models | 17 |
| V. | EXPERIMENTAL AND CODE MODELING RESULTS | 20 |
| | A. Shock Transmission Tests (NF85) | 20 |
| | B. Shock-Tube Ventilation System Tests (NF85) | 42 |
| | C. Hydrogen/Air Ventilation System Tests (EVENT84) | 55 |
| | D. Blasting Cap Ventilation System Tests (EVENT84) | 58 |
| VI. | SUMMARY. | 63 |
| REFERENCES | | 68 |

# COMPUTER CODE SIMULATIONS OF EXPLOSIONS IN FLOW NETWORKS AND COMPARISON WITH EXPERIMENTS

by

W. S. Gregory, B. D. Nichols, J. A. Moore, P. R. Smith,
R. G. Steinke, and R. D. Idzorek

## ABSTRACT

A program of experimental testing and computer code development for predicting the effects of explosions in air-cleaning systems is being carried out for the Department of Energy. This work is a combined effort by the Los Alamos National Laboratory and New Mexico State University (NMSU). Los Alamos has the lead responsibility in the project and develops the computer codes; NMSU performs the experimental testing. The emphasis in the program is on obtaining experimental data to verify the analytical work. The primary benefit of this work will be the development of a verified computer code that safety analysts can use to analyze the effects of hypothetical explosions in nuclear plant air cleaning systems. The experimental data show the combined effects of explosions in air-cleaning systems that contain all of the important air-cleaning elements (blowers, dampers, filters, ductwork, and cells).

A small experimental set-up consisting of multiple rooms, ductwork, a damper, a filter, and a blower was constructed. Explosions were simulated with a shock tube, hydrogen/air-filled gas balloons, and blasting caps.

Analytical predictions were made using the EVENT84 and NF85 computer codes. The EVENT84 code predictions were in good agreement with the effects of the hydrogen/air explosions, but they did not model the blasting cap explosions adequately. NF85 predicted shock entrance to and within the experimental set-up very well. The NF85 code was not used to model the hydrogen/air or blasting cap explosions.

---

## I. INTRODUCTION

Accidental explosions can occur within nuclear plants, and therefore, safety analysts are required to evaluate their possibility and effects thoroughly. For this reason, we want to (1) develop computer codes to evaluate the effect of possible explosion-induced releases from a facility, (2) perform scoping studies involving a multitude of explosion scenarios, and (3) evaluate the effectiveness of different protective designs. To simulate these explosive effects accurately, we must be sure that the computer codes we use will perform as expected. This can be done by comparing the calculated simulations with small-scale experiments.

This report describes (1) two computer codes (EVENT84 and NF85) that have been developed by the Los Alamos National Laboratory for the Department of Energy, Office of Nuclear Safety, to simulate explosive effects within nuclear plants and (2) an experimental apparatus consisting of multiple rooms, ductwork, a damper, a filter, and a blower. Explosions were simulated using a large shock tube, and hydrogen/air-filled gas balloons and blasting caps were used to create actual explosions. The data obtained from these experiments and their comparison with the computer codes are described below.

## II. TEST EQUIPMENT

### A. Two-Dimensional Shock Transmission Set-Up

Figure 1 is a plan view of the experimental apparatus, which is located on the campus of New Mexico State University (NMSU) in Las Cruces, New Mexico, and is operated under contract with Los Alamos. The shock tube is connected to the experimental apparatus with a 0.305-m (1-ft)-i.d. pipe that is 2.72 m (8.92 ft) long. These experiments were designed to obtain two-dimensional data in the transition region where the 0.91-m (3-ft)-i.d. shock tube connects to the smaller 0.305-m (1-ft)-i.d. pipe.

The shock tube is a 48-m (160-ft)-long, 0.91-m (3-ft)-diam tube. The driven (low-pressure) section of the shock tube is 36 m (118 ft) long. The driver (high-pressure) section has a variable length, but it was fixed at 3.0 m (10 ft) for this study. (A complete description of the shock tube is given by Smith and

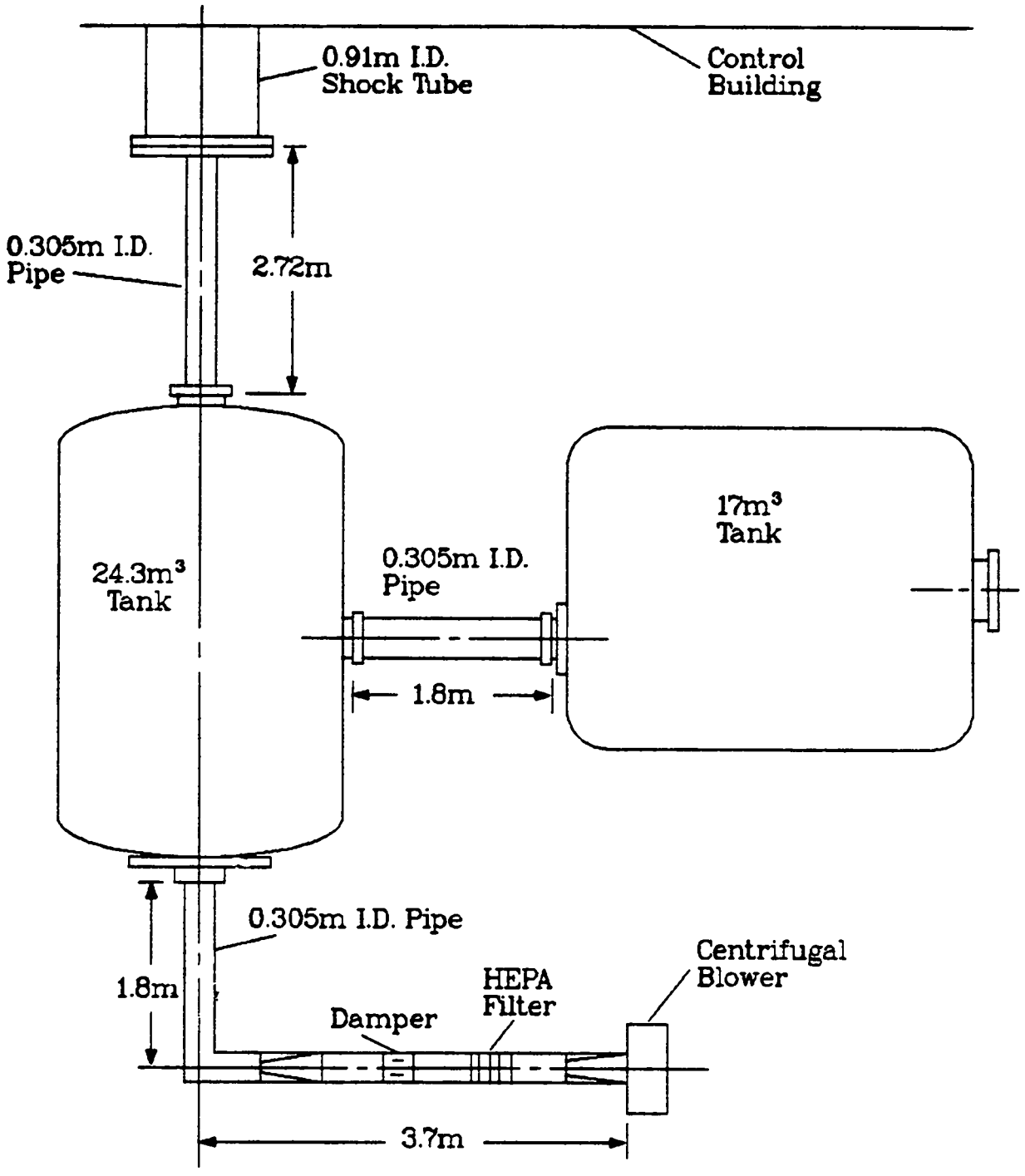


Fig. 1.
Plan view of the model ventilation system.

Gregory.[1]) At the end of the driven section of the shock tube, there is an abrupt contraction to a 0.305-m (1-ft)-diam, 2.72-m (8.92-ft)-long pipe that leads to the small ventilation system..

Pressure measurements were taken at the eight locations shown in Fig. 2 and labeled 1 through 8. Channel 1 is located on the side wall of the shock tube 0.91 m (3 ft) ahead of the abrupt contraction. Channels 2--4 are located on the dead-end portion of the abrupt contraction (an area-reducing plate) at the radial positions of 0.35 m (1.16 ft), 0.28 m (0.92 ft), and 0.20 m (0.67 ft), respectively. These three measurements are referred to as "head-on pressure measurements." Channels 5--8 were located at positions on the 0.305-m (1-ft)-diam pipe as shown in Fig. 2. These four measurements were "side-on pressure measurements." All eight channels used Kulite model XT-190 miniature pressure transducers with a range of 0 to 689 kPa (0 to 100 psi). The experimental data were digitized and recorded by a CAMAC data acquisition system using a digital computer (a Digital Equipment Corporation PDP 11/10).

The operation of the shock tube is explained in detail in Ref. 2. All eight pressure transducers were calibrated against a pressure standard before each experiment. The driver then was pressurized to the desired driven pressure, and the diaphragm was ruptured. The resulting shock wave traveled down the shock tube and, upon passing a triggering pressure transducer, automatically started the data acquisition system.

B. Shock-Tube Ventilation System Test Set-Up

The experimental set-up for this series of tests was the same as described in Sec. II.A. However, the experiments focused on obtaining data throughout the ventilation system and then comparing them with an NF85 model of the system. The shock tube again was used to simulate the explosive transient. Figure 3 shows the system set-up and the location of the pressure transducers (marked as "PT-X"). All pressure measurements except those in the tanks were side-on measurements. The rest of the instrumentation and data acquisition system were the same as described in Sec. II.A.

C. Hydrogen/Air and Blasting-Cap Ventilation System Test Set-Up

The experimental arrangement is the same as outlined above except for disconnecting the shock tube.

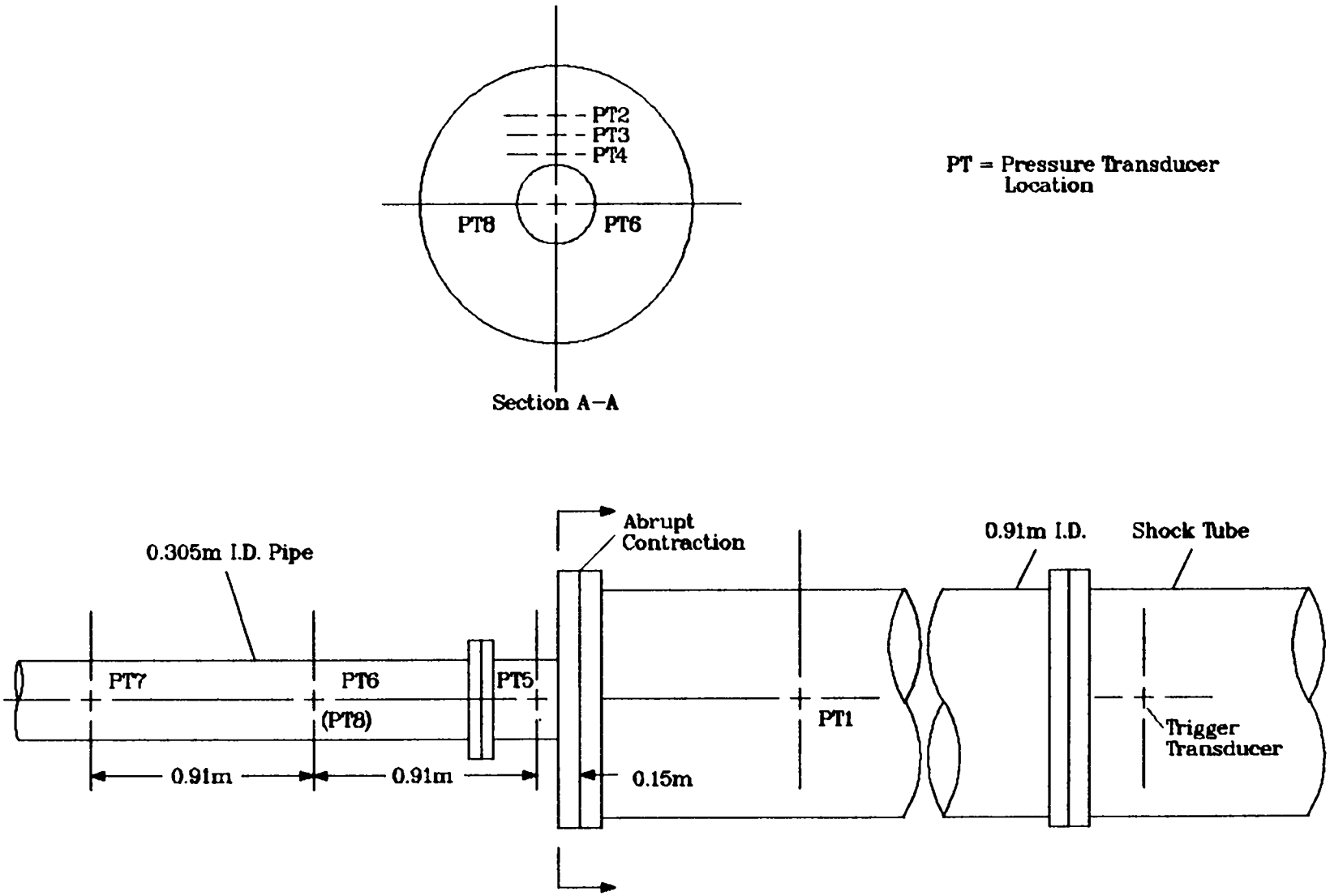


Fig. 2.
Location of pressure transducers for shock-transmission tests.

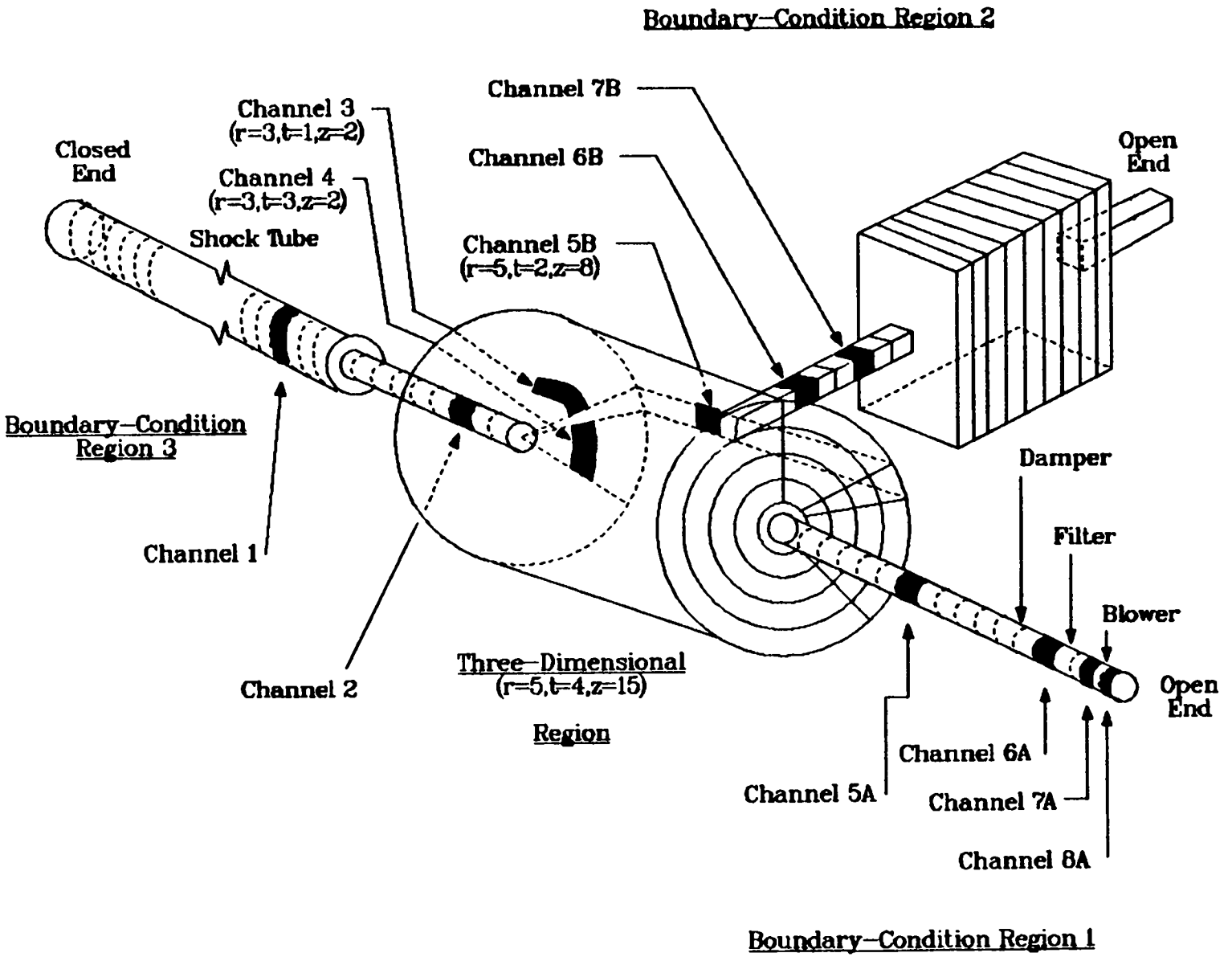


Fig. 3.
Numerical model used by the NF85 computer program to analyze shock transmission tests TMET11 to TMET16.

The gaseous explosions were created by exploding hydrogen/air-filled latex rubber balloons nominally 50.8 cm (20 in.) in diameter. The balloons were filled using a Matheson model 7372T gas proportional flowmeter through which the hydrogen and air flow simultaneously (Fig. 4). This system is shown in Fig. 5; Fig. 6 is a photograph of the spark generator used to initiate the explosion. Figure 7 shows a filled balloon just before detonation. All seven pressure transducers were calibrated against a pressure standard before each experiment, and the balloons were filled at a known flow rate for each gaseous component for a measured length of time. A small electrical impulse then caused the hydrogen/air mixture to explode, and the resulting shock wave automatically started the data acquisition system when it encountered a nearby trigger transducer.

The same tanks and ductwork system were used in the solid explosive tests. The blasting caps were arranged so that they would be detonated by a small electrical impulse.

## III. COMPUTER CODE DESCRIPTIONS

### A. The EVENT84 Computer Code

The EVENT84 computer code uses a lumped-parameter formulation to model a ventilation system or any other air pathway. No spatial distribution of parameters is considered in this approach, but the effect of spatial distribution can be approximated by noding. Network theory (using lumped-parameter methods) includes a number of system elements called branches joined at certain points called nodes. Ventilation system components that exhibit flow resistance (such as dampers, ducts, and filters) and flow potential (such as blowers) are located within the branches of the system. The connecting points of branches are nodes for components that have finite volumes (such as rooms, gloveboxes, plenums, and ducts) and for boundaries where the volume is practically infinite. Therefore, all internal nodes should possess some finite volume where fluid mass and energy storage can be taken into account.

The explosion source terms used in EVENT84 are simulated in several ways.

- Mass and energy prescription
- Mass and pressure prescription
- Mass and temperature prescription
- Pressure and temperature prescription
- Chamber model

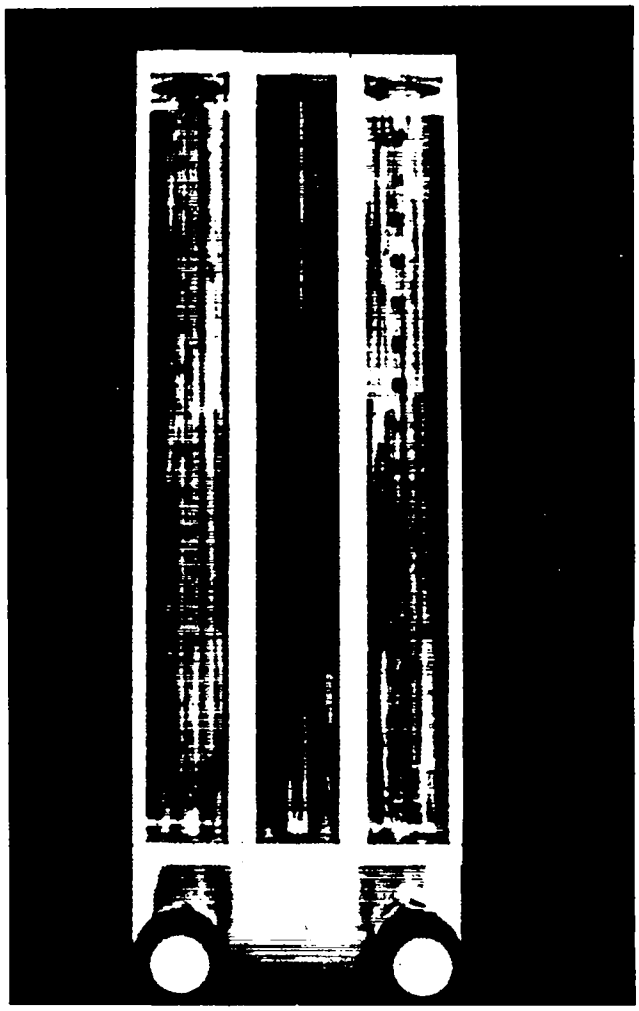

Fig. 4.
Hydrogen and air flowmeters.

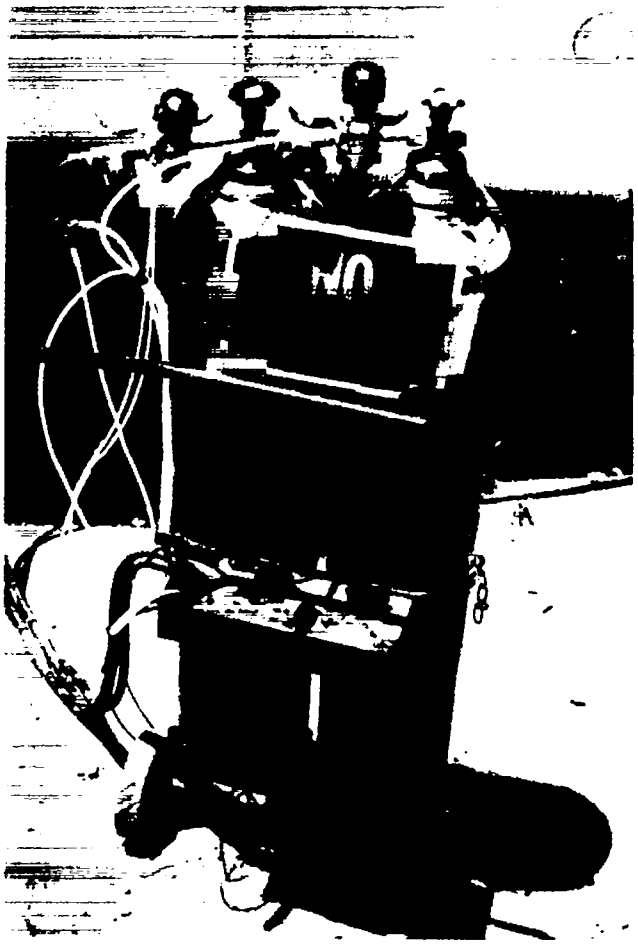

Fig. 5.
Hydrogen and air cylinders.

Fig. 6.
Spark generator for explosion initiation.

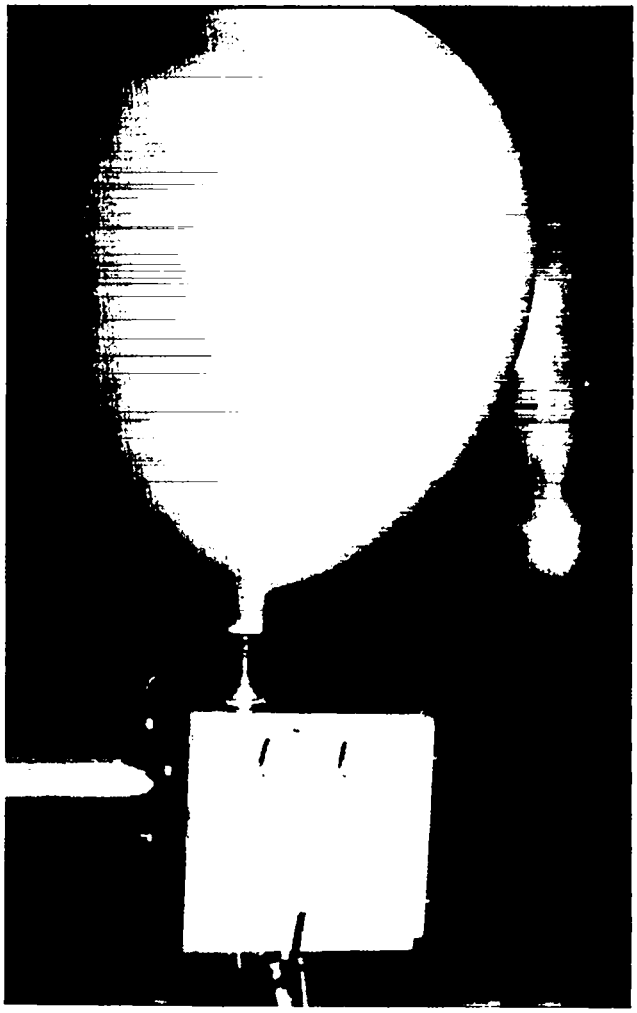

Fig. 7.
Hydrogen/air filled balloon before detonation.

The last option (the chamber model) allows specialty quantities of TNT, hydrogen oxygen, red oil, or acetylene to be used, and the explosion source term is calculated automatically.

The following equations are used in the EVENT84 computer code for conserving air.

Mass: $$V \frac{d\rho}{dt} = \sum_k q_k \dot{m}_k + \dot{m}_s \quad ,$$

Motion: $$\frac{\ell}{A} \frac{d\dot{m}}{dt} = -(P_2 - P_1) - \frac{f\ell}{D} \frac{1}{A^2} \frac{\dot{m}|\dot{m}|}{2\rho} \quad , \text{ and}$$

Energy: $$\frac{dp}{dt} = \frac{R}{C_v V} \left[\sum_k q_k \dot{m}_k \left(C_p T_k + \frac{V_k^2}{2}\right) + \dot{m}_s C_p T_s + \dot{e}_s\right] \quad ,$$

where

$V$ is the volume of the node,
$q_k$ is equal to +1 for downstream node and -1 for the upstream node,
$\dot{m}_k$ is the mass flow in branch k,
$\dot{m}_s$ is the specified mass source per unit time,
$t$ is the time,
$\rho$ is the air density,
$\ell$ is the duct length,
$A$ is the cross-sectional area,
$f$ is the Moody friction factor,
$D$ is the hydraulic diameter,
$P_2$ and $P_1$ are the pressures at the upstream and downstream nodes,
$C_v$ and $C_p$ are the specific heats at constant volume and constant pressure,
$T_k$ is the branch air temperature,
$V_k$ is the branch air velocity,
$T_s$ is the mass source temperature, and
$e_s$ is the energy source per unit time.

B. The NF85 Computer Code

The NF85 computer code is a multidimensional, gas-dynamics code designed to predict the effects of an explosion within a room. The NF85 code provides detailed modeling near the location of the explosion. This near-field modeling can provide a more accurate driving force than the chamber model used in EVENT84. NF85 is designed to operate alone or to be coupled to EVENT84.

The gas-dynamic equations solved in the NF85 computer code are the following partial-differential equations conserving air.

$$\text{Mass:} \quad \frac{\partial \rho}{\partial t} + \underline{\nabla} \cdot \rho \underline{V} = m_s \quad ,$$

$$\text{Motion:} \quad \frac{\partial \underline{V}}{\partial t} + \underline{V} \cdot \underline{\nabla}\, \underline{V} = -\frac{1}{\rho}\, \underline{\nabla} P - K\, |\underline{V}|\underline{V} + \underline{g} \quad , \text{ and}$$

$$\text{Energy:} \quad \frac{\partial \rho e}{\partial t} + \underline{\nabla} \cdot \rho e \underline{V} = -P \underline{\nabla} \cdot \underline{V} + m_s e_s \quad ,$$

where

- $t$ is time,
- $\rho$ is air density,
- $\underline{V}$ is air velocity (a vector),
- $m_s$ is the equivalent air mass per unit time per unit volume source from an explosion,
- $P$ is air pressure,
- $K$ is the friction-factor coefficient for air drag on structure surface,
- $\underline{g}$ is the acceleration of gravity (a vector),
- $e$ is air internal energy per unit mass, and
- $e_s$ is the internal energy plus combustion energy per unit mass from an explosion.

These equations are solved by finite-difference methods. Time and space are broken down into time steps and mesh-cell volumes over which the above conservation equations are applied. The semi-implicit, time-differencing technique with a first-order, donor-cell convection model is applied to these equations to give

a system procedure. This provides a numerically stable solution algorithm for time steps that exceed the sonic Courant limit (the time interval needed for a pressure wave to move across a mesh cell). To allow time steps to increase beyond the material Courant limit (the time interval needed for air mass to move across a mesh cell), NF85 applies the stability-enhancing two-step method to the semi-implicit equations. With this solution procedure, the time-step size is limited only by the rate of the transient being analyzed, not by the Courant limits for numerical stability. An appropriate time-step size for the rate of the transient is evaluated internally by NF85 based on five time-step criteria. To provide an accurate time-differencing approximation for a parameter of the transient solution, each criterion limits the time-step size. The most limiting criterion after each time step defines the time-step size that is used to evaluate the next time step's solution.

The NF85 computer code was developed to analyze the effect of an explosion on the air dynamics in an enclosed region. An explosion (modeled as a mass and energy source) generates a shock wave. The reflection of the shock wave from interior and exterior surfaces and the interaction of reflected shock waves requires the multidimensional analysis capability of NF85 for accurate modeling. NF85 models the momentum drag on air flowing over a structure surface by a Fanning friction factor definition for K in the air motion equation with different forms for laminar- and turbulent-flow conditions. Air is defined to behave as an ideal gas defined by the equation of state:

$$P = (\gamma-1)\,\rho e \quad ,$$

where $\gamma$ is the ratio of specific heats at constant pressure and constant volume ($\gamma = C_p/C_v = 1.4$ for air). In general, the enclosed region containing the explosion has a portion of its external boundary open to airflow through vents, ducts, open doorways, penetration holes, and so on that significantly affect the air-dynamics solution in the multidimensional region. This allows the feedback effect of air behavior in these passageways on the air-dynamics solution in the multidimensional region to be modeled explicitly and taken into account.

## IV. COMPUTER CODE MODELING

### A. NF85 Shock Transmission Model

The shock-transmission tests have been analyzed by the NF85 computer program to provide a benchmark for determining NF85's ability to evaluate shock-wave transmission, reflection, and interaction. A multidimensional region in (r,z) cylindrical geometry with a (9,24) spatial mesh was used to model the vicinity of the cross-section-area-reducing plate at the open end of the shock tube. By neglecting the small effect on the solution of gravitational acceleration normal to the axial (z) direction, azmuthal ($\theta$) dependence was eliminated to reduce calculative effort. Radial (r) dependence was evaluated to model its effect at the area-reducing plate, where the shock wave pulse is partially reflected and transmitted. Almost all of the 0.91-m (3-ft)-diam shock tube was modeled by a one-dimensional region with 750 mesh cells attached at the z = 0 boundary face of the (r,z) region. At the z = 24 boundary face of the (r,z) region, another one-dimensional region with 179 mesh cells was attached to model a 0.305-m (1-ft)-diam pipe, a 24.3-m ($859\text{-ft}^3$) tank, and another 0.305-m (1-ft)-diam pipe, all of which are downstream of the area-reduction plate. Figure 8 is a diagram of the mesh-cell spatial model of the shock-transmission experiment. The darkened mesh cells indicate the locations of the eight pressure transducers in the experiment.

### B. NF85 Shock-Tube Ventilation System Model

Figure 3 is a coarse [30-cm (12-in.)]-mesh spatial model of the shock tube/ventilation system set-up. The model consists of a three-dimensional region representing the cylindrical tank and three one-dimensional regions representing the boundary-condition regions. The boundary condition regicns consisted of the pipes containing the damper, the high-efficiency particulate air (HEPA) filter, and the blower; the rectangular tank; and the shock tube. Initially, the blower is operated at steady-state conditions with airflow into the open end of the boundary condition region 1 pipe and out the open end of the boundary-condition region 2 pipe.

Several changes had to be made to NF85 to perform calculations that model the entire ventilation system. A one-dimensional boundary condition region had to be coupled to a three-dimensional external boundary area having more than one

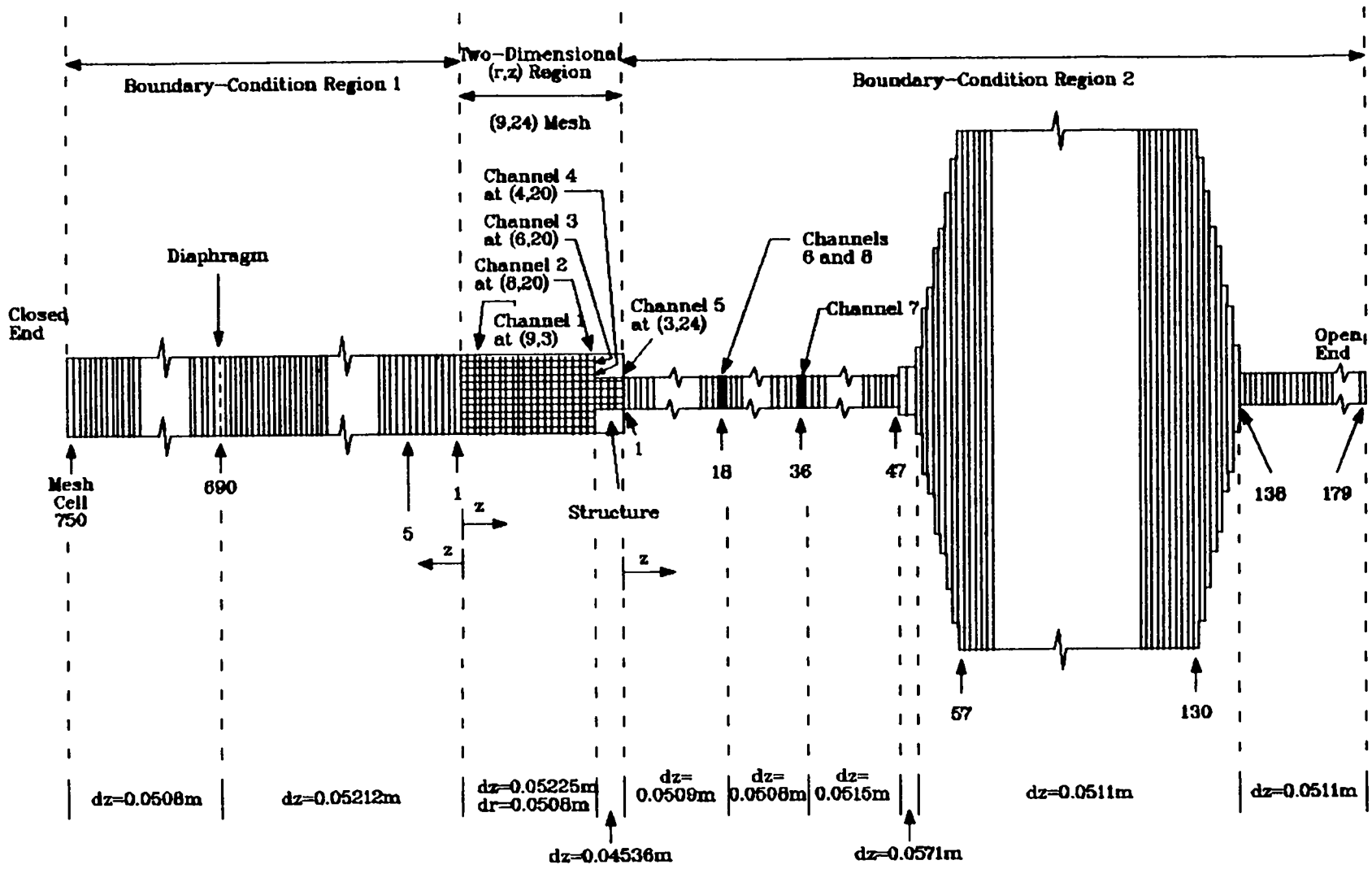


Fig. 8.
Mesh-cell spatial model used by the NF85 Computer Program to analyze the shock transmission tests.

mesh cell in the theta direction. In the initial calculations, a numerical instability with error growth was observed at this junction location. Reprogramming the implicit coupling to connect all junction mesh cells directly rather than couple them to the three-dimensional regions' average condition at the junction eliminated this instability.

C. EVENT84 Hydrogen/Air and Blasting Cap Explosion System Models

Certain assumptions are made to model a system using EVENT84: perfect gas (air), compressible flow, momentum balance with friction and inertia, choking, linear and nonlinear filters, certain blower characteristics, and mass and energy addition to the gas phase. As stated earlier, the model uses a lumped-parameter formulation; that is, no spatial distribution of parameters within network components is included. In addition, the analytical model must have the same arrangement of components, friction characteristics, capacitance, duct lengths, cross-sectional areas, boundary pressures, and driving forces as the experimental model.

The energy conservation equations are applied to internal (capacitance) nodes using a lumped-parameter formulation assuming a homogeneous mixture and thermodynamic equilibrium. A momentum equation that includes the effect of wall friction and inertia is used to relate the flow rate to the pressure drop across a duct; choking is imposed on the duct flow if the conditions warrant it. A filter provides only resistance to the flow. A quasi-steady relation is imposed between the pressure head and the flow rate for a blower.

The network system models for EVENT84 are shown in Figs. 9 and 10. The inlets on the rectangular and cylindrical tanks can be open or closed. Two arrangements were used for modeling the experiments. In Model 1, the rectangular tank inlet is open, and in Model 2, the cylindrical tank inlet is open.

Models 1 and 2 consist of 11 nodes (including 2 boundary nodes and 9 internal nodes) and 10 branches. The symbols used on the schematic represent dampers, blowers, duct resistance, filters, volumes of the ductwork, and cylindrical and rectangular tanks. For example, in Model 1, the numbers enclosed in parentheses represent branches, and numbers without parentheses represent nodes. Branches contain blowers, dampers, duct resistance, and filters. The nodes represent points such as the explosion chamber and the cylindrical tank. Pressures and temperatures are calculated at the nodes, whereas flows are calculated for the branches.

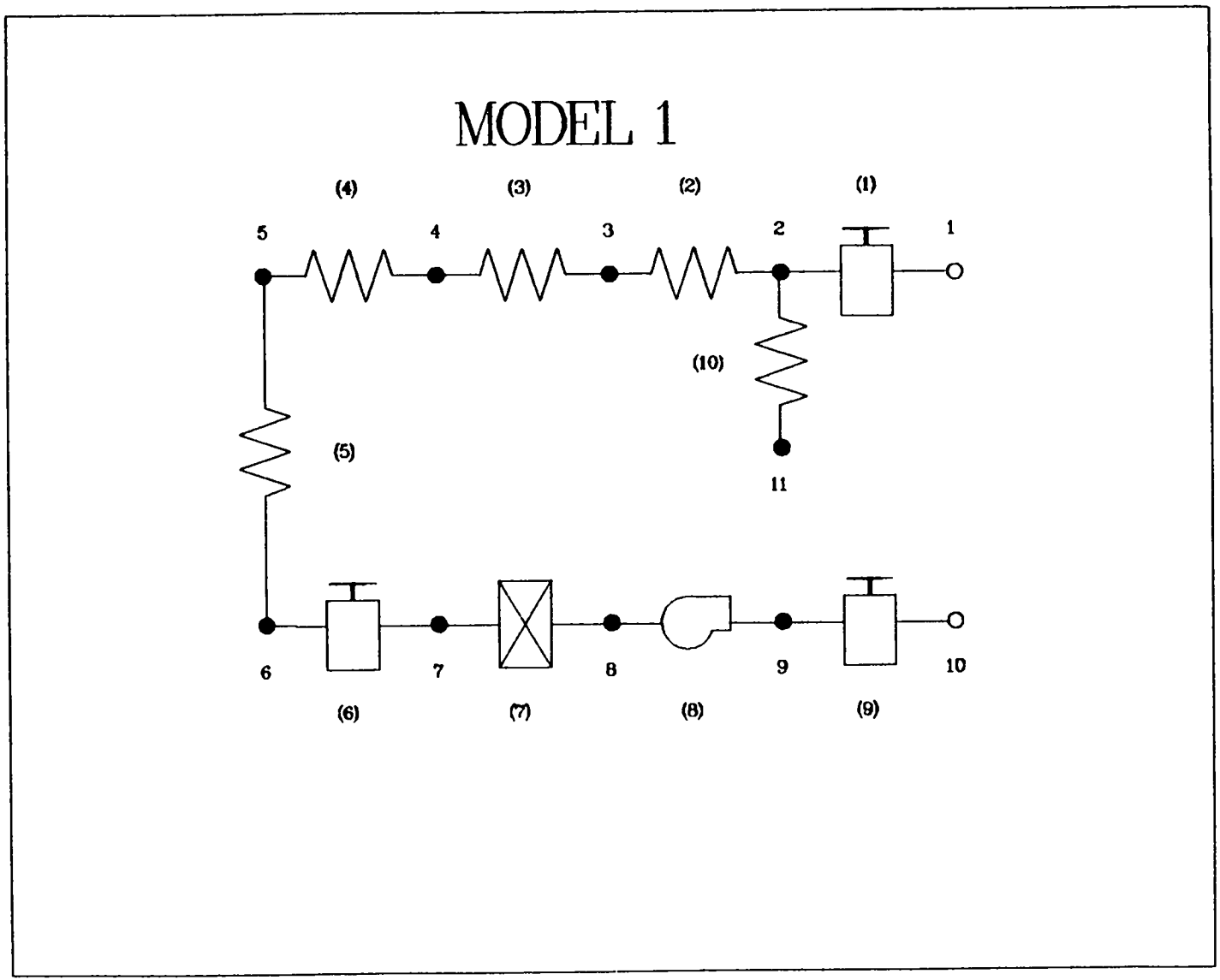


Fig. 9.
Computer network schematic for Model 1.

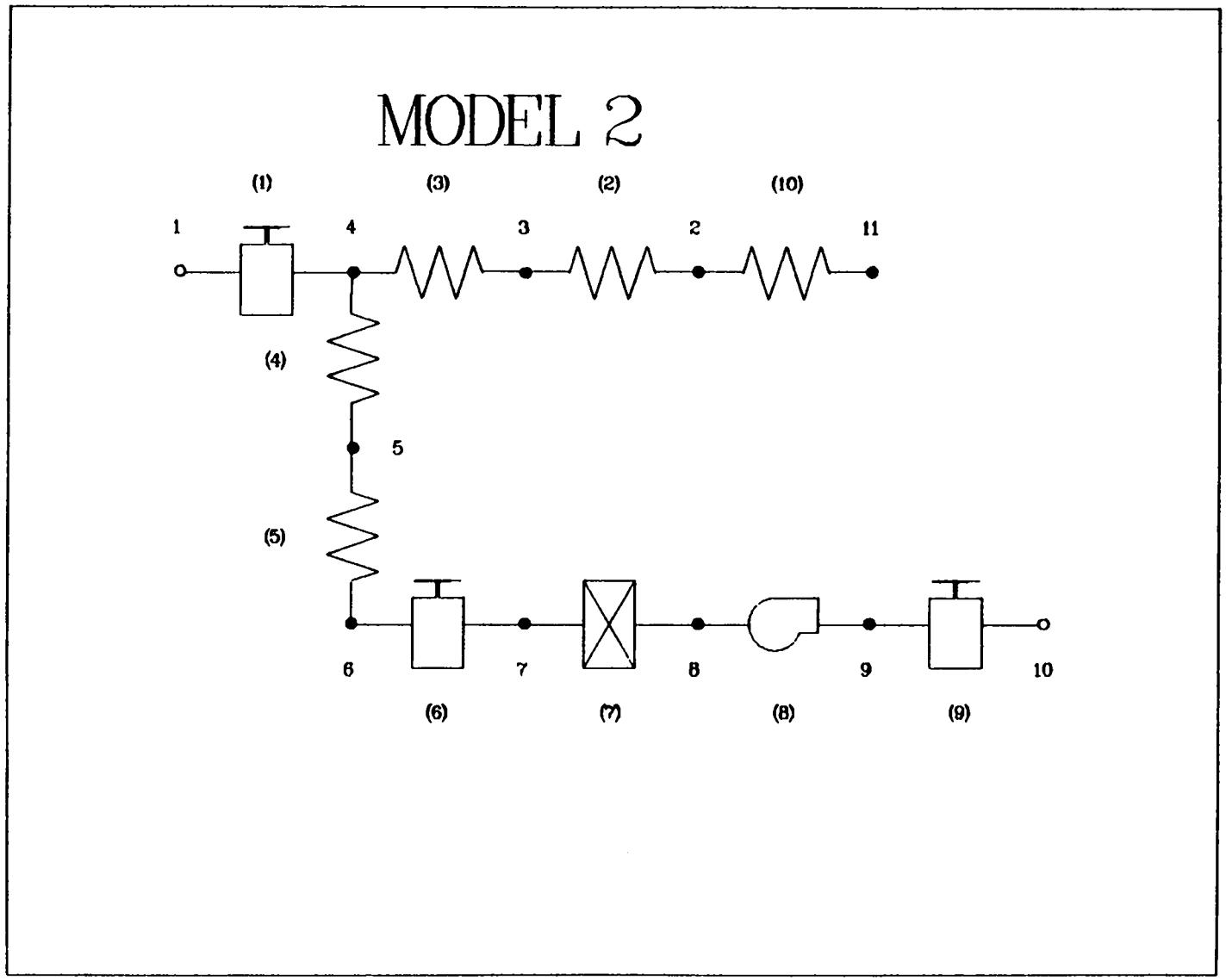


Fig. 10.
Computer network schematic for Model 2.

To accurately determine the resistance coefficient for each branch, each component (the 90-degree bend, the damper, the filter, and the blower) is modeled as a separate branch. In addition, the entrance and exit for the system are modeled as dampers (branches) to account for the entrance or exit losses. The duct between the two tanks is divided into two branches. The explosions take place within a balloon in the rectangular tank. The balloon is modeled as a separate node, with a flow area into the tank equal to the surface area of the balloon. The explosion is simulated as a mass and energy input into the balloon node, either as user-calculated time functions or through the explosion chamber subroutine.

The models described above were essentially the same for the solid explosive experiments. The only difference was that the node representing the balloon was not included. The explosive energy and mass were injected directly into node 2 on both models. Two explosive levels were used, 1.2 g (two blasting caps) and 3.0 g (five blasting caps) of "black powder."

## V. EXPERIMENTAL AND CODE MODELING RESULTS

### A. Shock Transmission Tests (NF85)

The shock-transmission tests involved measuring air pressure at eight locations in the vicinity of the area-reduction plate as a shock-wave pulse passes through the region. The shock-wave pulse is generated by breaking two diaphragms between the high- and low (atmospheric)-pressure ends of the shock tube. The shock-wave front travels down the low-pressure length of the shock tube at essentially the sonic velocity of the air medium ahead of it. It is followed by an air-mass front moving at the much lower air velocity. In the opposite direction, a rarefaction (expansion)-wave front travels up the high-pressure length of the shock tube until it reaches the closed end, where it is reflected. It then travels down the high-pressure and low-pressure lengths of the shock tube at the sonic velocity plus air-mass velocity. The expansion wave has both a front and a tail; the tail travels at a slightly slower velocity. The expansion wave catches up to the air-mass front very quickly and passes through it. The expansion wave eventually catches up to the shock wave, but this does not happen in the experiment until after both waves have passed the pressure transducer locations. The pressure transducers measure a shock-wave pulse where the

air pressure rises initially when the shock-wave front crosses the transducer location. The expansion wave front crosses the transducer location a short time later, causing the air pressure to fall until the expansion-wave tail crosses the transducer location.

This shock-transmission test provides a very sensitive benchmark for calculating shock- and expansion-wave transmission, reflection, and interaction. The channel 1 pressure transducer first encounters the shock-wave front and then encounters its front partially reflected from the area-reduction plate. Soon thereafter it encounters the expansion wave that was reflected from the shock tube's high-pressure end and that interacted with the air-mass front and the partially reflected shock front. The pressure transducers for channels 2--4 measure the air pressure at the area-reduction reflecting surface. The pressure transducers of channels 5--8 encounter the shock and expansion waves that have been transmitted partially through the abrupt area-reduction-plate opening.

NF85 was used to evaluate the shock-transmission tests in three different ways.

1. The calculation starts at the breaking of the diaphragms using the numerical model in Fig. 8 with the shock and air-mass fronts initially 36.1 m (118 ft) from the channel 1 location.
2. The calculation starts from an analytic solution for the shock pulse after it has traveled down the shock tube and is approximately 0.13 m (0.43 ft) from the channel 1 location and uses the numerical model in Fig. 8.
3. The calculation is done in two stages. First, only the shock tube is modeled with the 750-mesh-cell region 1 attached to a one-cell multidimensional region, and the test is analyzed from the breaking of the diaphragms until the shock front is approximately 0.13 m (0.43 ft) from the channel 1 location. The second stage uses the restart data dump from region 1 instead of the analytic solution as the initial condition for a calculation similar to that in item 2.

Calculative statistics from the nine analyzed shock-transmission tests are shown in Table I. The second procedure described above was used to analyze all the tests from initiation until 0.065 s; the total number of time steps and Cray-1 computer time required by NF85 for each test are reported in the left half of

TABLE I

NF85 CALCULATION STATISTICS FROM ANALYZING THE NMSU SHOCK-TRANSMISSION TESTS

| Pressure Difference Across Diaphragms (psi) | Shock-Front Overpressure (psi) | Calculated from Analytic Solution: Problem Time (s) | Time Steps | CRAY Time (s) | Calculated From Diaphragm Break: Problem Time (s) | Time Steps | Cray Time (s) | Transmission Time to the Area-Reduction End of the Shock Tube: Analytic (s) | Calc. (s) | Error (%) |
|---|---|---|---|---|---|---|---|---|---|---|
| 6.830 | 3.000 | 0 to 0.065 | 186* | 69.4[a] | 0 to 0.160 | 199 | 87.9 | 0.09642 | 0.09530 | -1.12 |
| 7.250 | 3.163 | 0 to 0.065 | 105 | 42.4 | 0 to 0.160 | 199 | 88.8 | 0.09700 | 0.09583 | -1.13 |
| 7.500 | 3.257 | 0 to 0.065 | 105 | 42.8 | 0 to 0.160 | 199 | 89.2 | 0.09639 | 0.09531 | -1.11 |
| 58.000 | 15.646 | 0 to 0.065 | 688 | 307.9 | 0 to 0.074 | 0 to 1665 | 127.6 | | | |
| | | | | | to 0.140 | to 2301 | 305.4 | | | |
| | | | | | | | 433.0 | 0.07418 | 0.07894 | +6.40 |
| 58.000 | 15.653 | 0 to 0.065 | 685 | 306.4 | 0 to 0.076 | 0 to 1697 | 129.6 | | | |
| | | | | | to 0.140 | to 2294 | 293.2 | | | |
| | | | | | | | 442.8 | 0.07445 | 0.07926 | +6.46 |
| 59.985 | 16.000 | 0 to 0.065 | 690 | 314.7 | 0 to 0.140 | 0 to 2403 | 917.0 | 0.07423 | 0.07899 | +6.42 |
| 60.000 | 16.012 | 0 to 0.065 | 706 | 316.0 | 0 to 0.076 | 0 to 1775 | 135.1 | | | |
| | | | | | to 0.140 | to 2396 | 301.4 | | | |
| | | | | | | | 436.5 | 0.07444 | 0.07935 | +6.60 |
| 90.000 | 20.547 | 0 to 0.065 | 1248 | 553.2 | 0 to 0.072 | 0 to 2759 | 208.8 | | | |
| | | | | | to 0.140 | to 3622 | 401.5 | | | |
| | | | | | | | 610.3 | 0.06954 | 0.07575 | +8.92 |
| 98.000 | 21.603 | 0 to 0.065 | 1395 | 620.0 | 0 to 0.070 | 0 to 2933 | 223.3 | | | |
| | | | | | to 0.135 | to 3881 | 430.1 | | | |
| | | | | | | | 653.4 | 0.06808 | 0.07436 | +9.21 |

[a]This calculation's time-step size was constrained for most of the analysis by a maximum time-step size of 0.0005 s; the other calculations used a maximum time-step size of 0.0001 s.

the table. The right half of the table reports the same statistics when using the first procedure for tests with shock-front overpressures of 20.7, 21.8, 22.4, and 110.2 kPa (3.000, 3.163, 3.257, and 16.000 psi) and the third procedure for the other tests. The first and third procedures give the same solution, but Table I shows that the Cray-1 computer times for the 107.8, 107.85, and 110.3 kPa (15.646, 15.653, and 16.012 psi) shock-front overpressure tests evaluated with the third procedure required half the calculative effort of the 110.2-kPa (16.0-psi) test evaluated with the first procedure. The second procedure required a half to a third the calculative effort of the first procedure. At the far right of Table I is a comparison of the analytic and calculated transmission times for the shock-wave front to reach the area-reduction plate. The transmission times for small shock-front overpressures are calculated accurately but tend to overestimate the times as the shock-front overpressures increase. The time at which the shock front reaches the area-reduction plate was determined based on calculating half the shock-front overpressure rise at the plate.

Time plots of calculated air pressure and pressure transducer measurements are shown in Figs. 11--13 for the 21.8-, 110.3-, and 141.5-kPa (3.163-, 16.012-, and 20.547-psi) shock-front overpressure tests, respectively. The results from seven of the eight pressure-transducer locations are shown; the results from channel 3 are omitted because of their similarity to the results from channels 2 and 4. Overall, the results from all the tests are of two different forms: the 20.7-, 21.8-, and 22.4-kPa (3.000-, 3.163-, and 3.257-psi) shock-front overpressure tests have similar results, and the other tests with shock-front overpressures greater than 103.35 kPa (15 psi) have similar results. This similarity can be seen by comparing Figs. 12 and 13.

The pressure transducer measurements are plotted along with NF85 calculative results using the first or third procedure shown by the dotted curve [labeled 36.1 m (119.1 ft), the initial distance of the shock-wave front from channel 1] and using the second procedure shown by the solid curve [labeled 0.13 m (0.43 ft)]. The first or third procedure is more convenient for the NF85 user because the entire solution, starting with breaking the diaphragms, is evaluated by NF85. However, having NF85 evaluate the shock-wave pulse transmission down the 36-m (118.8-ft) length of the shock tube low-pressure section introduces spatial smearing to the solution. The second procedure avoids this numerical-solution error by starting with the analytic solution for the shock-front pulse just before it reaches channel 1.

In Fig. 13, we can see that the spatial smearing error is excessive for the 20.7-kPa (3-psi) shock-front overpressure test calculations. Backward smearing of the shock-wave front and forward smearing of the expansion-wave front result in their overlapping and diminishing the amplitude of the pulse. Starting from the shock-front pulse analytic solution 0.13 m (0.43 ft) before channel 1, the solid-curve solution initially has very little spatial smearing and is in reasonable agreement with the measurements. However, after 0.020 s, spatially dependent effects also begin to be smeared out in space and in time at a fixed location because of convection. Note the reduction in amplitude of the pressure pulse at the channel 7 location in even the solid curve because of the shock and expansion wave overlapping-effect error.

The calculative results in Figs. 12 and 13 show almost no spatial-smearing error in the shock-wave front. Forward spatial smearing of the expansion-wave front diminishes the amplitude of the shock pulse (as shown by the dotted curve

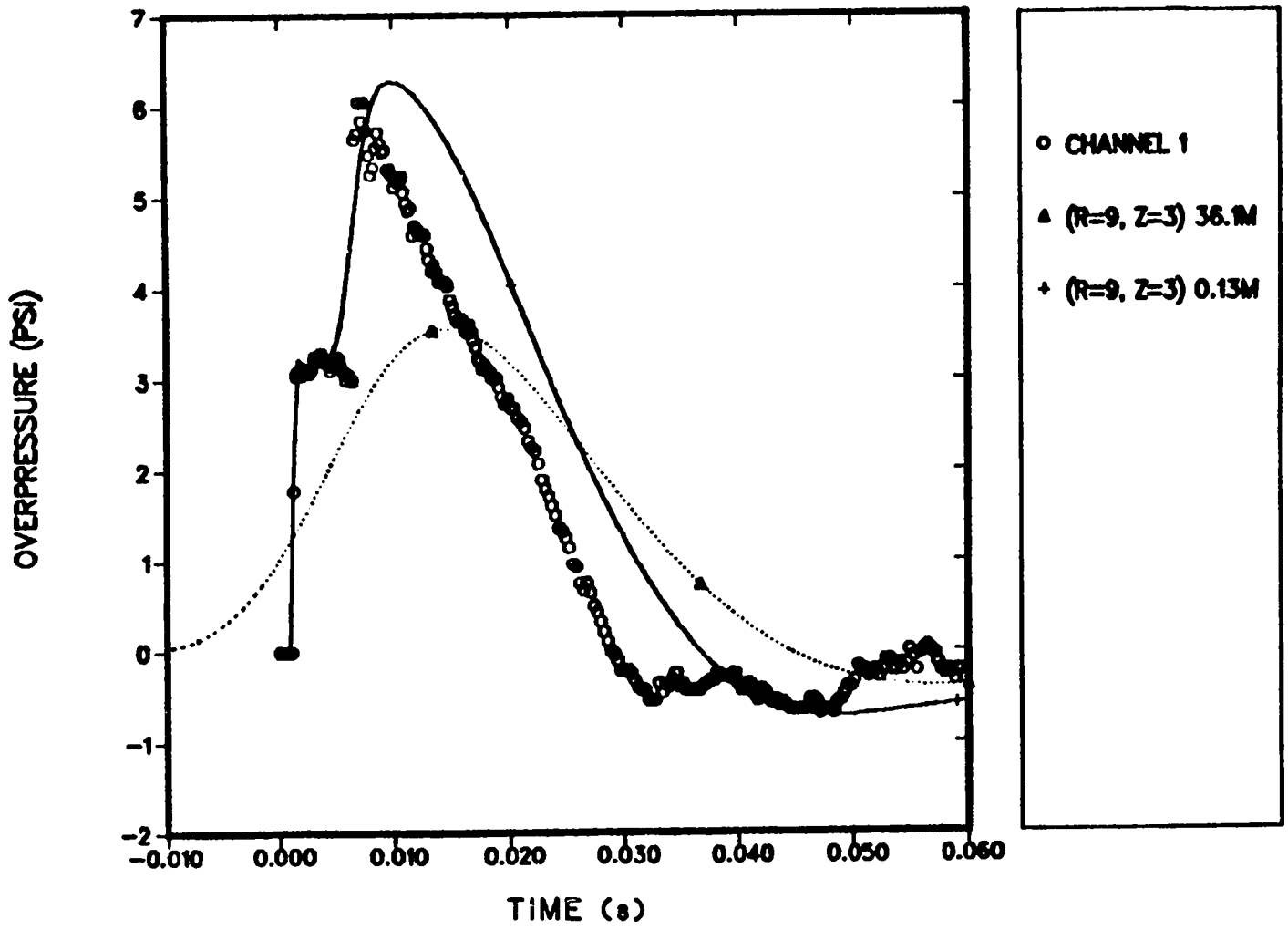


Fig. 11.
Shock transmission test with 21.8-kPa (3.163-psi) shock pressure.

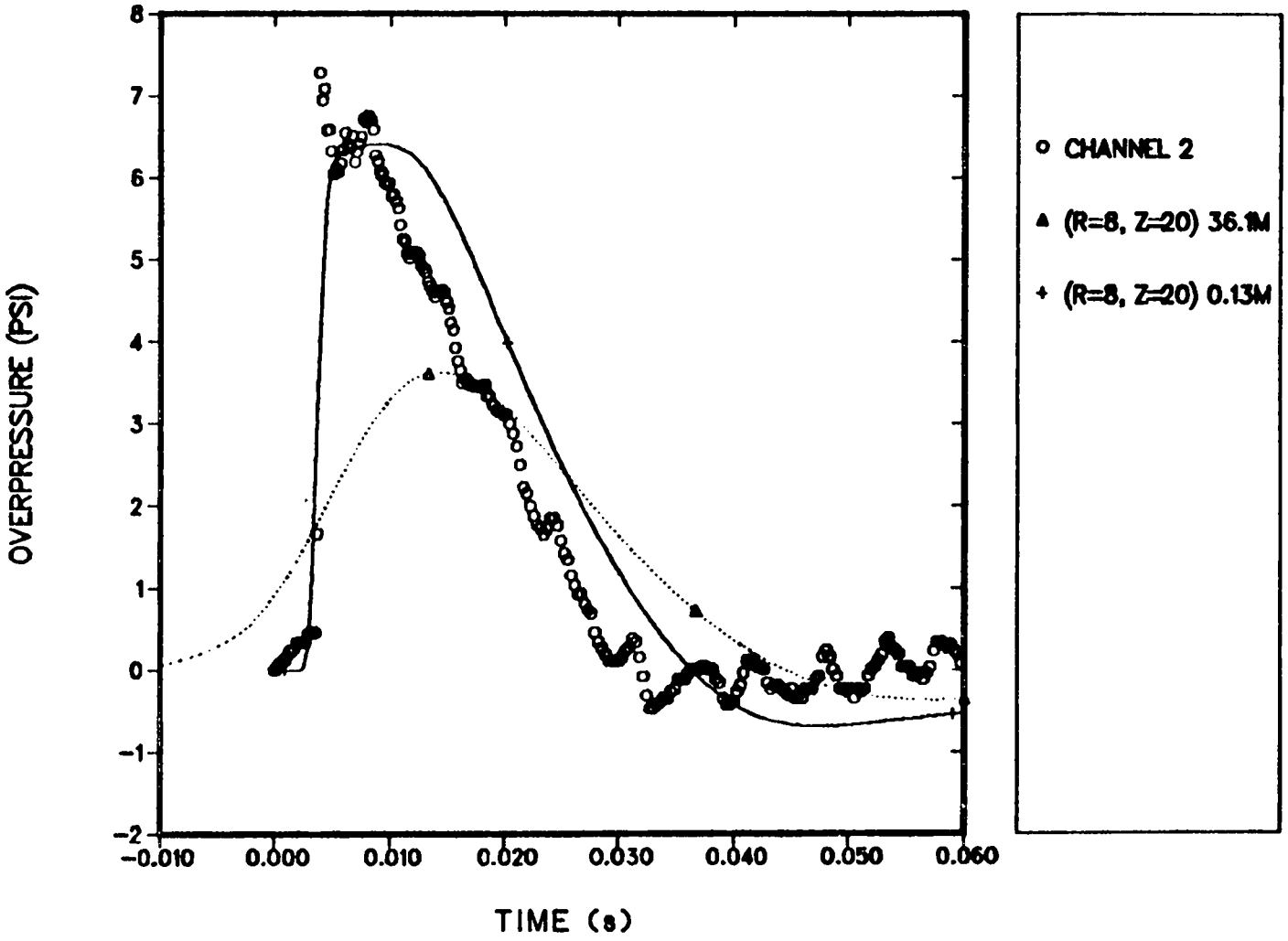


Fig. 11 (cont).
Shock transmission test with 21.8-kPa (3.163-psi) shock pressure.

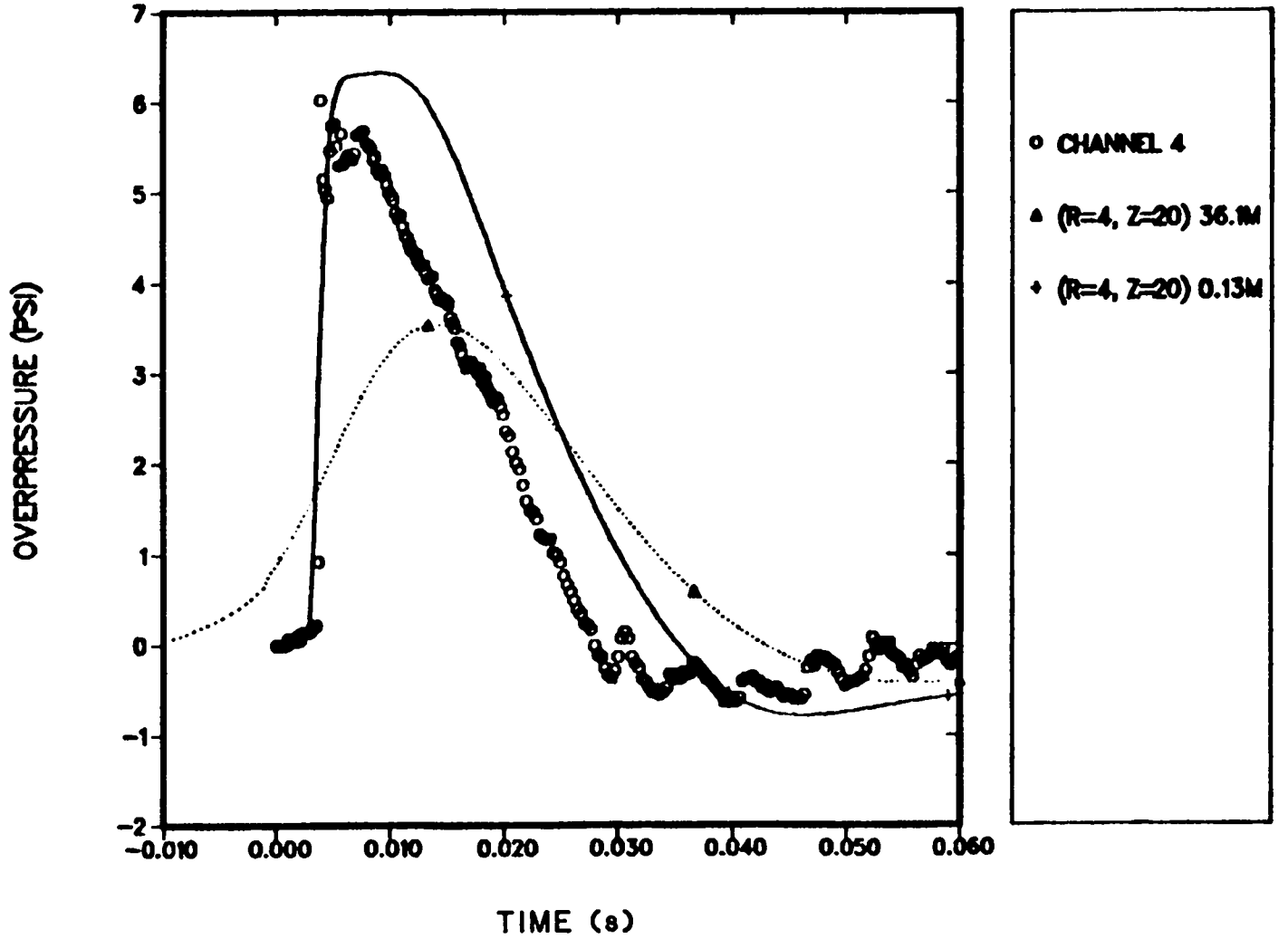


Fig. 11 (cont).
Shock transmission test with 21.8-kPa (3.163-psi) shock overpressure.

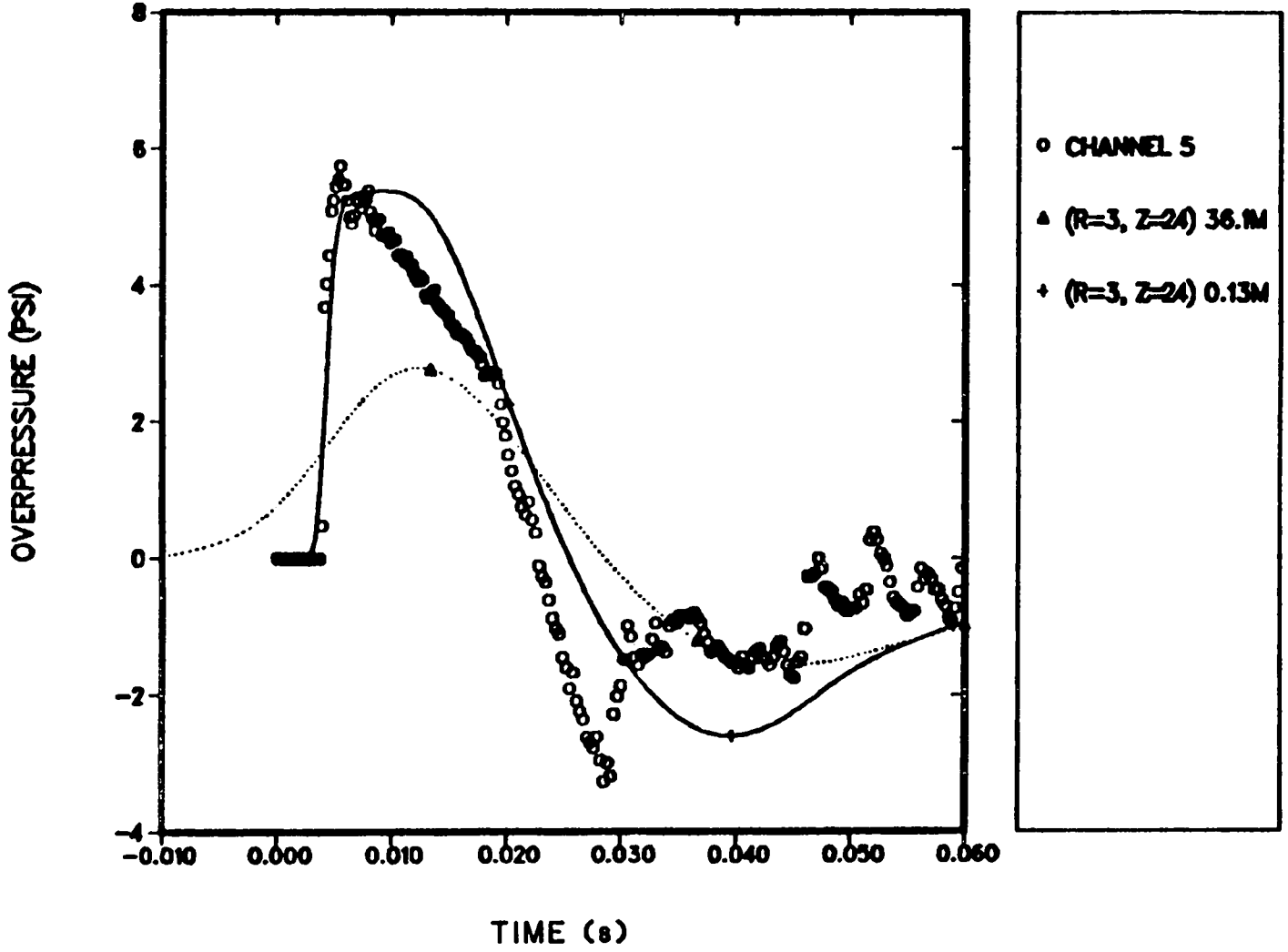


Fig. 11 (cont).
Shock transmission test with 21.8-kPa (3.163-psi) shock overpressure.

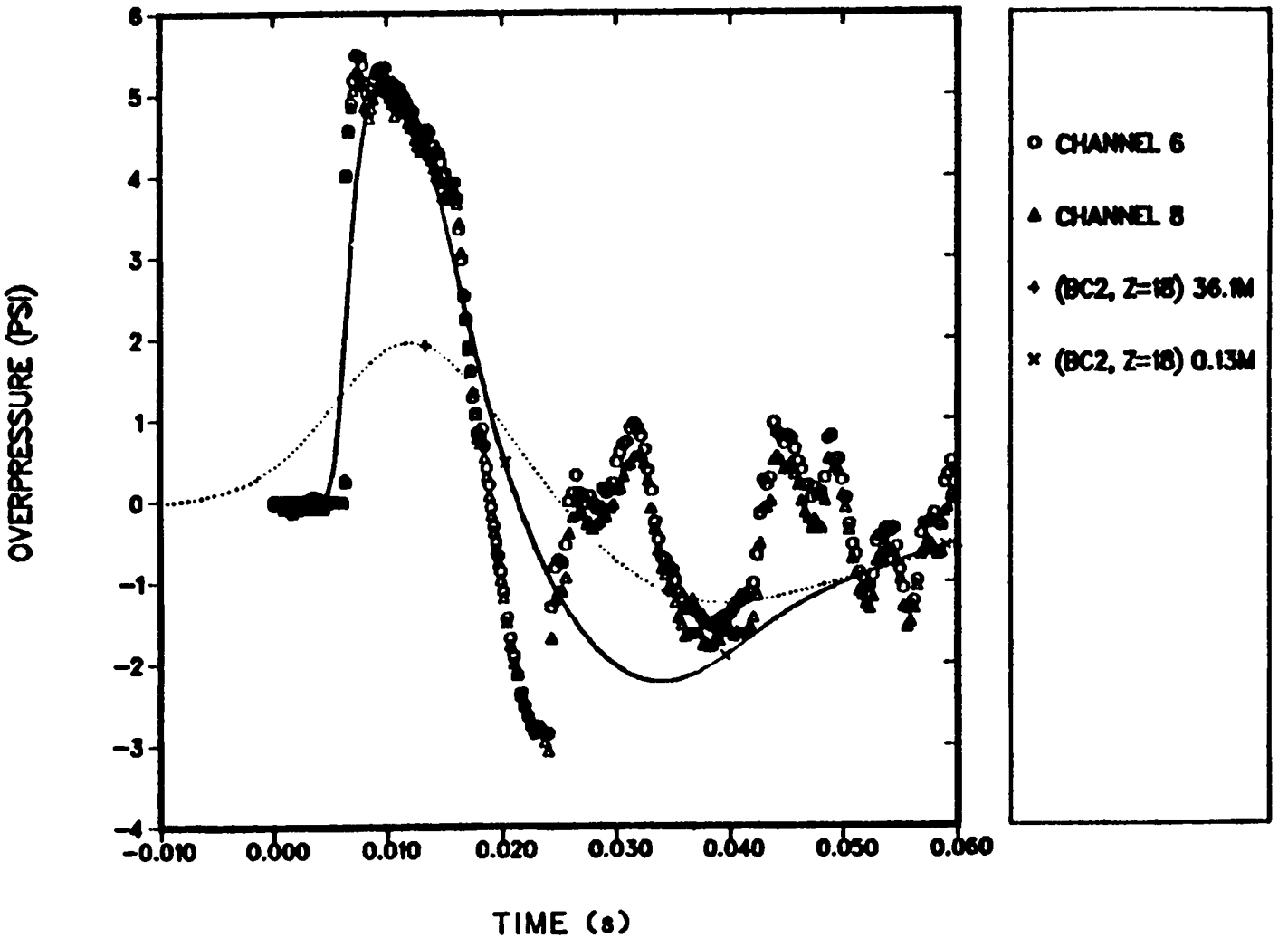


Fig. 11 (cont).
Shock transmission test with 21.8-kPa (3.163-psi) shock overpressure.

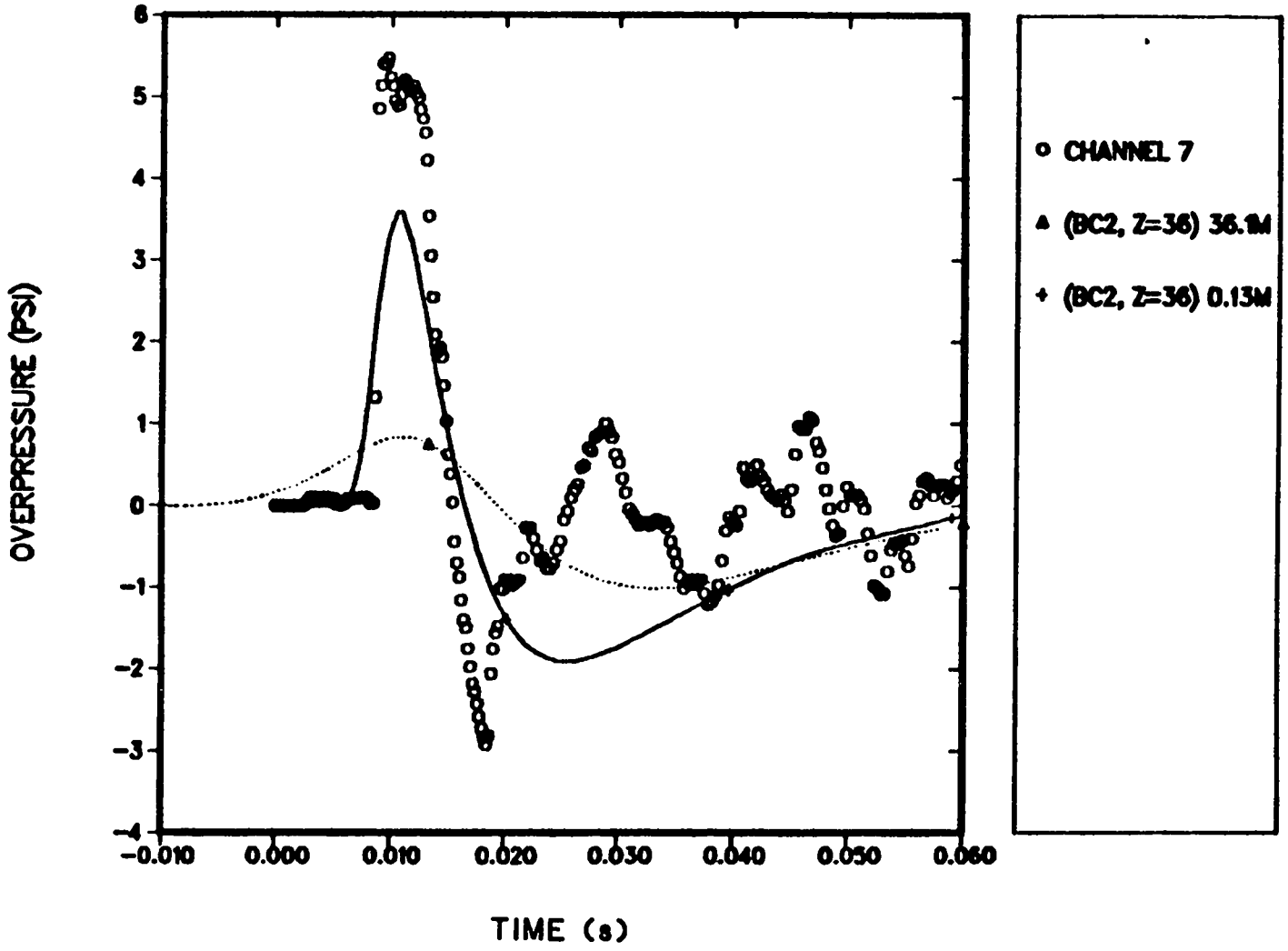


Fig. 11 (cont).
Shock transmission test with 21.8-kPa (3.163-psi) shock overpressure.

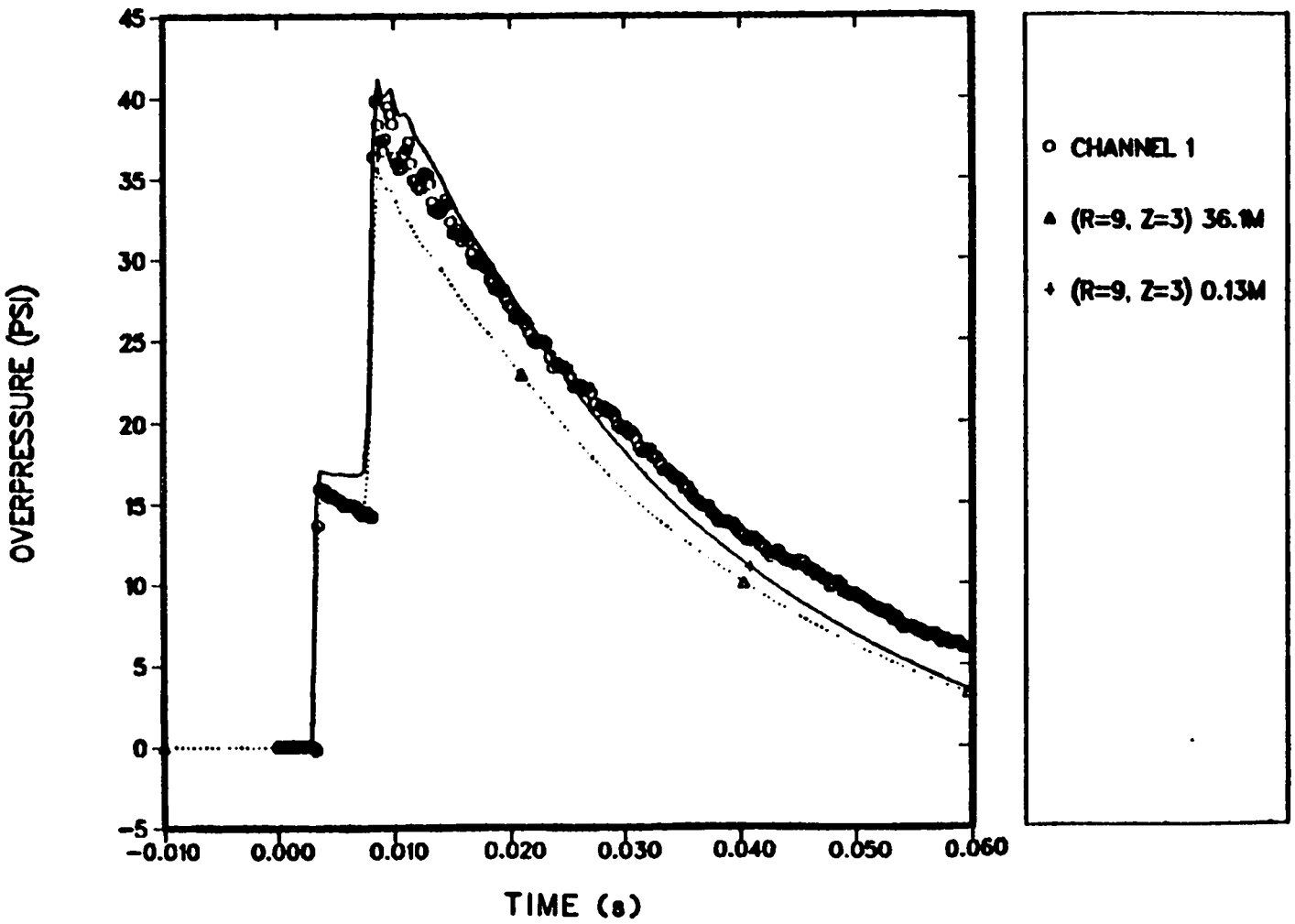


Fig. 12.
Shock transmission test with 110.3-kPa (16.012-psi) shock overpressure.

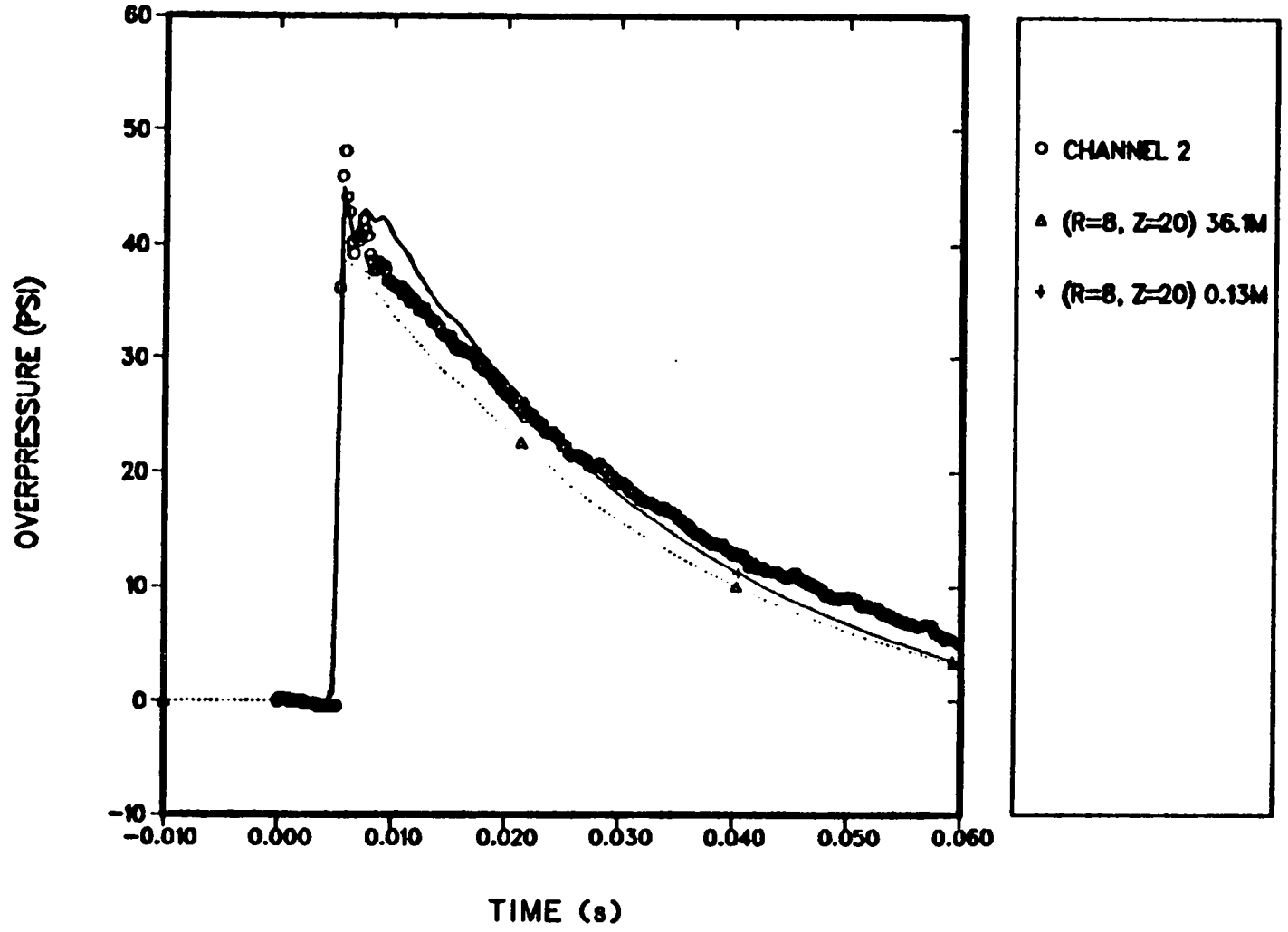


Fig. 12 (cont).
Shock transmission test with 110.3-kPa (16.012-psi) shock overpressure.

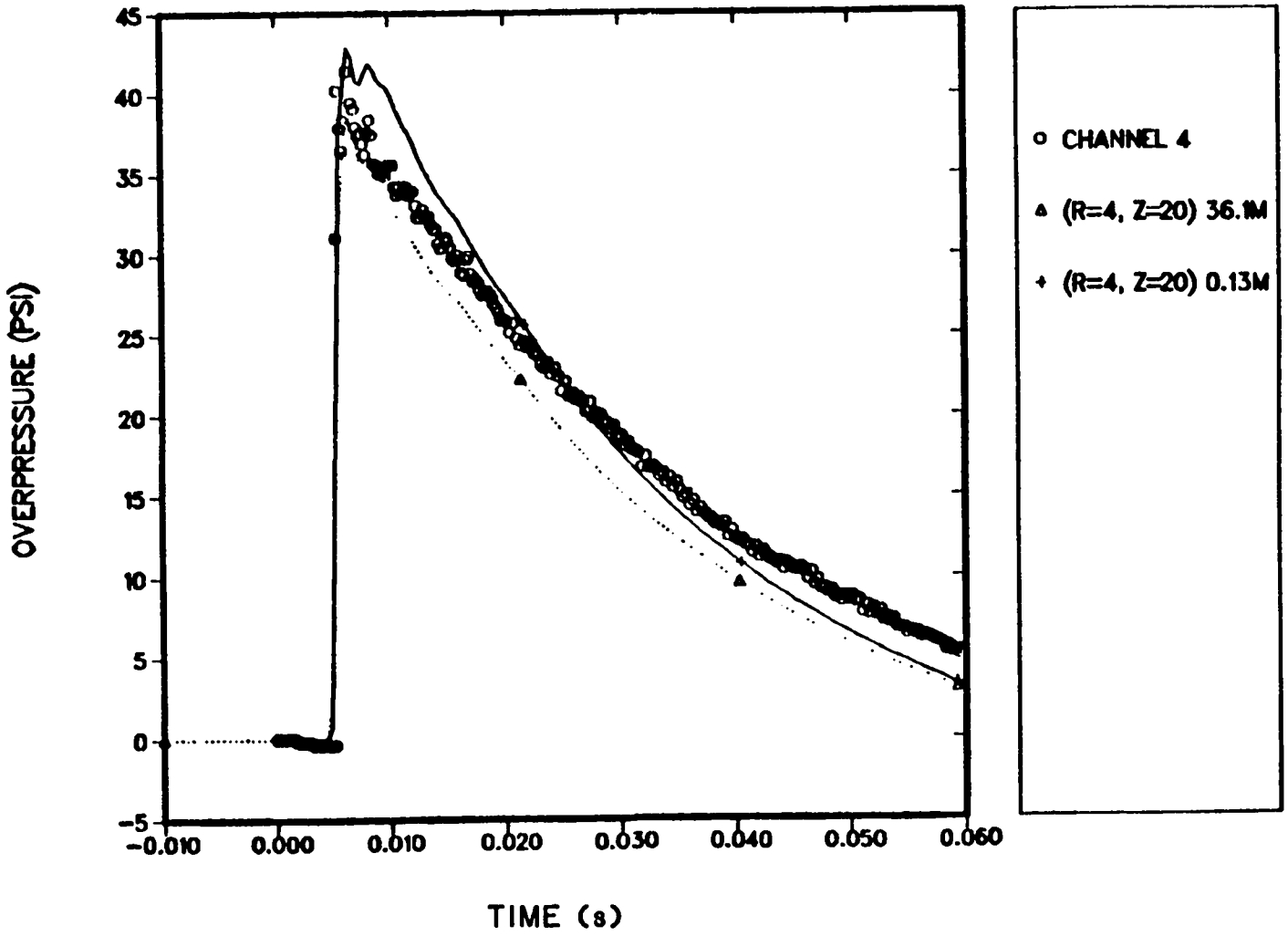


Fig. 12 (cont).
Shock transmission test with 110.3-kPa (16.012-psi) shock overpressure.

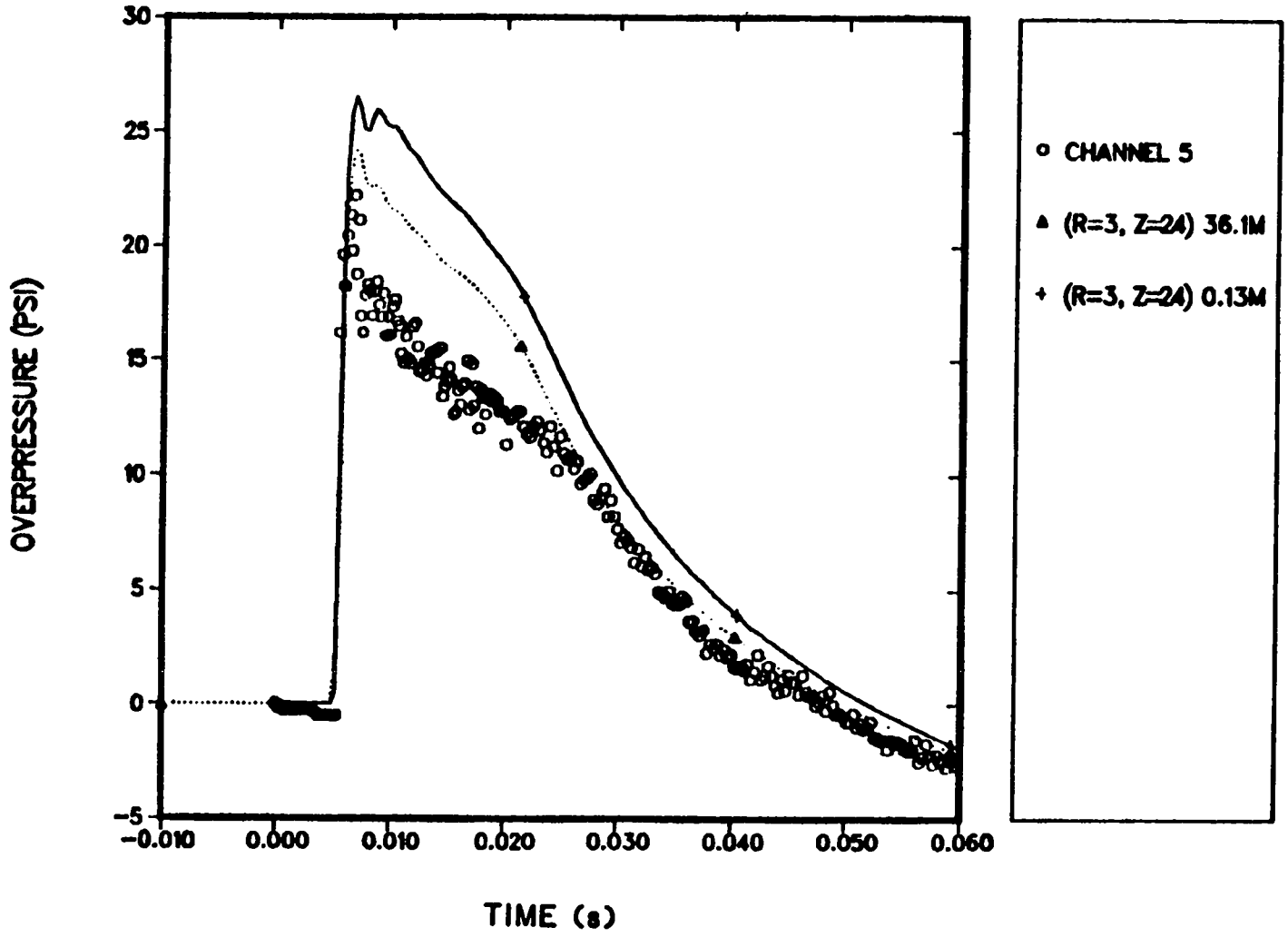


Fig. 12 (cont).
Shock transmission test with 110.3-kPa (16.012-psi) shock overpressure.

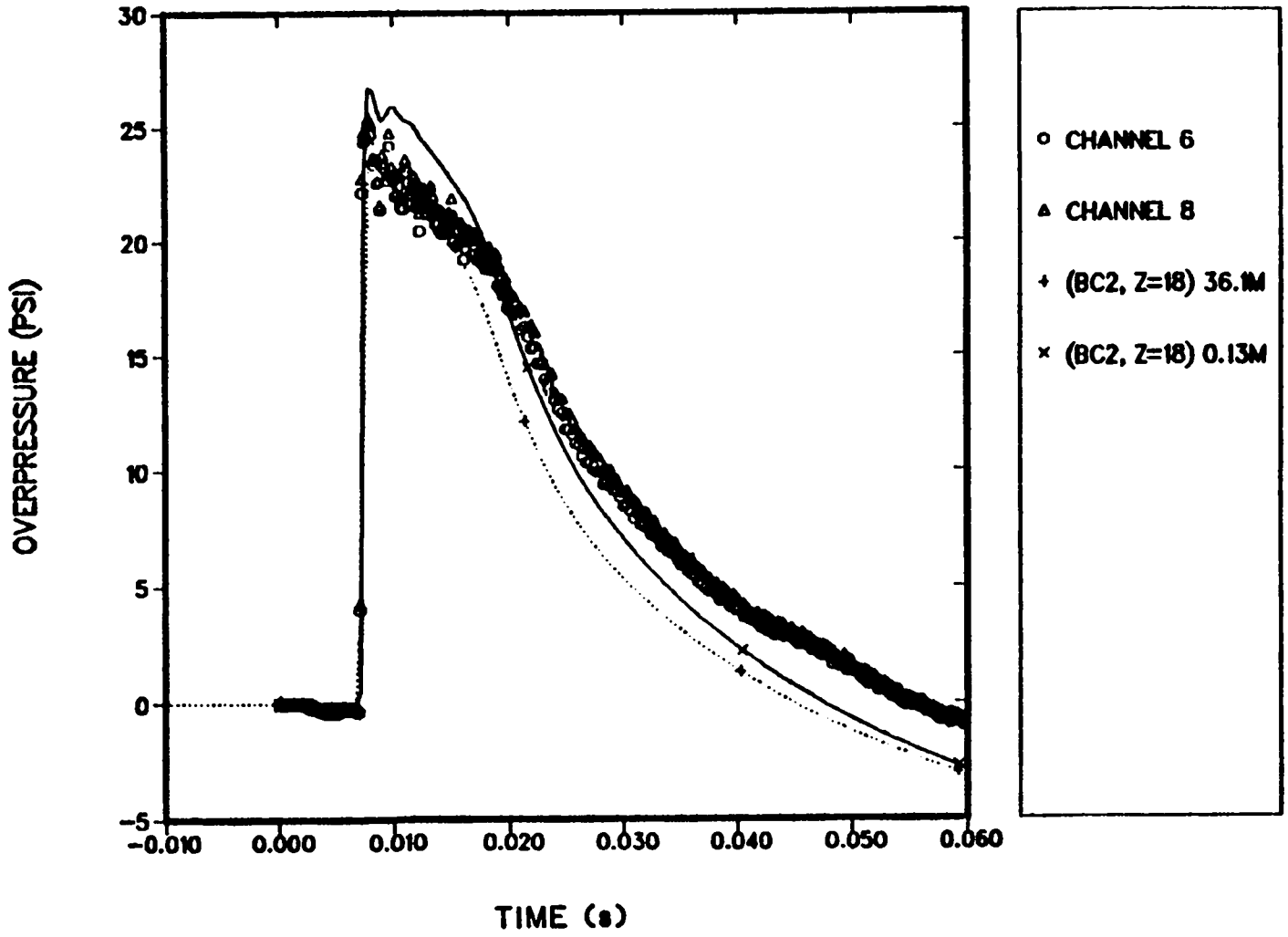


Fig. 12 (cont).
Shock transmission test with 110.3-kPa (16.012-psi) shock overpressure.

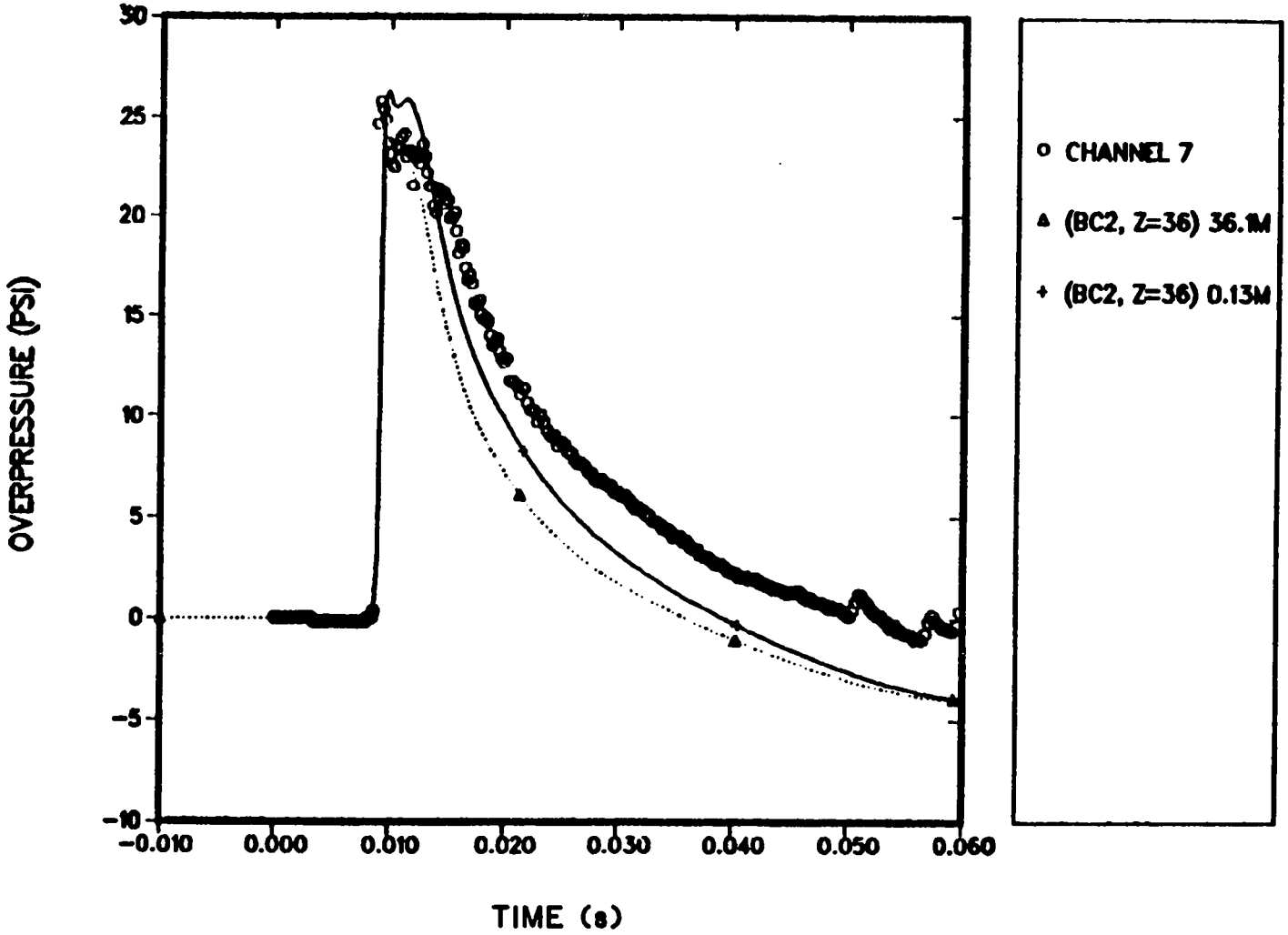


Fig. 12 (cont).
Shock transmission test with 110.3-kPa (16.012-psi) shock overpressure.

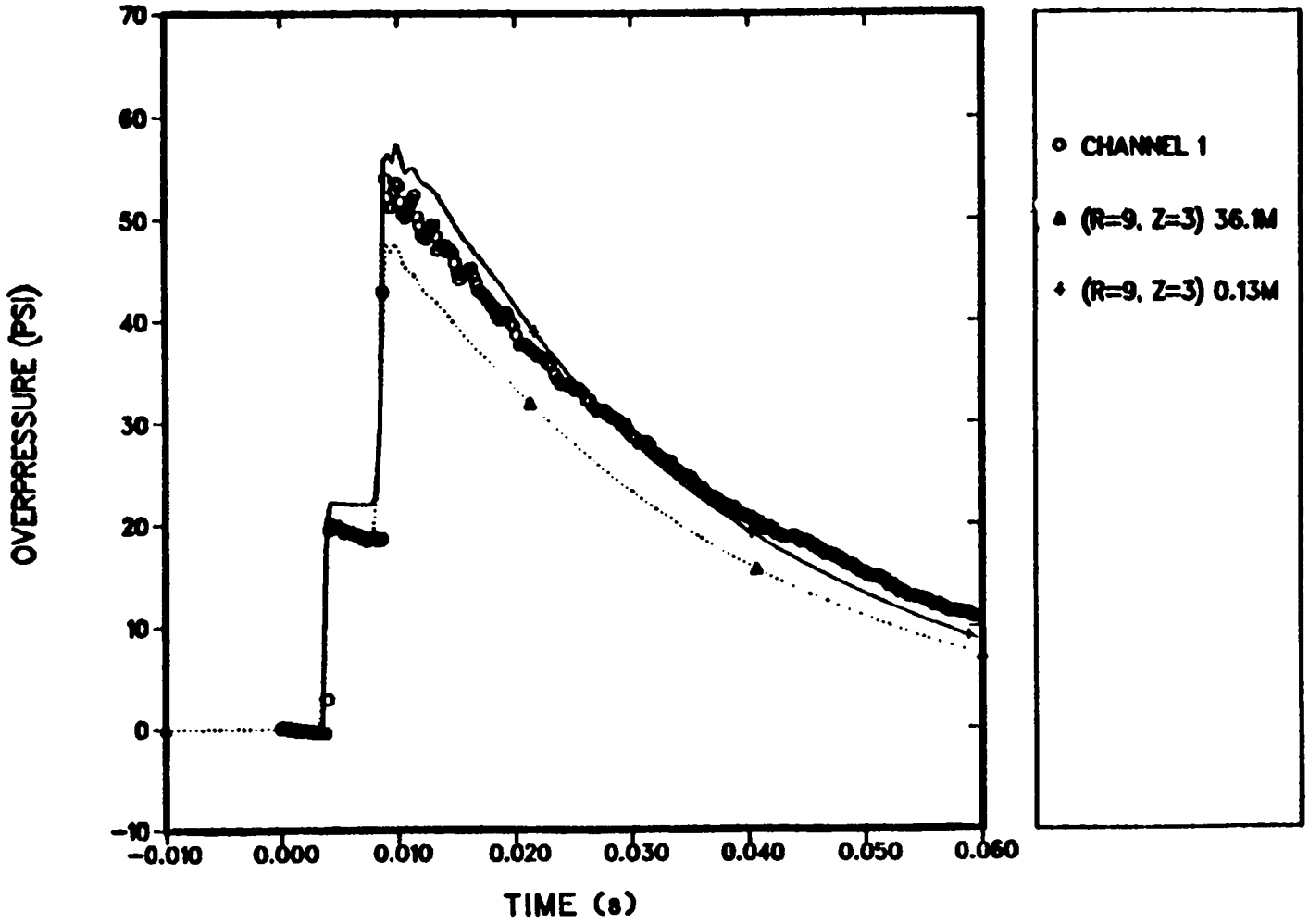


Fig. 13.
Shock transmission test with 141.5-kPa (20.547-psi) shock overpressure.

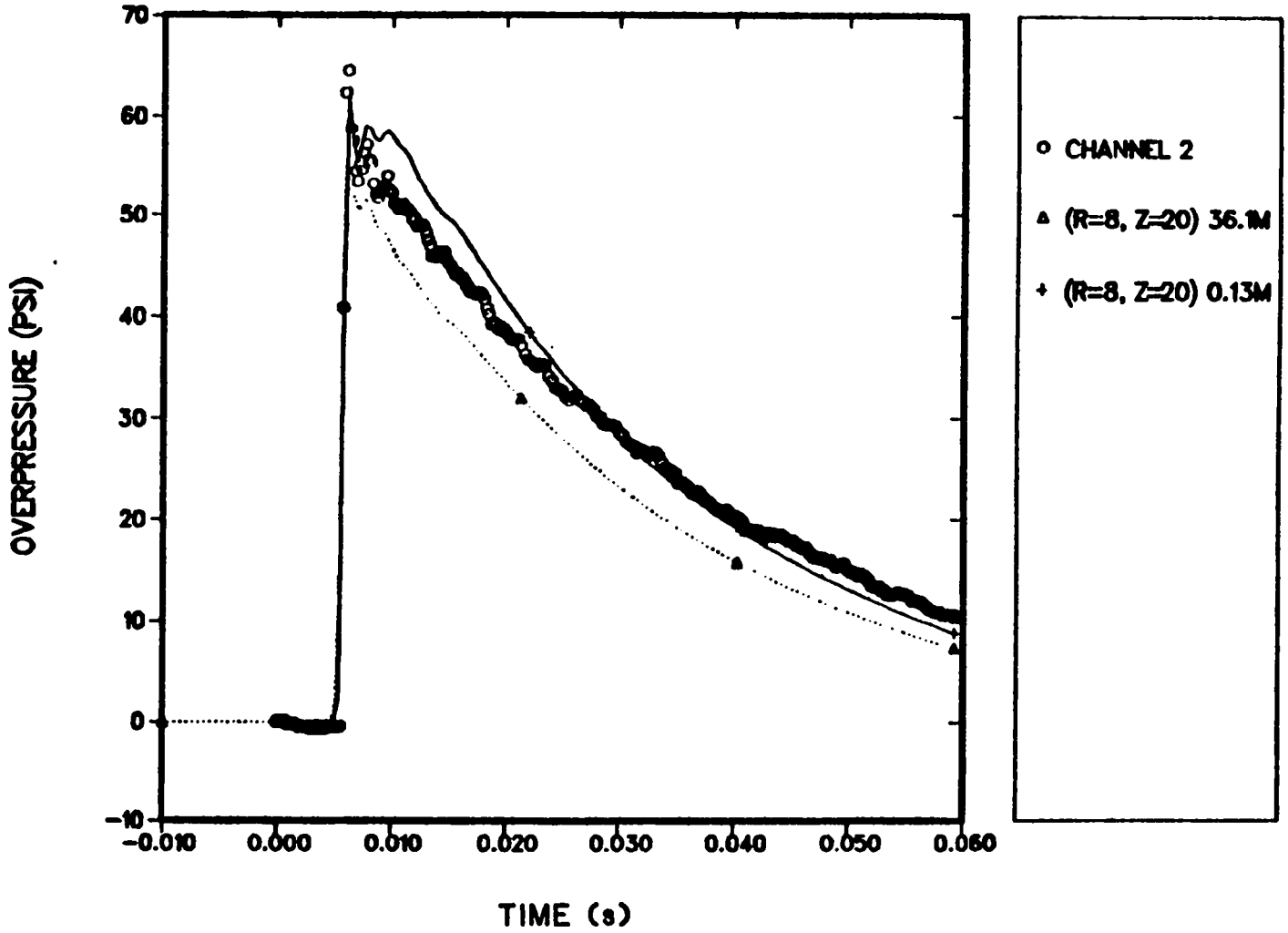


Fig. 13 (cont).
Shock transmission test with 141.5-kPa (20.547-psi) shock overpressure.

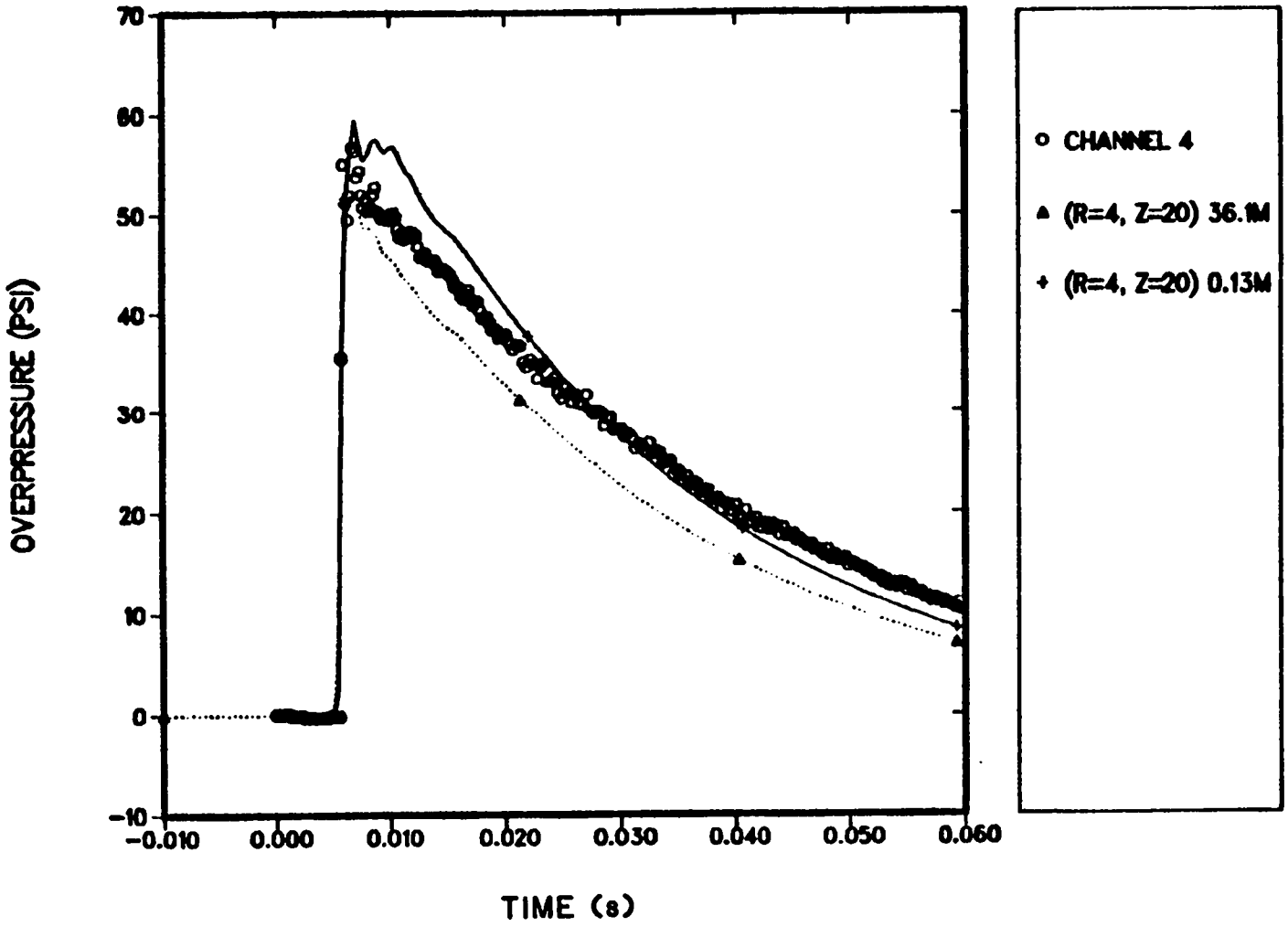


Fig. 13 (cont).
Shock transmission test with 141.50kPa (20.547-psi) shock overpressure.

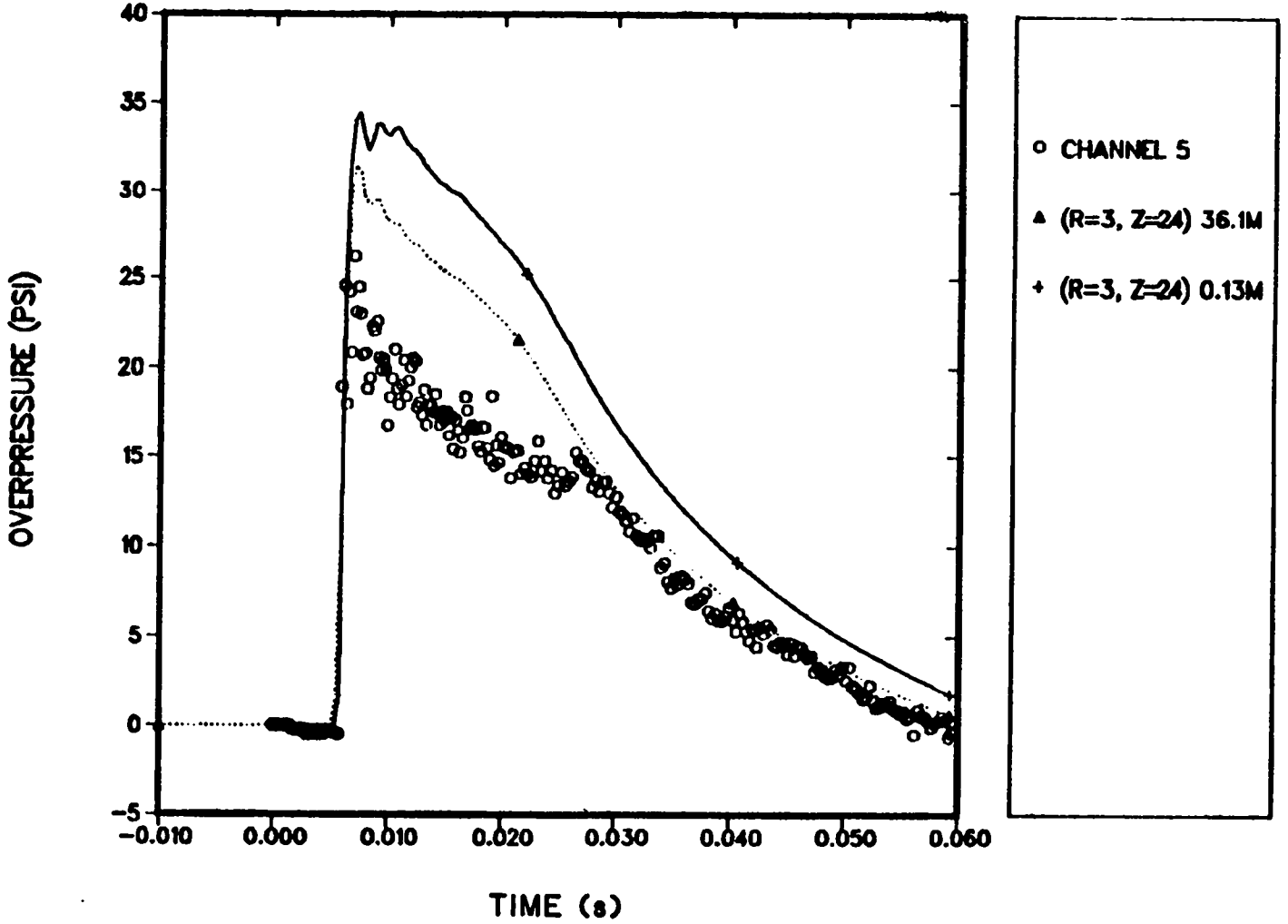


Fig. 13 (cont).
Shock transmission test with 141.5-kPa (20.547-psi) shock overpressure.

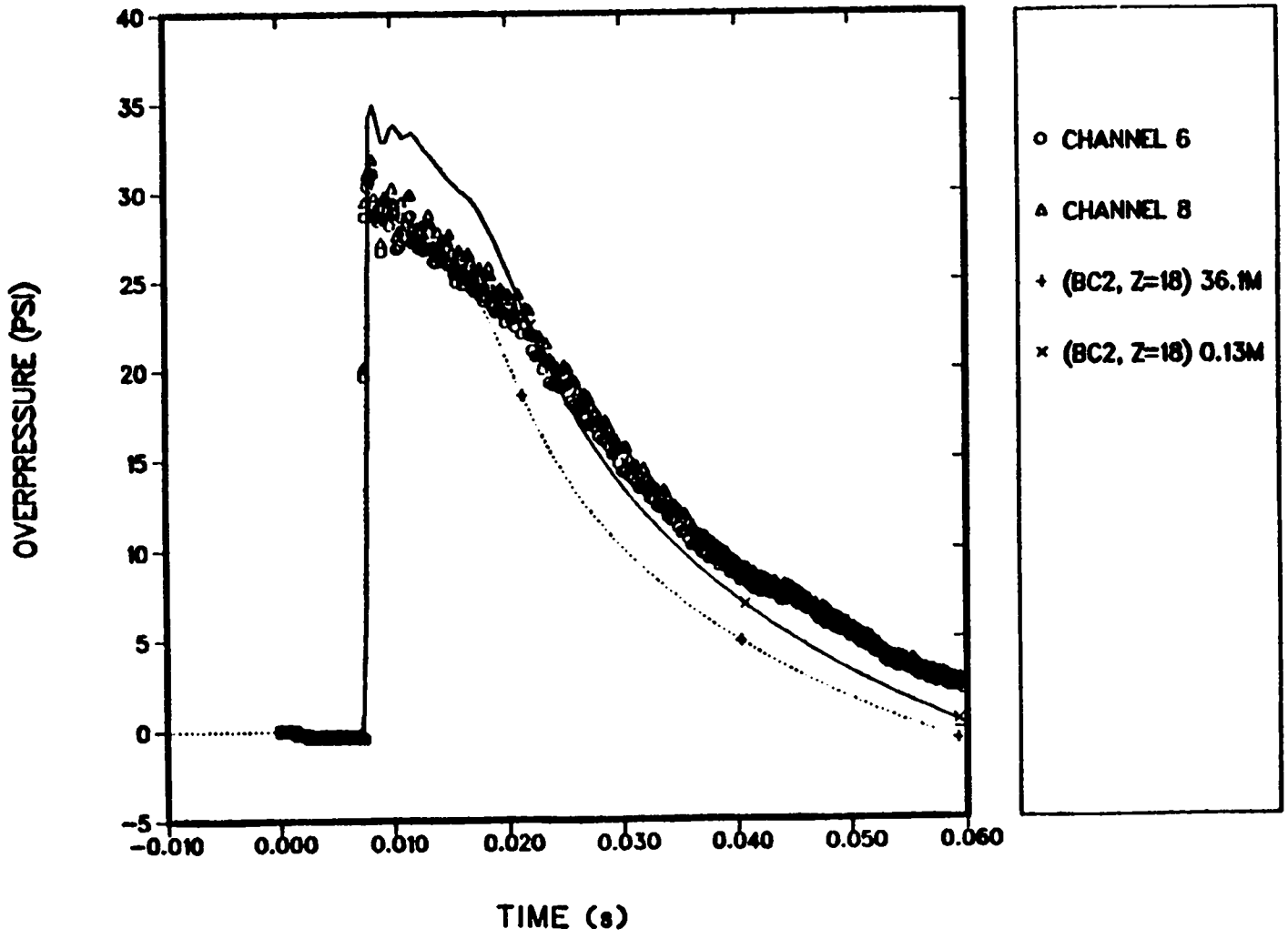


Fig. 13 (cont).
Shock transmission test with 141.5-kPa (20.547-psi) shock overpressure.

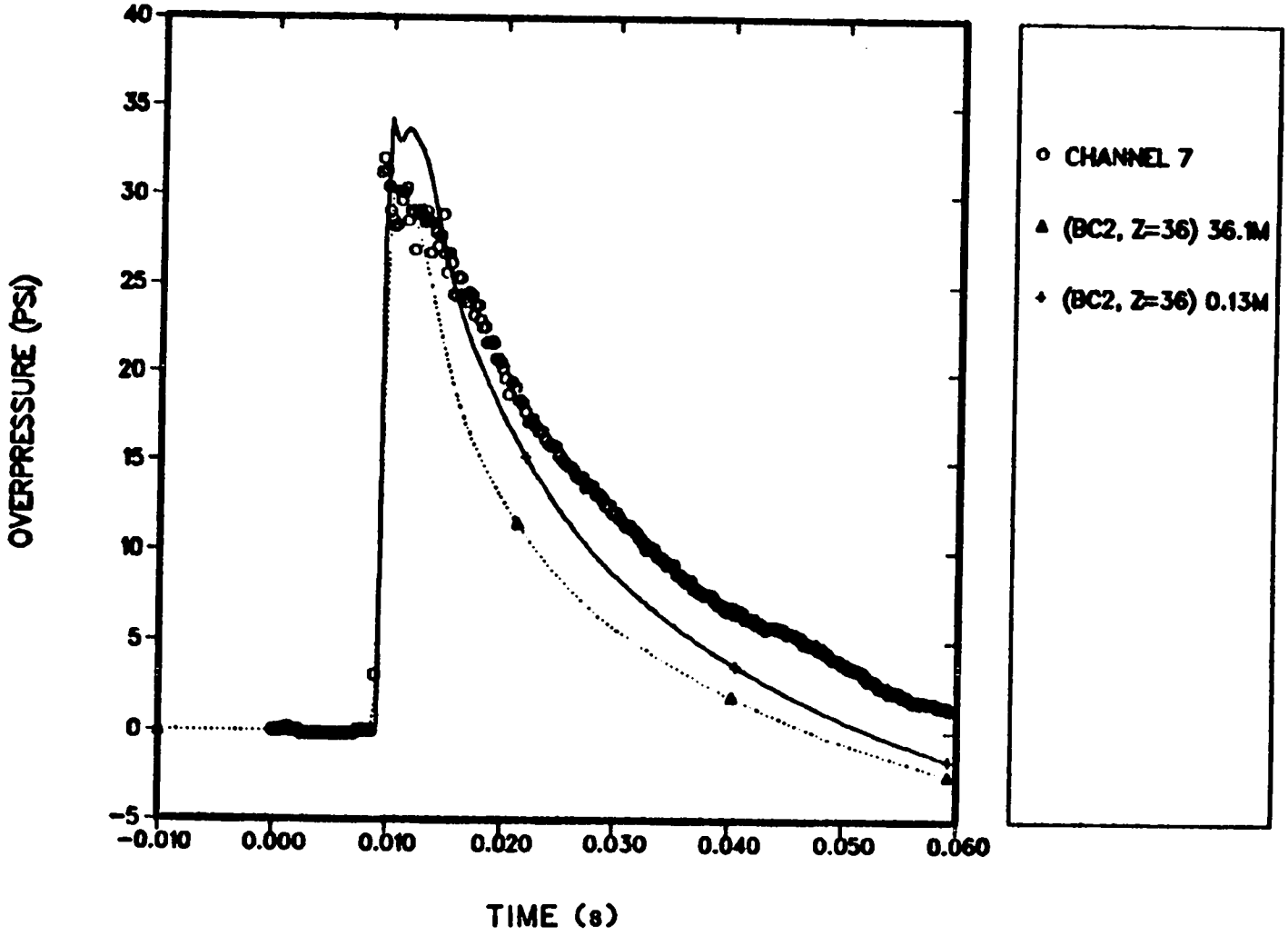


Fig. 13 (cont).
Shock transmission test with 141.5-kPa (20.547-psi) shock overpressure.

lying below the solid curve), but the error is small. We see the calculated pressures decreasing faster in time than the measured pressures as a result of spatial smearing of the expansion wave. All in all, the calculated pressures are in reasonable agreement with their experimental measurements.

The lack of numerical spatial smearing of the shock-wave front for overpressures greater than 1--3.35 kPa (0.15--0.49 psi) is important to note. A first-order donor-cell convection technique as used by NF85 can calculate spatially sharp shock fronts even after long transmission distances and multiple reflections. We feel this is because of the physical phenomena of sonic waves piling up behind a shock-wave front acting in an opposite way to numerical diffusion to eliminate spatial smearing of the shock front. Larger shock-front overpressures appear to have enough of this effect to override numerical-diffusion error.

B. Shock-Tube Ventilation System Tests (NF85)

In the shock-tube ventilation system tests, a shock pulse (a shock front followed by an expansion wave) is generated, travels down the shock tube, and interacts with a flow-area reduction at the end of the shock tube. From this area reduction, the shock pulse encounters the cylindrical tank, then the other two pipes connected to the rectangular tank, and then the rest of the ventilation system.

Two tests were run to ensure repeatability and to capture pressure measurements in all parts of the system. These tests are referred to as TMET17 and TMET19. The experimental results are compared with NF85 predictions in Fig. 14 and Fig. 15. Figures 14--21 show the NF85 predictions compared with experimental data for both TMET17 and TMET19 for channels 1--4. Figures 22--25 show NF85 comparisons with experimental data for channels 5--8 for test TMET17. The repeatability of the two tests is quite good, particularly at Channel 1 with peak pressures of approximately 41.4 kPa (6 psi) in both cases. The experimental pressure drops off more quickly in TMET17 than in TMET19.

Channel 1 comparisons between experimental and analytical predictions are shown in Figs. 14 and 15 for both tests. This measuring point is at the end of the shock tube before the area reduction and the entrance to the cylindrical tank. In this case, the comparisons are quite close. The analytical peak pressure is 48.3 kPa (7 psi), and the experimental value is 41.4 kPa (6 psi).

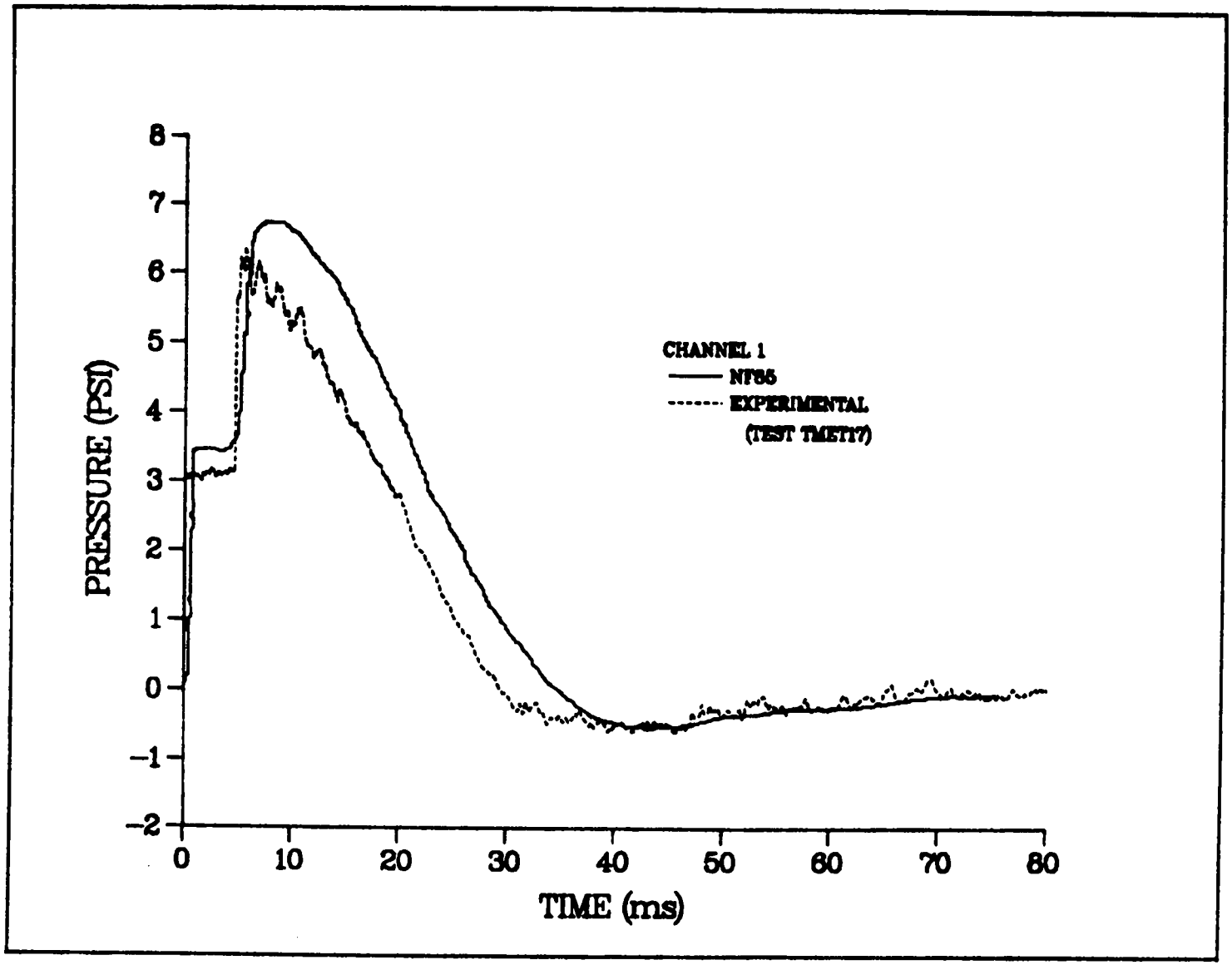


Fig. 14.
Comparison of experimental results with NF85 predictions of pressure at the exit of the shock tube.

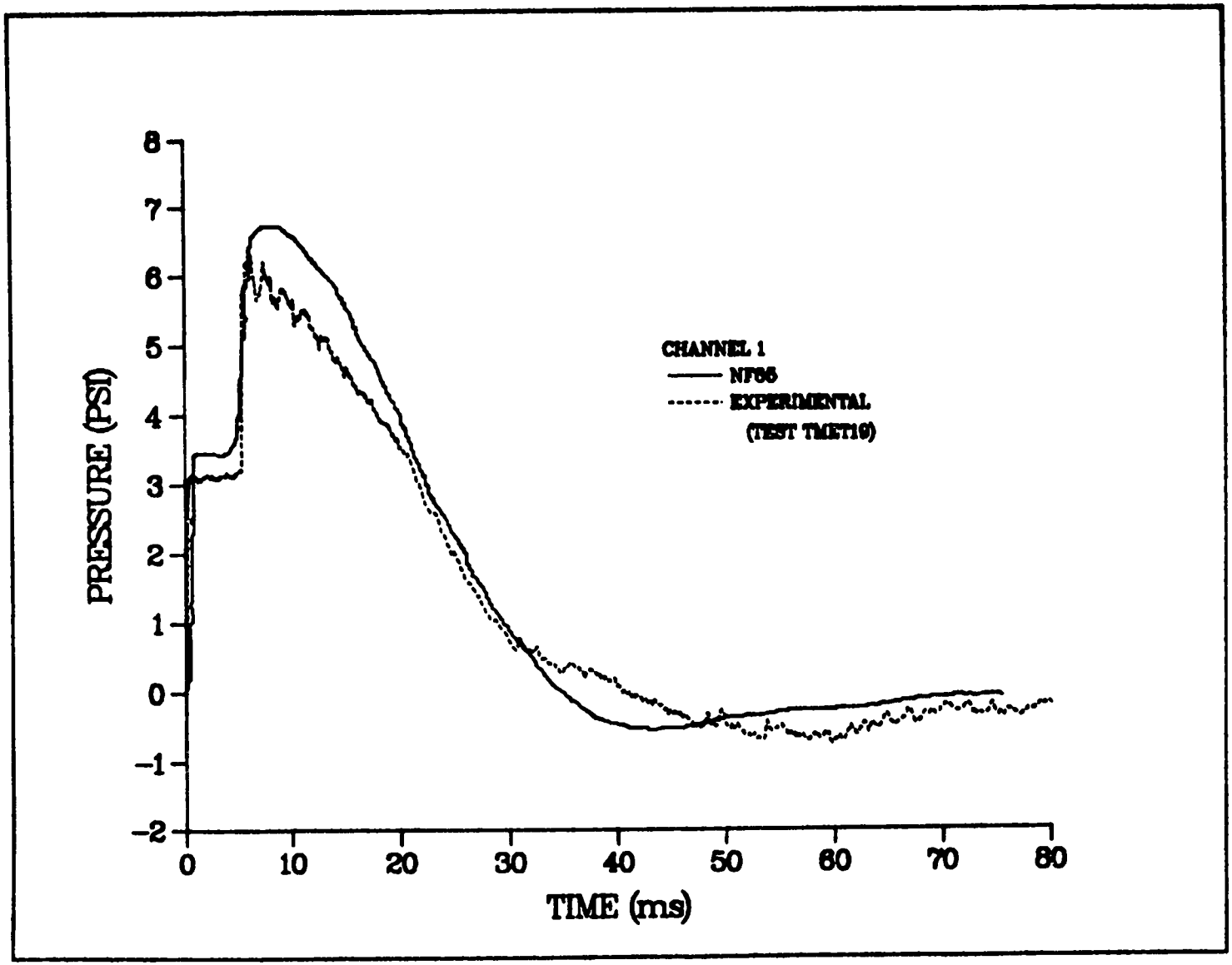


Fig. 15.
Comparison of TMET19 experimental results with NF85 predictions of pressure at the exit of the shock tube.

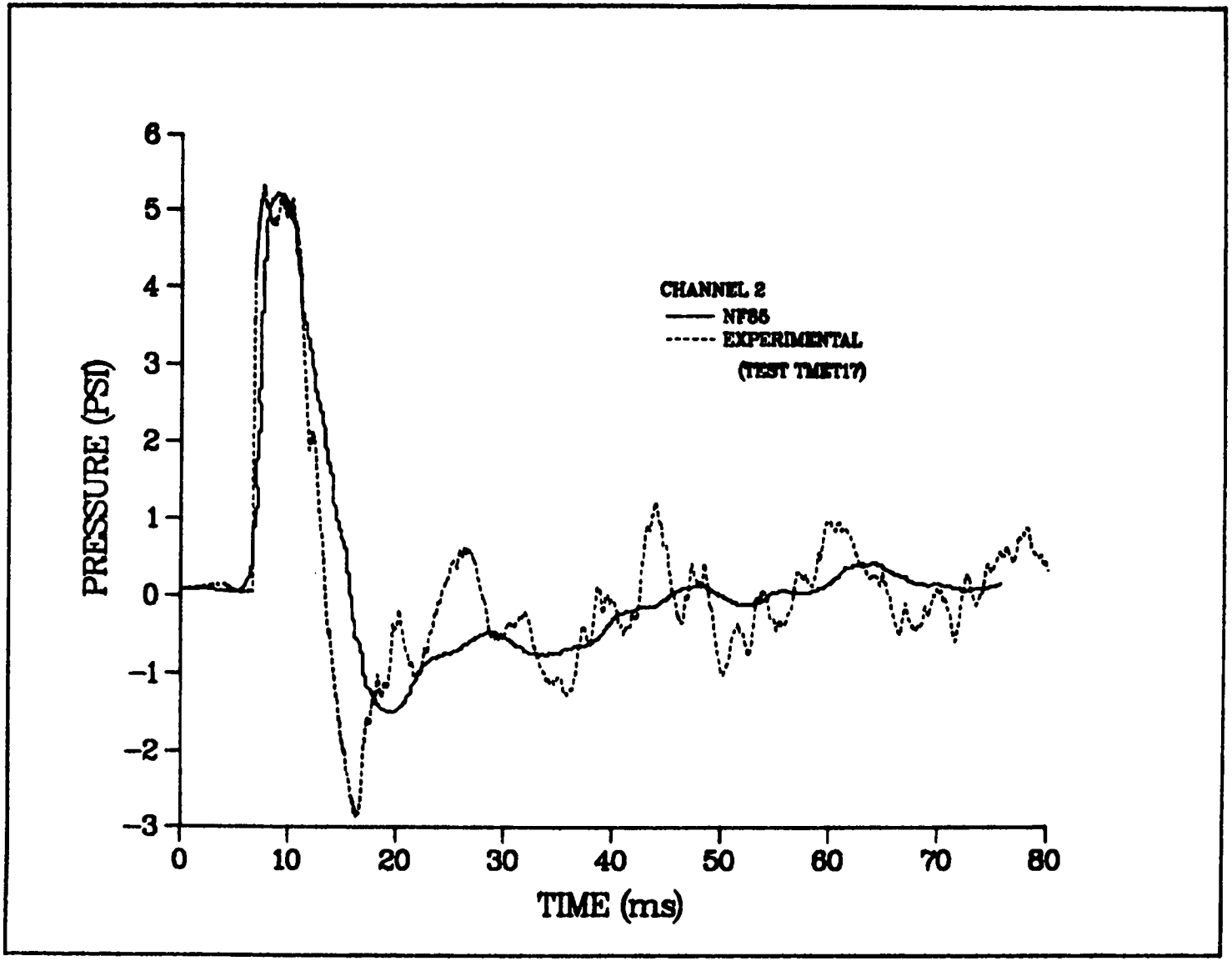


Fig. 16.
Comparison of TMET17 experimental results with NF85 predictions of pressure in the 1-ft-diam tube at the end of the shock tube.

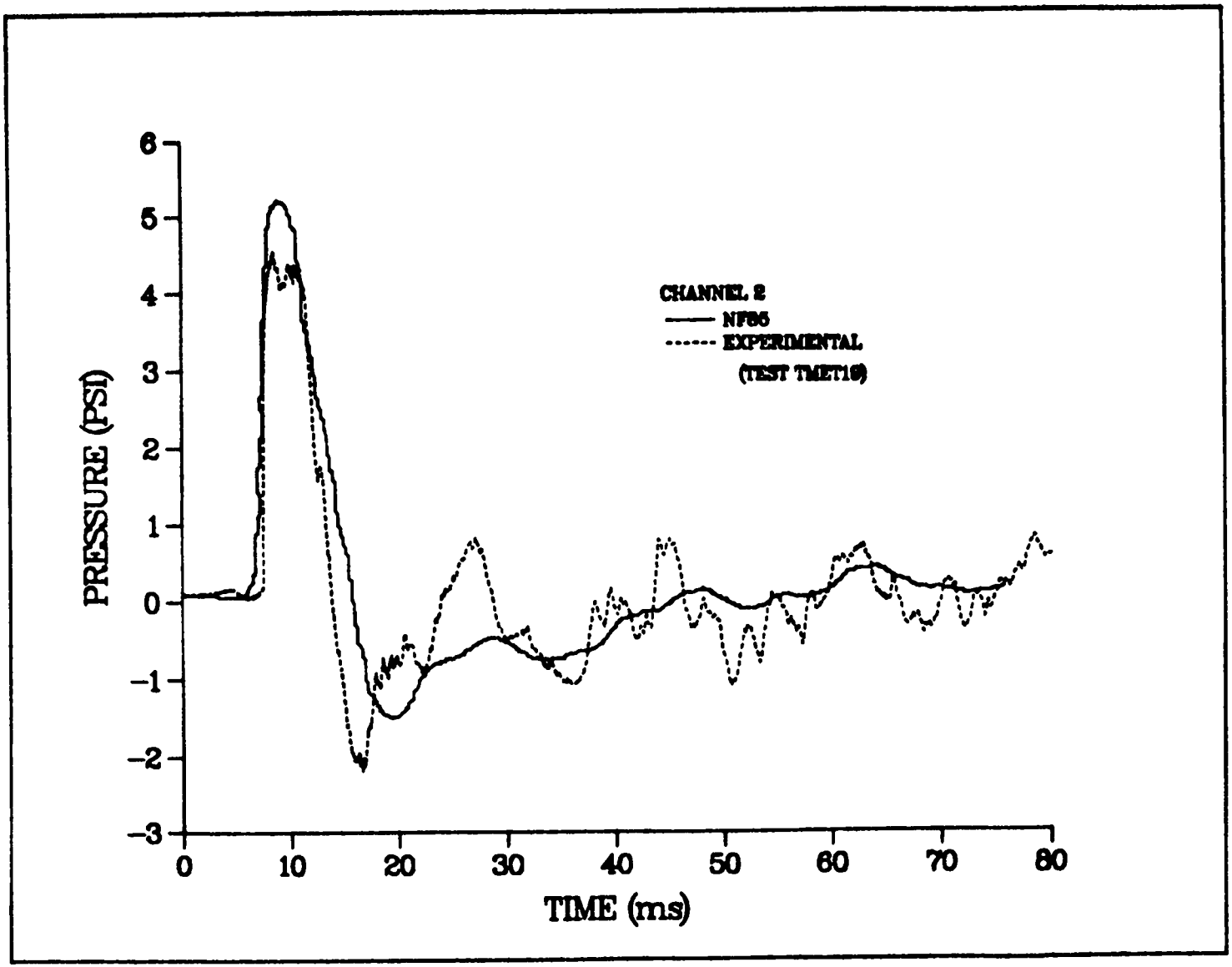


Fig. 17.
Comparison of TMET19 experimental results with NF85 predictions of pressure in the 1-ft-diam tube at the end of the shock tube.

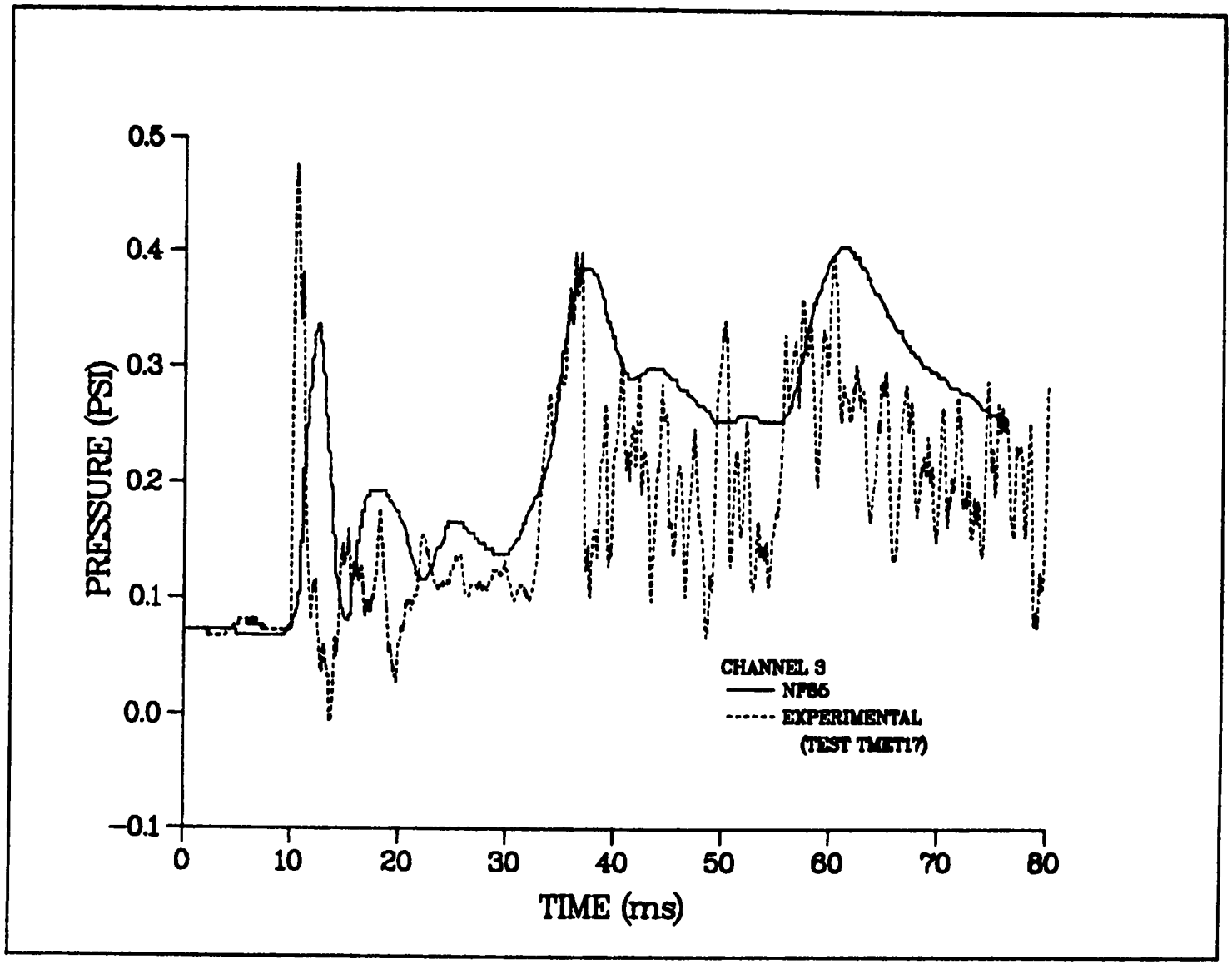


Fig. 18.
Comparison of the TMET17 experimental results with NF85 predictions of pressure at the end wall of the cylindrical tank.

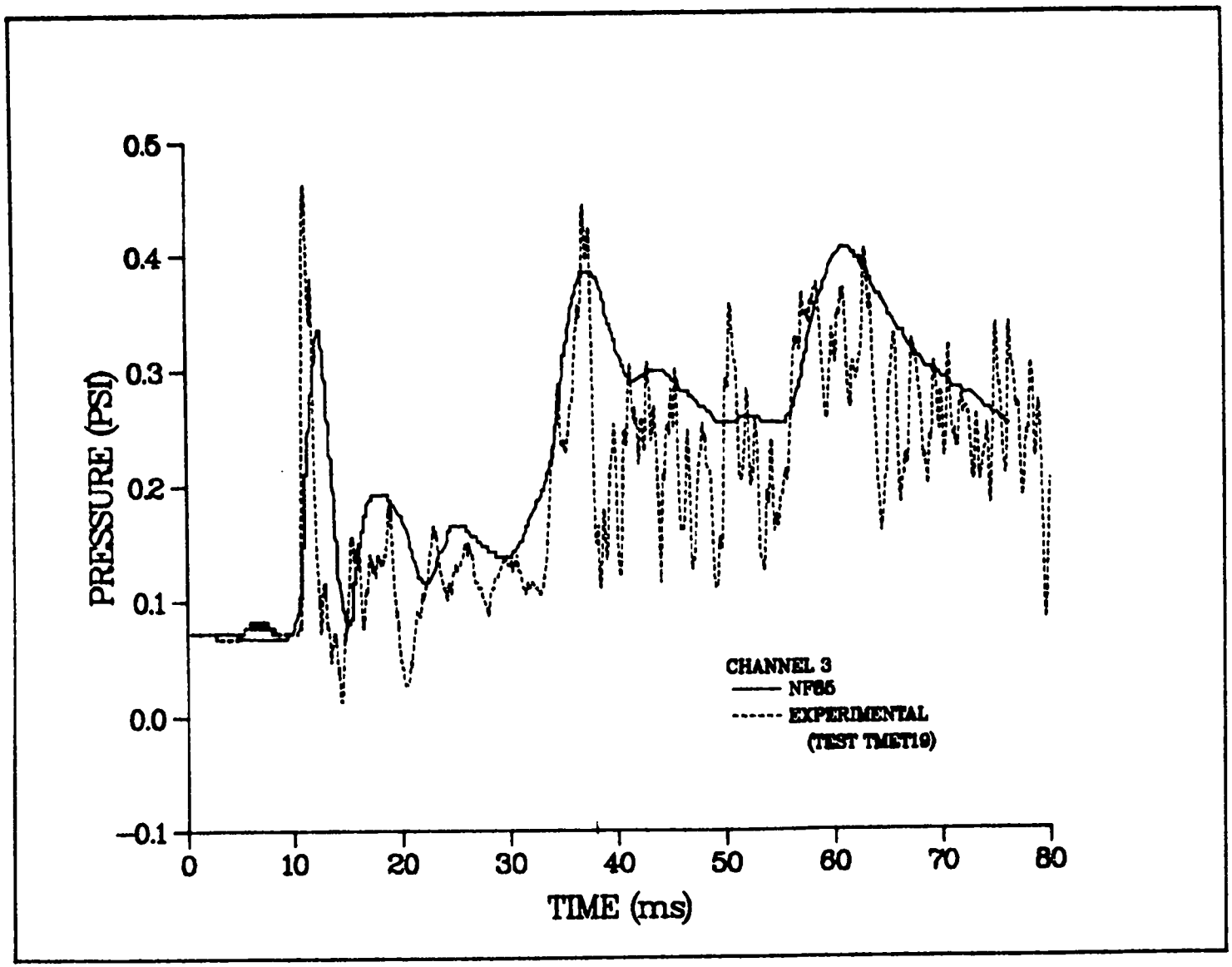


Fig. 19.
Comparison of TMET19 experimental results with NF85 predictions of pressure at the end of wall of the cylindrical tank.

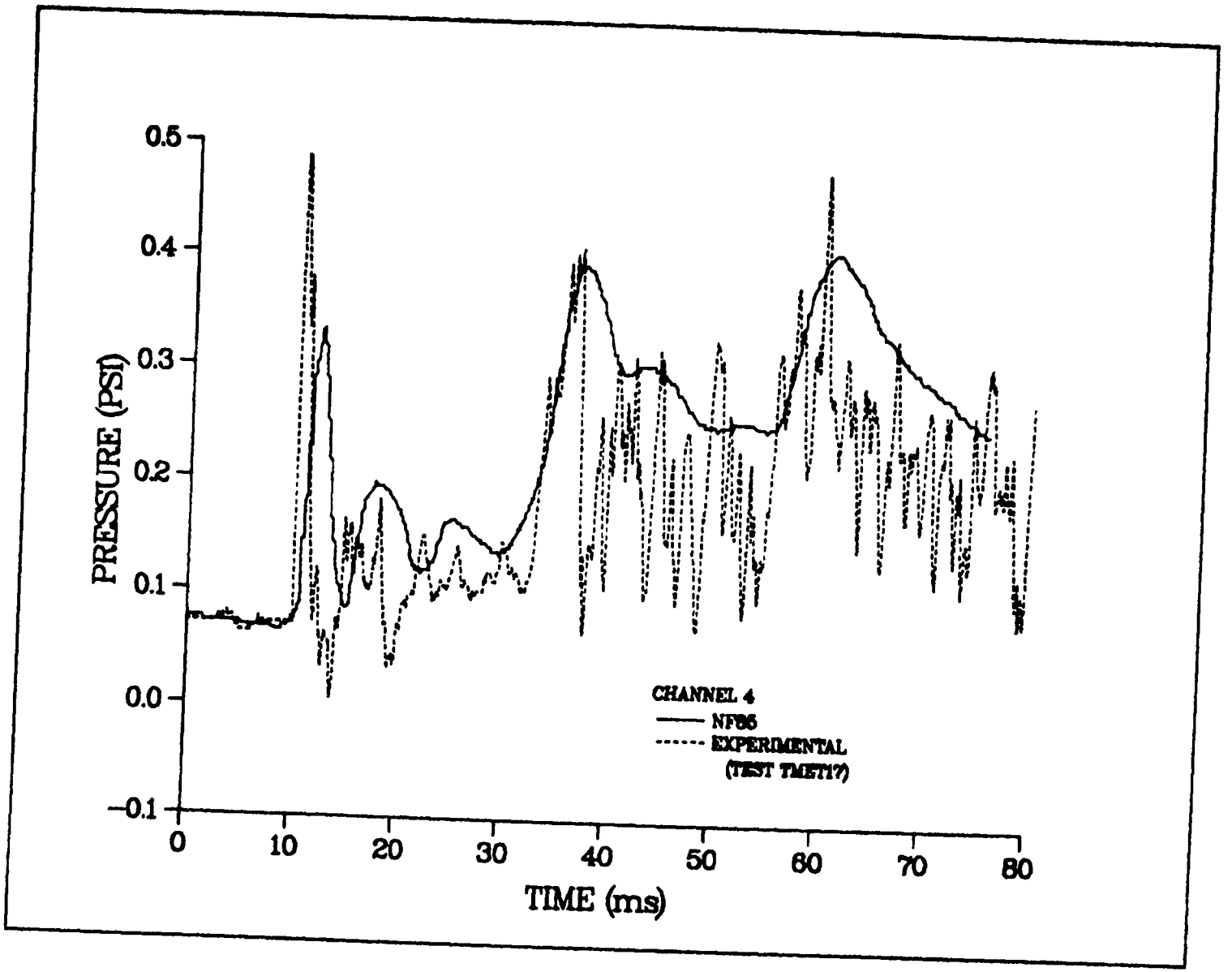


Fig. 20.
Comparison of the TMET17 experimental results with NF85 predictions of pressure at the end wall of the cylindrical tank.

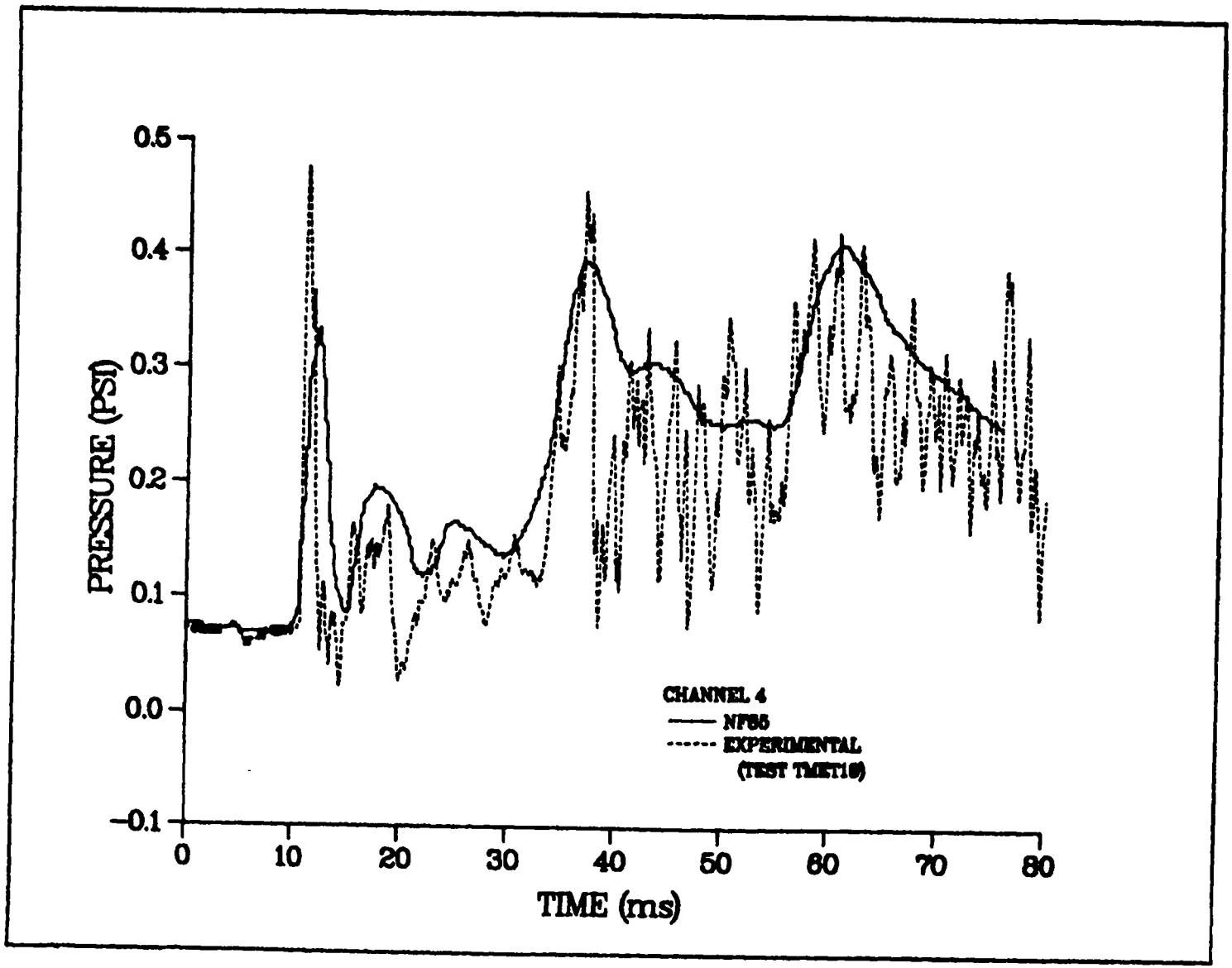


Fig. 21.
Comparison of the TMET19 experimental results with NF85 predictions of pressure at the end wall of the cylindrical tank.

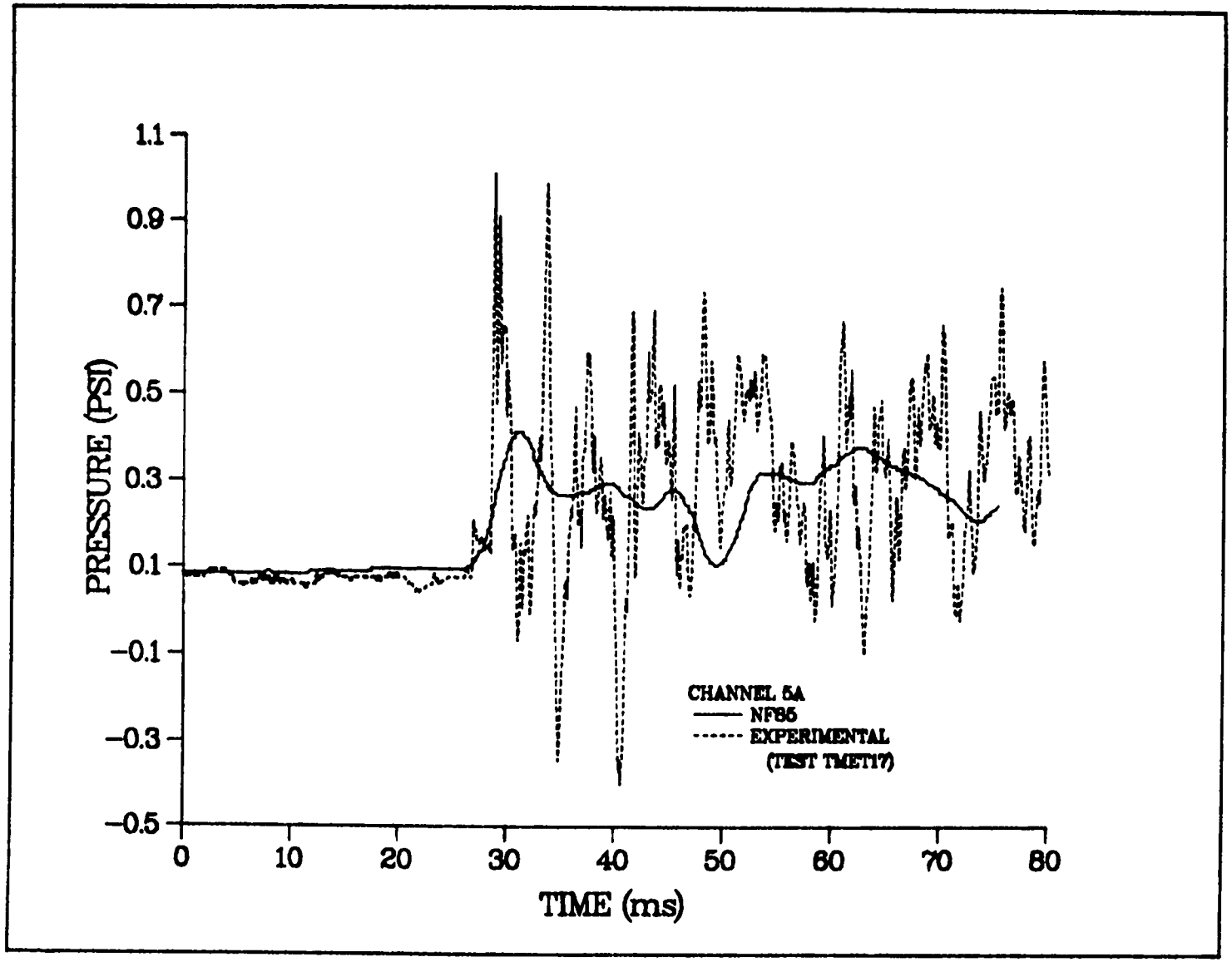


Fig. 22.
Comparison of TMET17 experimental results with NF85 predictions of pressure in the tube downstream of the cylindrical tank.

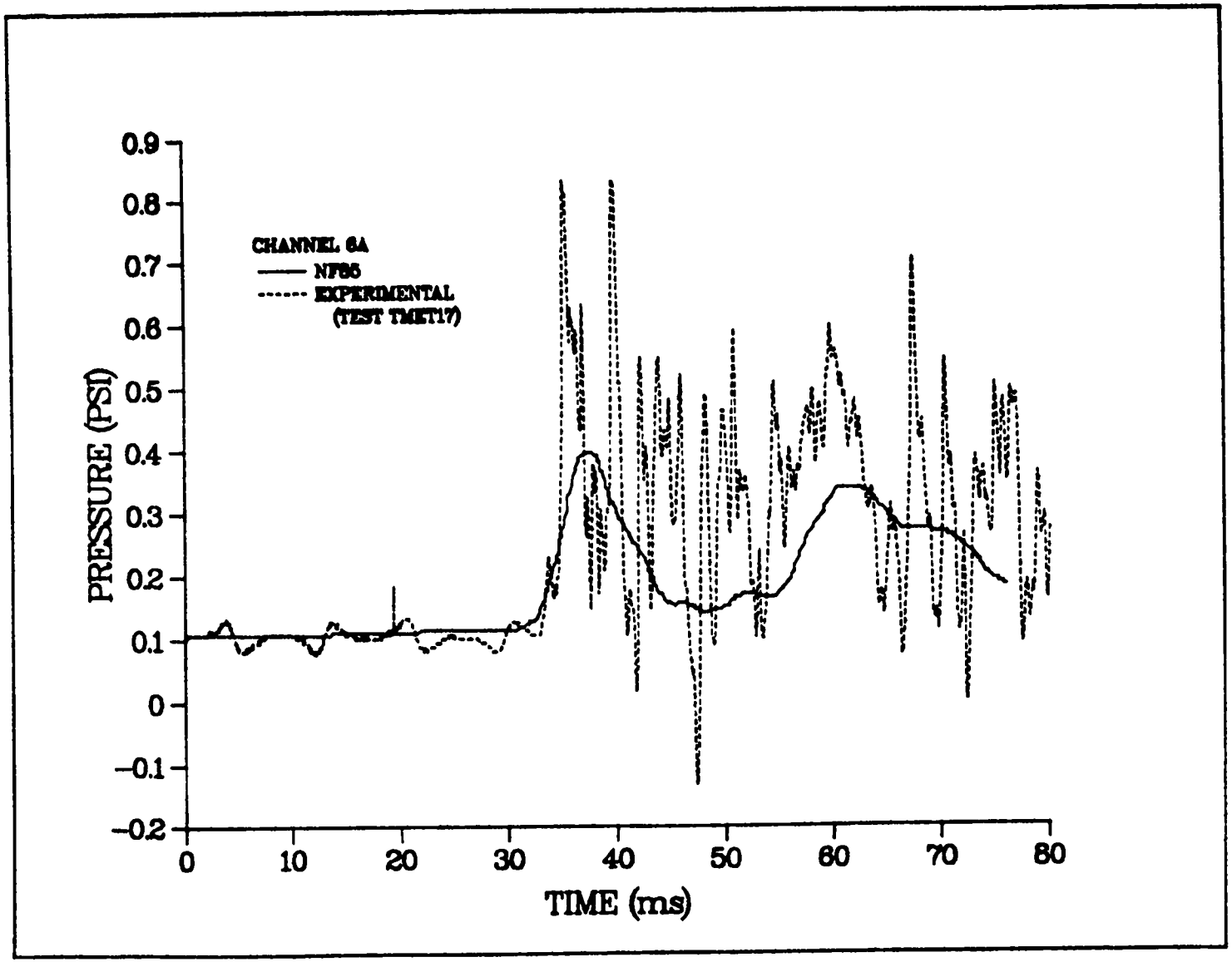


Fig. 23.
Comparison of TMET17 experimental results with NF85 predictions of pressure downstream of the damper.

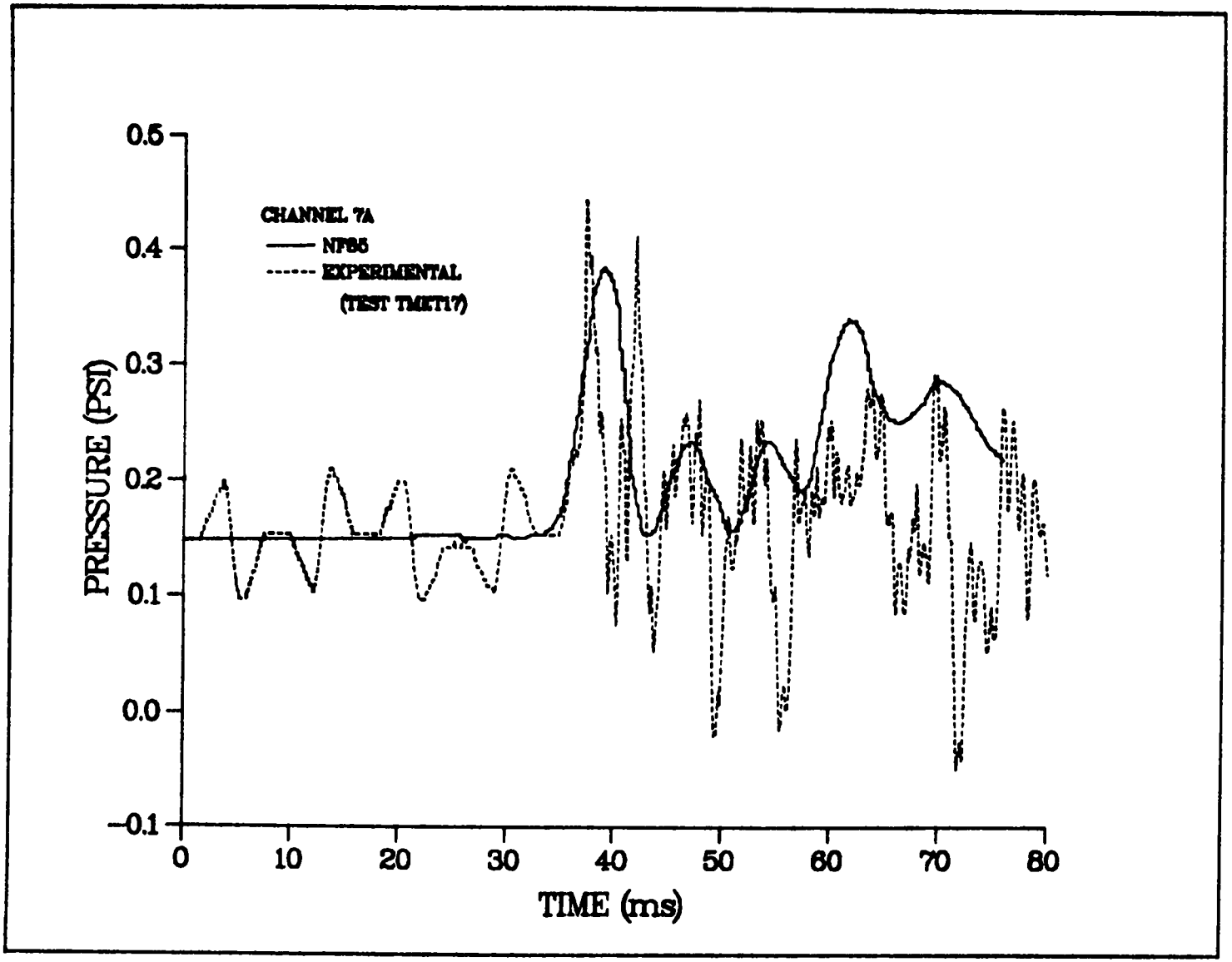


Fig. 24.
Comparison of TMET experimental results with NF85 predictions of pressure downstream of the HEPA filter.

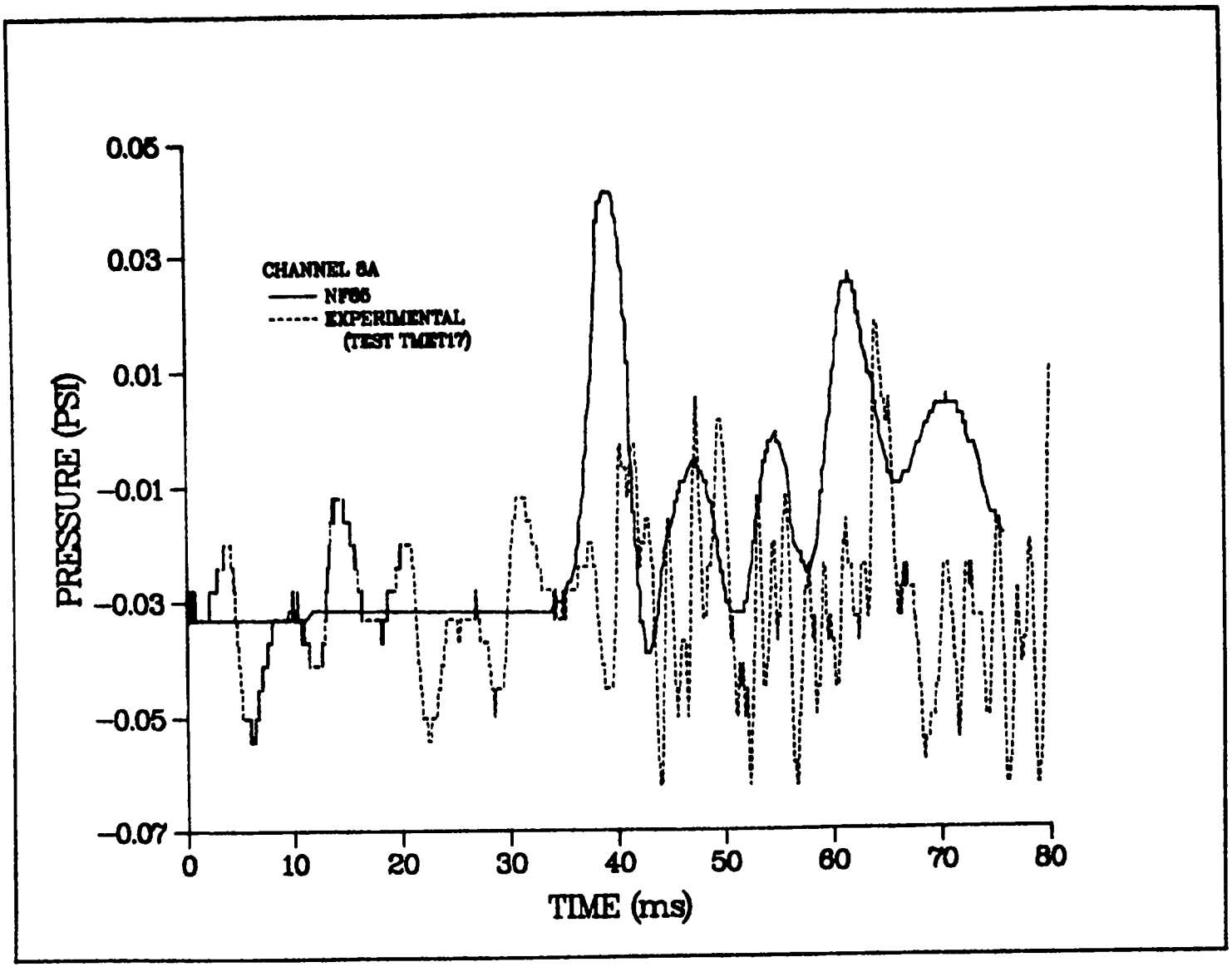


Fig. 25.
Comparison of TMET17 experimental results with NF85 predictions of pressure downstream of the blower.

Channel 2 is located in the 0.305-m (1-ft)-diam pipe, and the analytical/experimental comparison is shown in Figs. 16 and 17. As for channel 1, the major peak pressures coincide in time and are quite close in magnitude.

Channels 3 and 4 are located inside the cylindrical tank and are mounted on one end wall as shown in Fig. 3. The comparisons for these tests are shown in Figs. 18--21. As expected, there is considerable oscillation from these pressure transducers. In this case, the shock waves probably are hitting the end walls of the cylindrical tank. The major peaks occur at approximately 30-ms intervals, which correlates with the tank dimensions and the sonic speed in air. Note that the peak pressures have decreased from approximately 27.6 kPa (4 psi) to 2.76 kPa (0.4 psi) with expansion from the tank. NF85 again shows a good match of peak pressures with the experimental data.

Channels 5A--8A are in the 0.305-m (1-ft)-diam pipe downstream from the cylindrical tank. Figures 22--24 show the results of these comparisons. The peak pressures are in the range of 5.52--2.07 kPa (0.8--0.3 psi) except after the blower, which shows a negative magnitude of approximately 0.14 kPa (0.02 psi). All of the comparisons are relatively good except for Channel 8A, which is after the blower. (See Fig. 25.) The NF85 prediction does not match the experimental data well at all. This is probably because of the complex configuration of the blower, which is difficult to take into account in the NF85 modeling.

In general, the NF85 code predictions were in good agreement with the experimental data. The peak pressures and the time of peak pressure occurrence were very close. The only exception was at Channel 8A, which was downstream of the blower.

## C. Hydrogen/Air Ventilation System Tests (EVENT84)

The experimental and code simulation results involve the following.

- Code simulations and comparison with experimental results in the explosion chamber
- Code simulations and comparison with experimental results just before the system filter
- Code simulations of pressures upstream and downstream of the filter
- Experimental results of pressures upstream and downstream of the filter

Both Models 1 and 2 were involved in the comparisons.

Figures 26 and 27 show the first set of experimental and code simulation results. Figure 26 shows that the two methods used to simulate the explosion

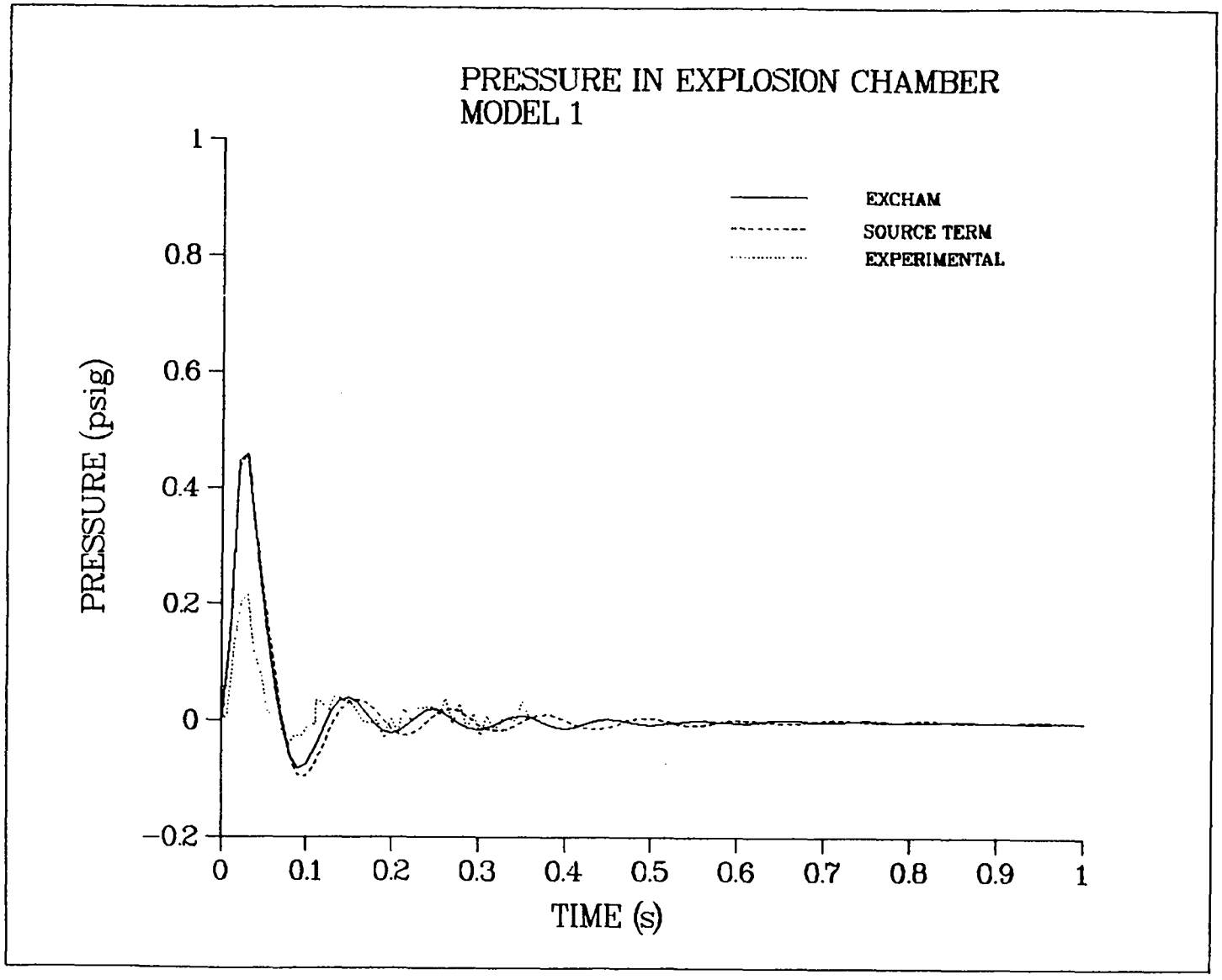


Fig. 26.
EVENT84 code simulation of pressure in explosion chamber and comparison with experimental results (Model 1).

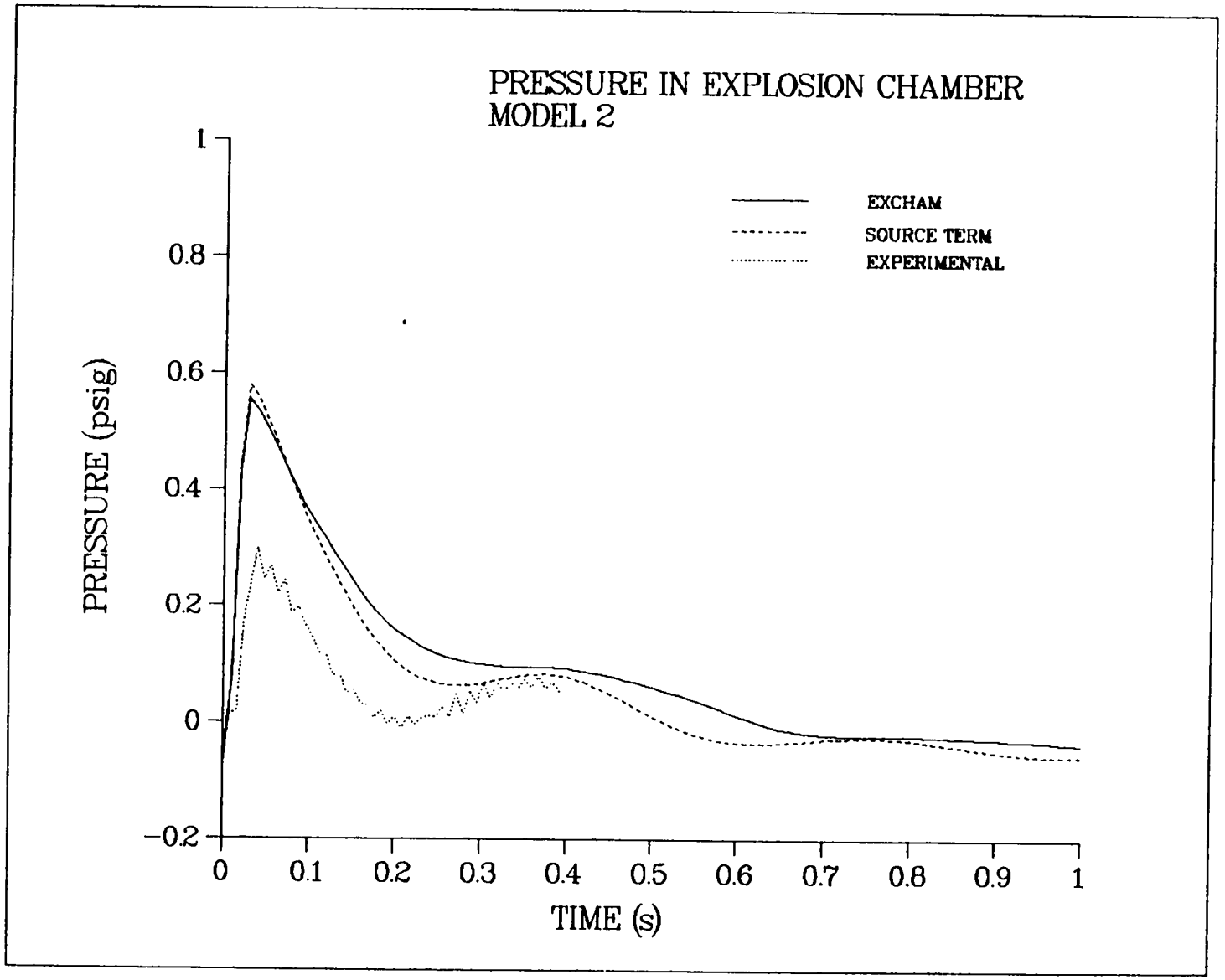


Fig. 27.
EVENT84 code simulation of pressure in explosion chamber and comparison with experimental results (Model 2).

(EXCHAM and SOURCE TERM) over-predict the pressure within the chamber. However, the shape of the pulse is very similar. The peak pressures predicted by the code were 3.174 kPa (0.46 psi), whereas the experimental values were 1.518 kPa (0.22 psi). The peak pressure times were in good agreement. In Fig. 27, Model 2 shows similar results. That is, the peak pressures are approximately twice the values obtained from the experiment. Again, the peak pressure times were in good agreement. Closing the explosion chamber door in Model 2 increases the peak pressure by about 50%. These results were expected based on the EVENT84 code results. That is, the code is expected to give conservative results in areas where the explosion takes place, which is why the NF85 code was developed to more closely simulate explosive effects near the source.

We must note that the experimental data were smoothed to make the information more presentable. This took out the highest peaks, which were of the same magnitude as the code results. The high peaks in the experimental data are caused primarily by shock reflections inside the explosion chamber.

Pressure comparisons were made downstream of the explosion (in the chamber right before the filter). This location corresponds to node 7 on Models 1 and 2. As in the results for pressure in the explosion chamber, the code conservatively over-predicts the pressure. However, the analytical and experimental results are much closer. The time at peak pressure is much closer for Model 2 than for Model 1. As shown in Figs. 28 and 29, the peak pressure is dissipated to 1.21 kPa (1.208 psi) after passing through the ductwork and the cylindrical tank. The closer EVENT84-predicted pressure transient results support our claim that the code predicts reasonable pressure levels in regions removed from the explosive source, particularly in areas where the final filters will be located.

Figures 30 and 31 are plots of the pressures upstream and downstream of the filter for Model 2. As shown in both figures, the filter essentially damps out the pressure wave. Figure 31 shows the code simulations of the pressures before and after the filter. These results indicate that the modeling does not indicate a complete damping of the pressure wave, but the peak pressure is reduced from 1.07 kPa (0.155 psi) to 0.345 kPa (0.05 psi).

## D. Blasting Cap Ventilation System Tests (EVENT84)

The experiment and code comparisons for the blasting cap experiments are similar to the hydrogen/air comparisons. That is, comparisons were made at the

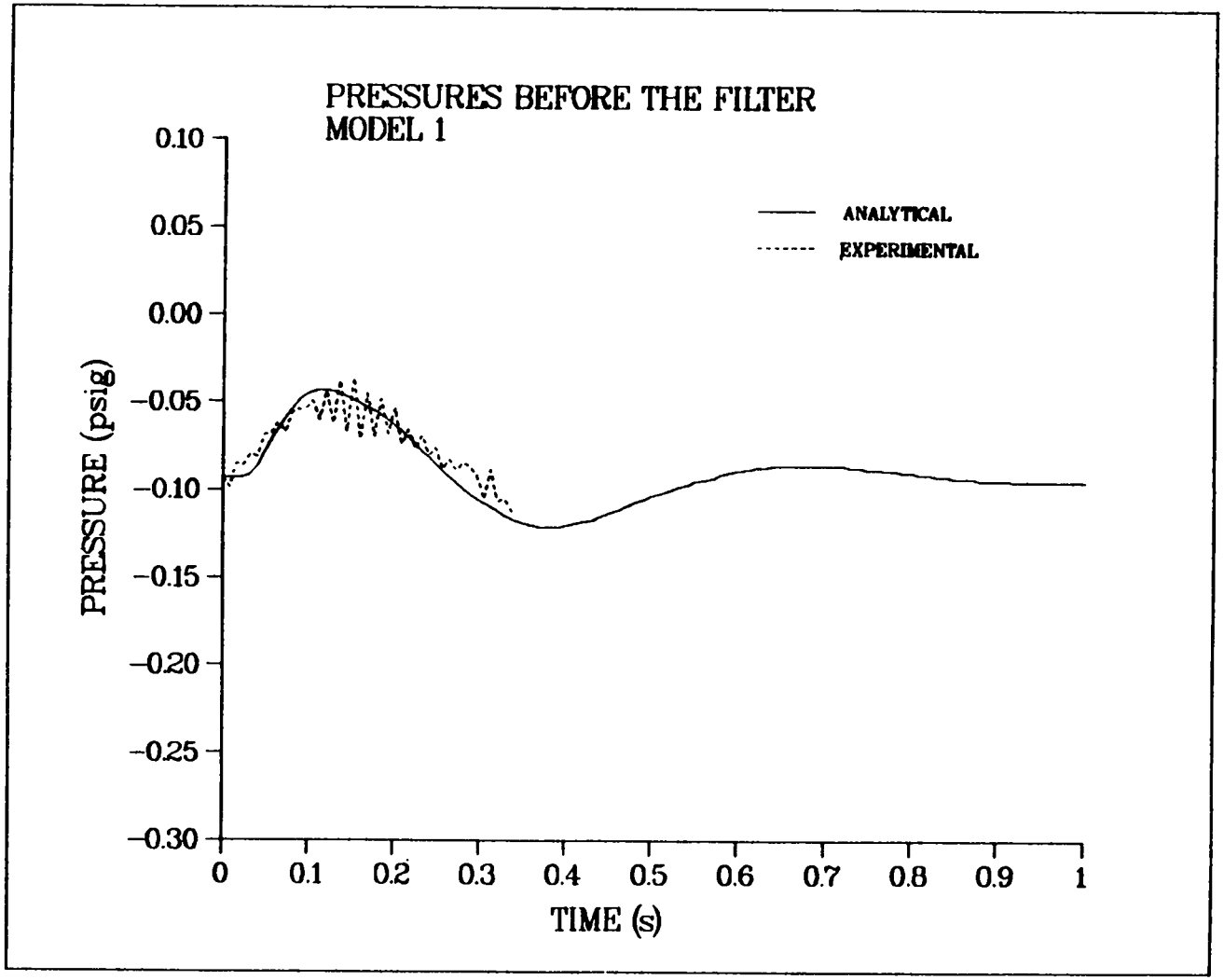


Fig. 28.
EVENT84 code simulation and experimental results of the pressure just before the filter in Model 1.

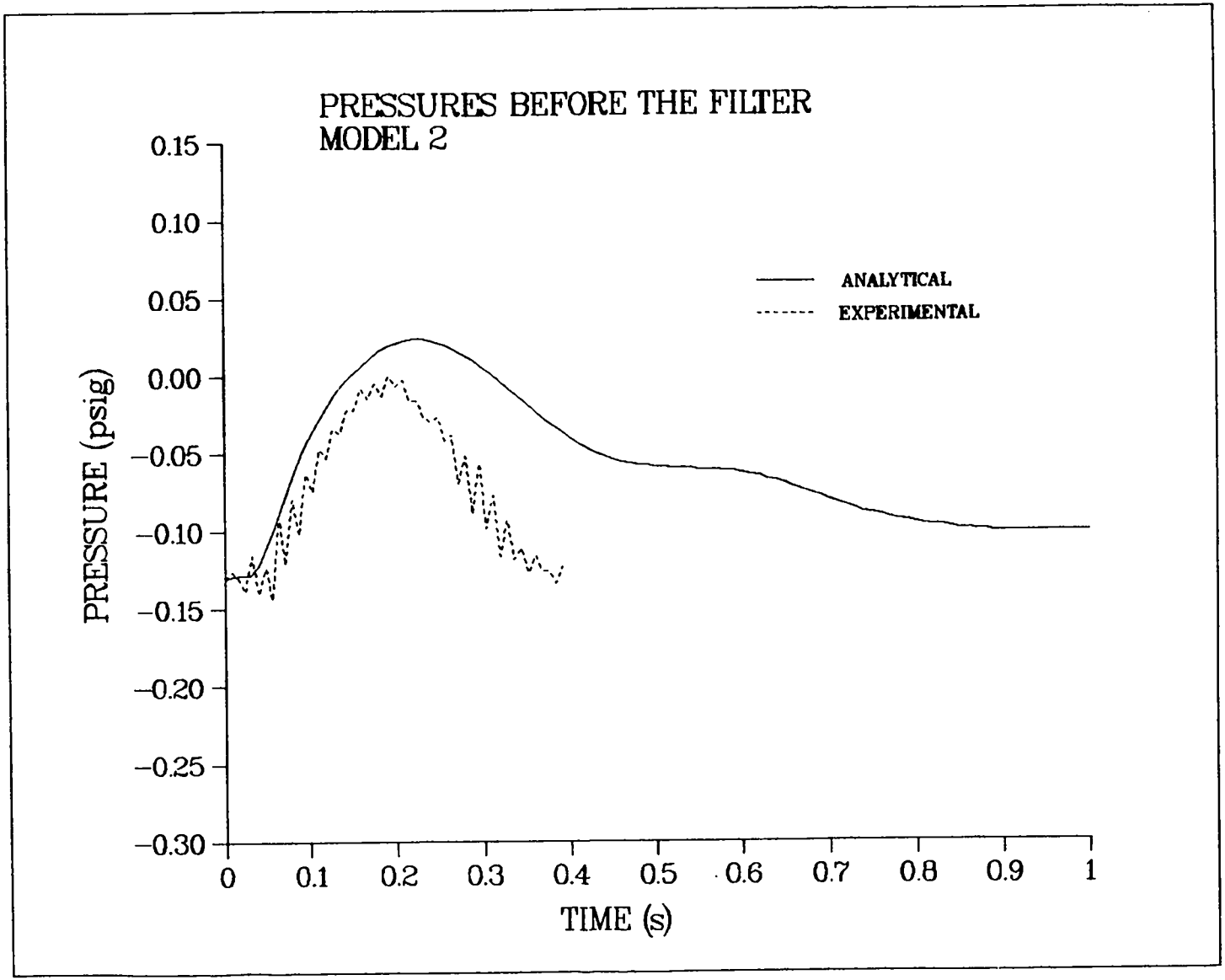


Fig. 29.
EVENT84 code simulation and experimental results of the pressure just before the filter in Model 2.

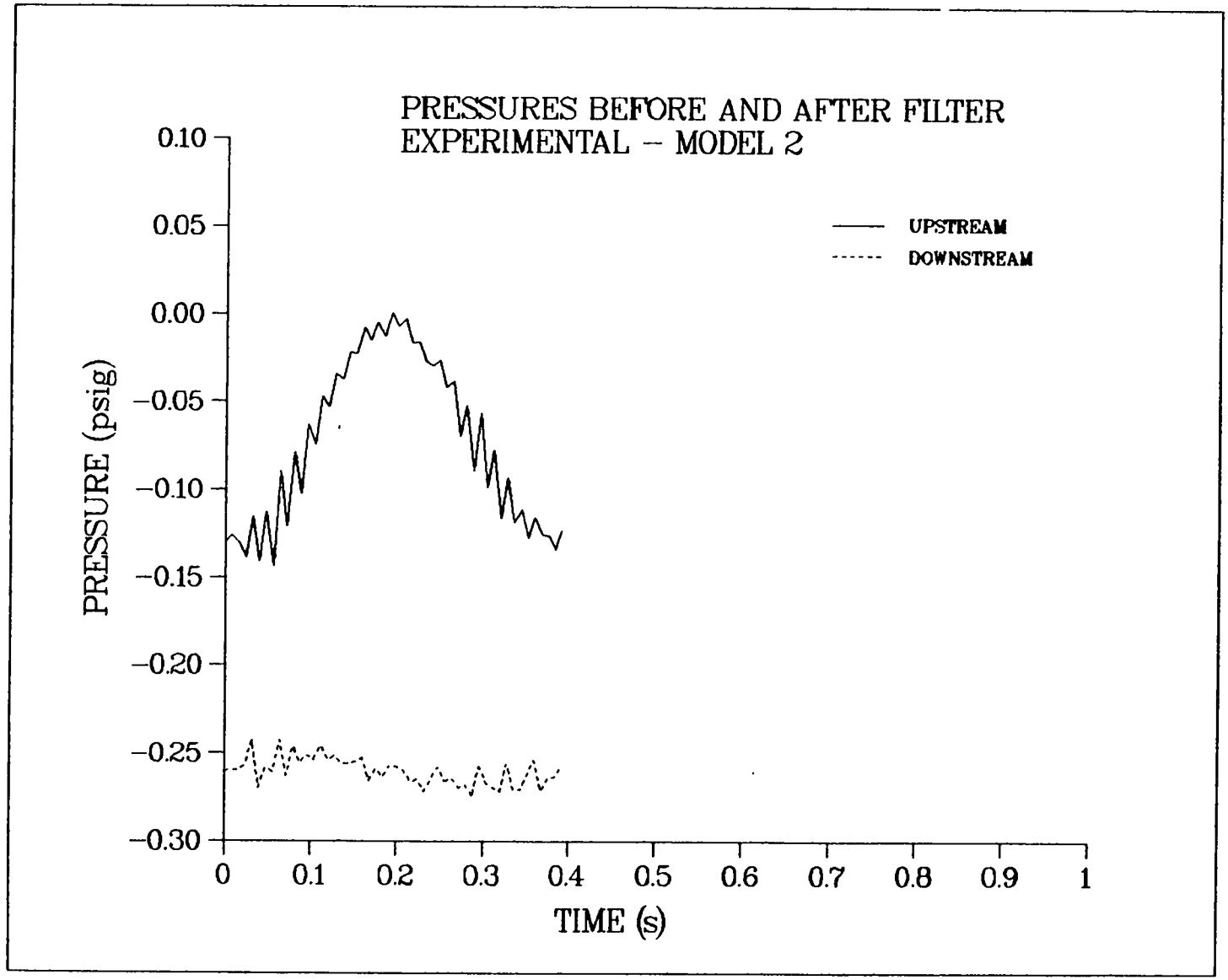


Fig. 30.
Experimental results for transient pressures upstream and downstream of the filter (Model 2).

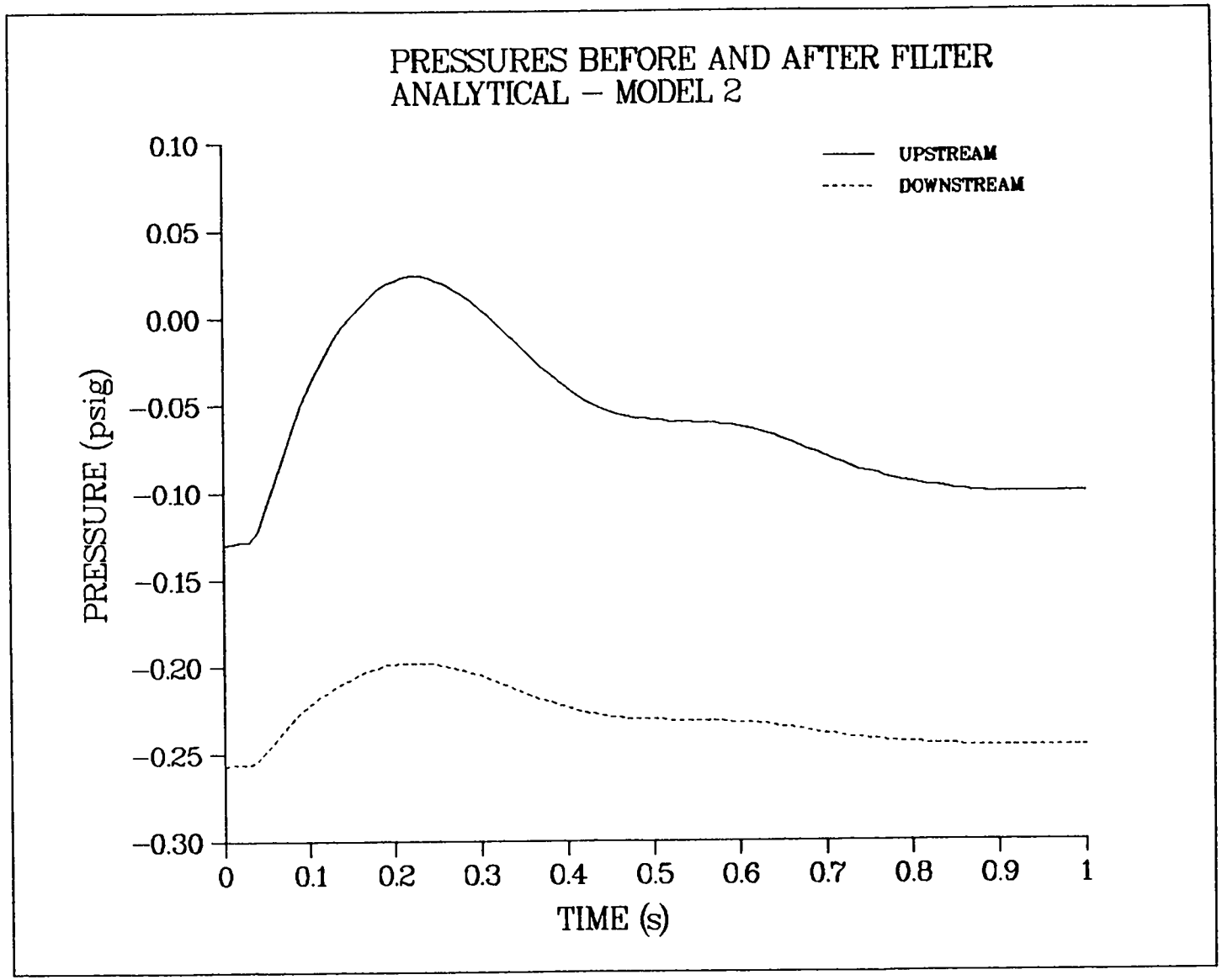


Fig. 31.
EVENT84 code simulation results of pressures upstream and downstream of the filter (Model 2).

explosion chamber and upstream and downstream of the HEPA filter. All of these comparisons are made using the explosion chamber model in EVENT84. However, the EVENT84 and experimental data comparisons for the blasting caps showed results that were quite different from the hydrogen-air explosions.

The blasting cap tests were performed using 1.2 and 3.0 g for the two model configurations. The analytical and experimental results for the explosion chamber are compared in Figs. 32--35. As shown in these figures, the EVENT84 results do not match the experimental data. The reason for this is the way EVENT84 models the explosion. In EVENT84, the mass and energy equivalence of the explosive are used to create a gas overpressure within the explosion chamber. In this case, the mass of the explosive used is so small that no appreciable pressure rise is possible. However, the experimental data show considerable pressure spikes that are probably a result of the shock waves impinging on the tank walls. In this case, the NF85 code should be used and probably would model the shock impingement quite well.

## VI. SUMMARY

Two computer codes that can be used to simulate explosions within flow networks (particularly nuclear air cleaning systems) have been developed at Los Alamos: NF85 and EVENT84. The EVENT84 code models the interconnected ducts and compartments of a flow network, providing pressures, temperatures, flows, and densities throughout the system. The NF85 code calculates the details of the explosion in three dimensions and can serve as the input or driver for EVENT84. Results from these codes were compared with experimental data from the Los Alamos test facility at NMSU. The explosions first were simulated with a large-diameter shock tube, and then small explosions using a hydrogen/air mixture and blasting caps were used. The NF85 code was used to simulate the shock tube tests, and the EVENT84 code was used to simulate the hydrogen/air and blasting-cap explosions.

The NF85 results showed very close agreement with the shock tube results for both shock transmission and shock propagation within the small experimental set-up that consisted of several tanks and connecting ductwork. The peak pressures and the times at peak pressure matched very well. The only exception to this was at a point downstream of the blower.

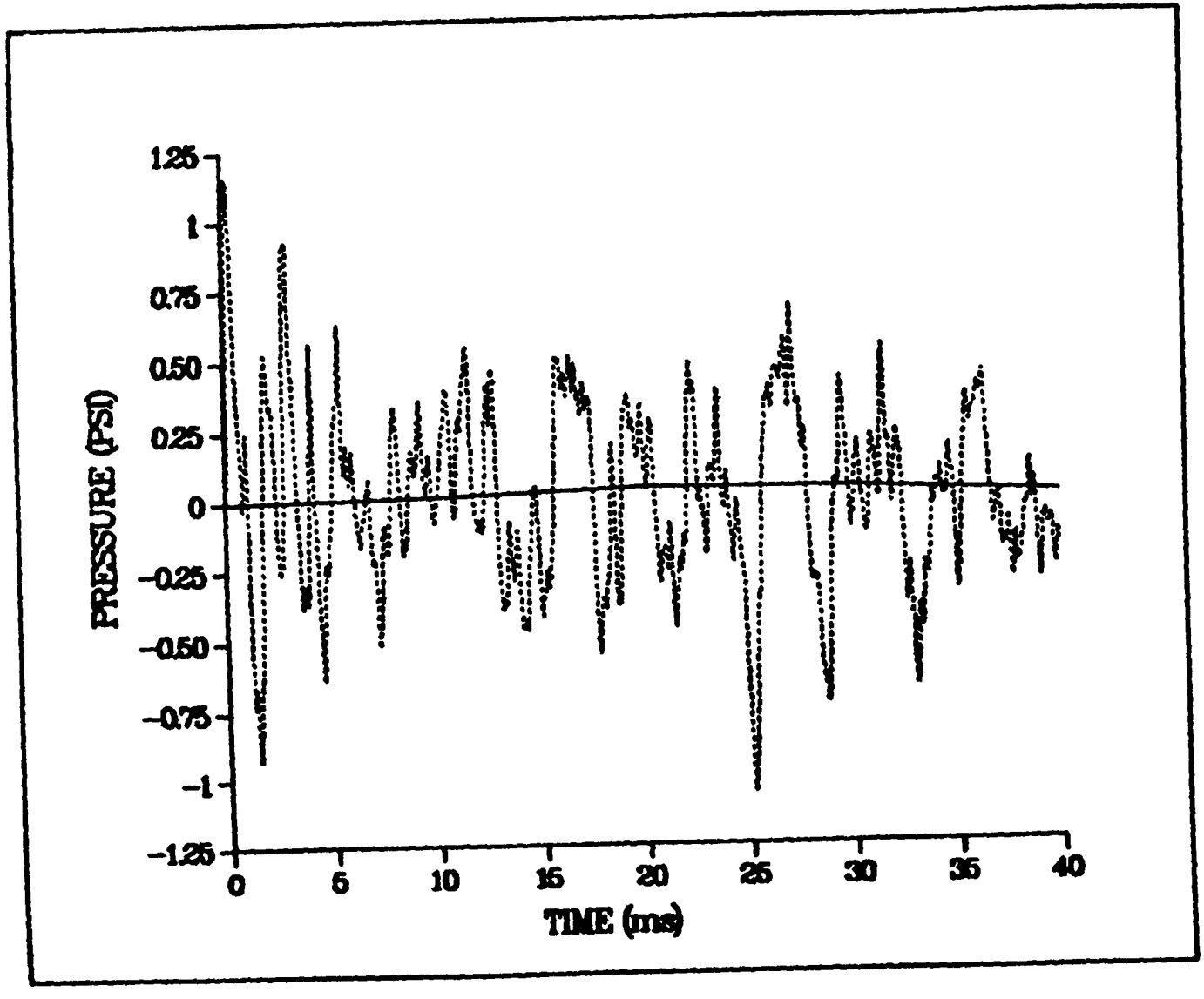


Fig. 32.
EVENT84 code pressure predictions in the explosion chamber compared with 1.2-g blasting cap experimental results.

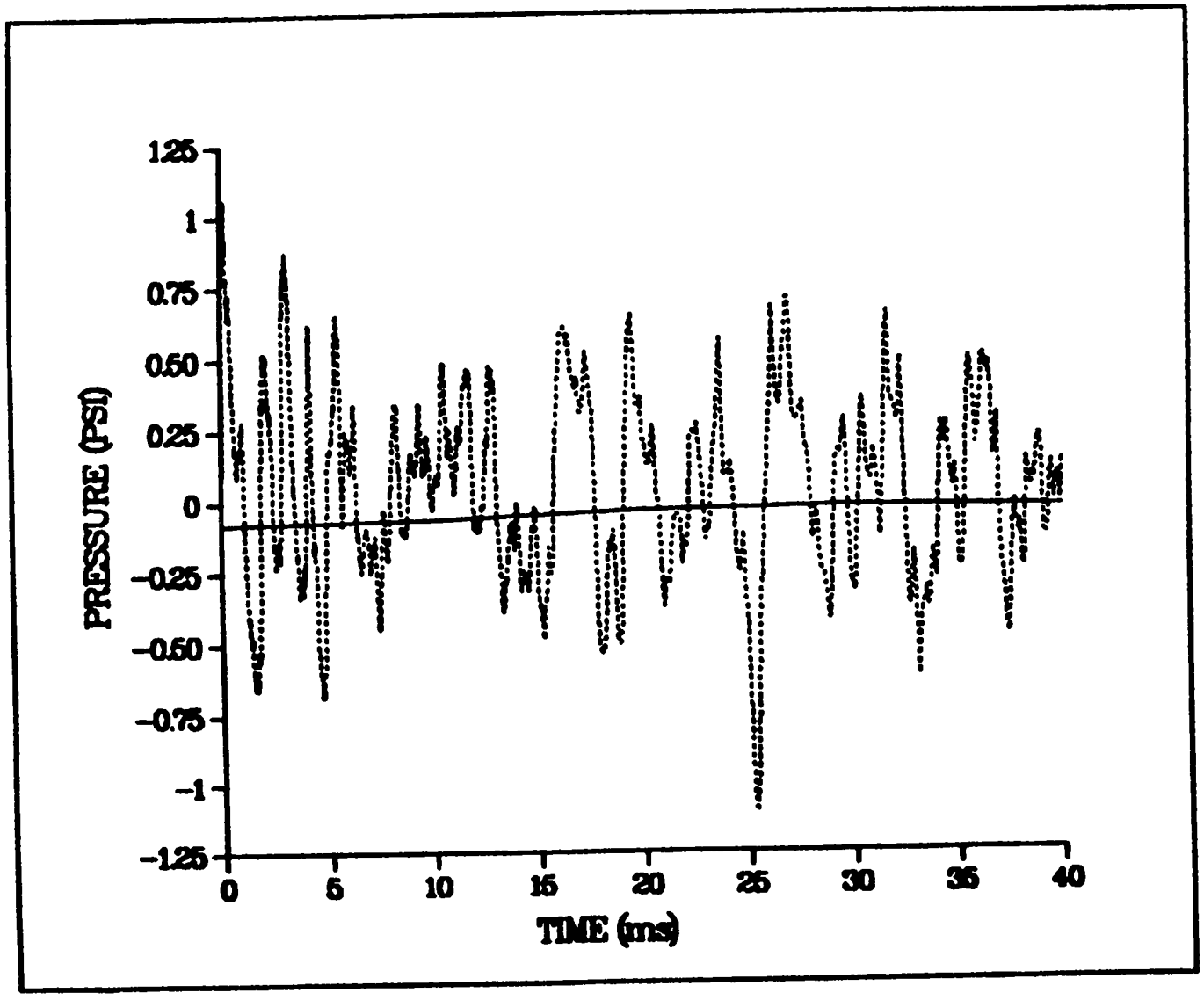


Fig. 33.
EVENT84 code pressure predictions in the explosion chamber compared with 1.2-g blasting cap experimental results.

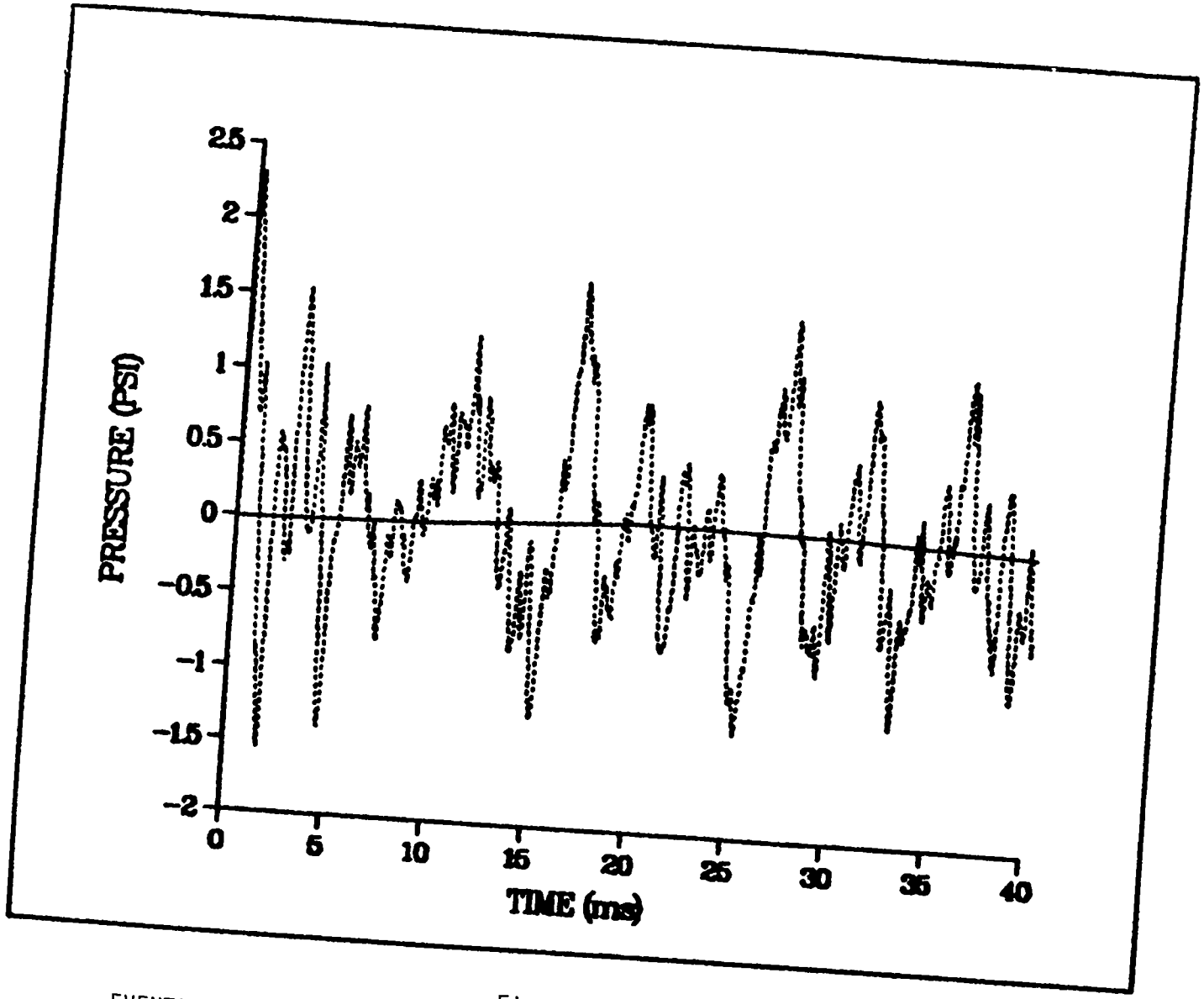


Fig. 34.
EVENT84 code pressure predictions in the explosion chamber compared with 3.0-g blasting cap experimental results.

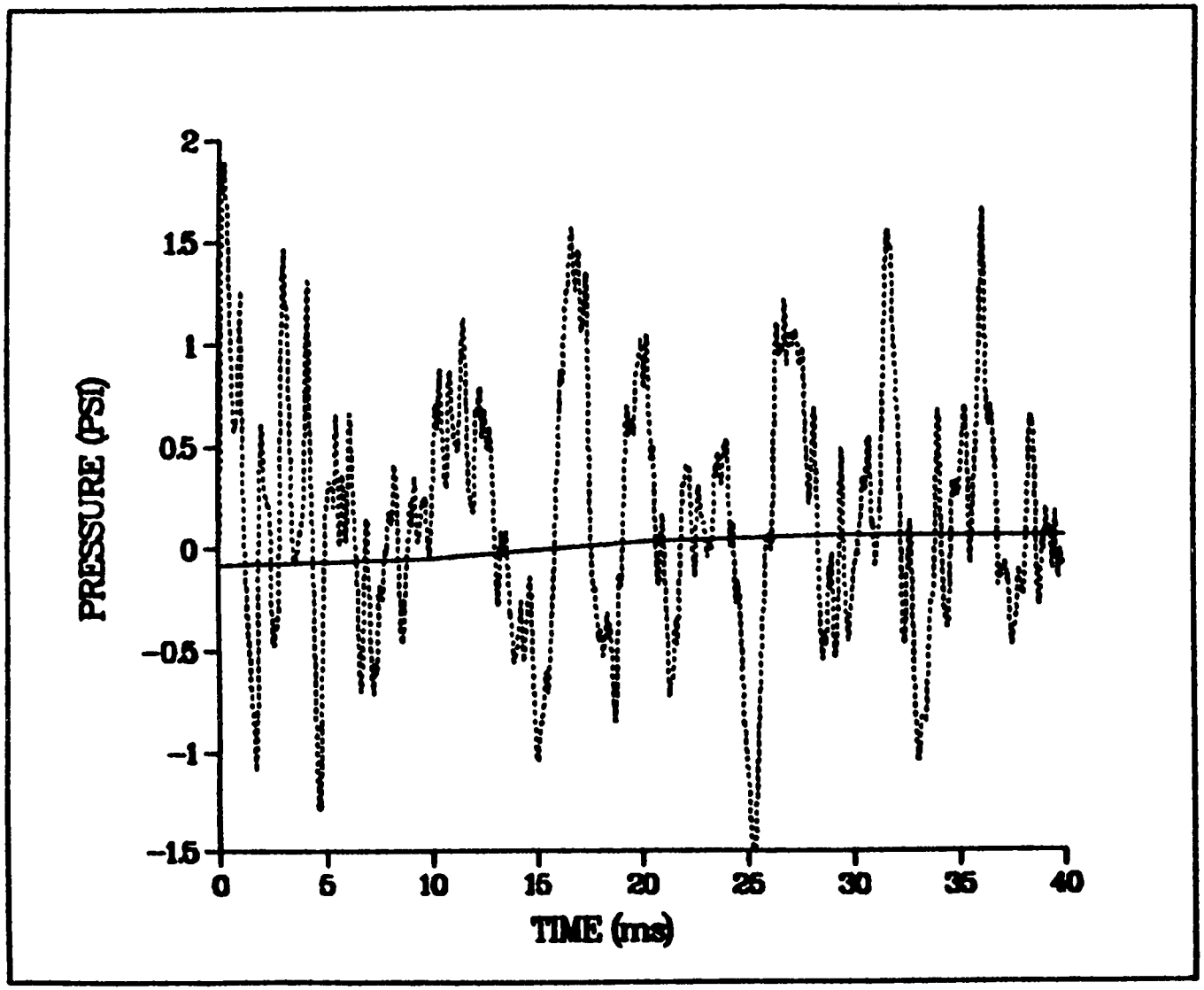


Fig. 35.
EVENT84 code pressure predictions in the explosion chamber compared with 3.0-g blasting cap experimental results.

The EVENT84 code results compared very well with the hydrogen/air experiments using an experimental set-up that consisted of two tanks, ductwork, dampers, a filter, and a blower. In the explosion chamber, the code predicted conservatively higher pressures than were measured. The downstream pressures across the dampers and filter also compared very well with the EVENT84 predictions. However, in the blasting cap experiments, EVENT84 did not match the experimental data. The problem seems to be that very small amounts of explosive are not enough to create the gas overpressure that is used to simulate an explosion in EVENT84. The experimental data show pressure peaks that indicate shock waves striking and reflecting off the walls of the chamber. EVENT84 does not model shock wave propagation.

We would recommend using NF85 to model the blasting-cap experiments. In addition, an effort to couple NF85 to EVENT84 should be pursued.

REFERENCES

1. W. S. Gregory and P. R. Smith, "Ventilation System Pressure Transients-Proposed Experiments and Shock Tube Conceptual Design," Los Alamos Scientific Laboratory report LA-7413-MS (September 1978).

2. W. S. Gregory and P. R. Smith, "Structural Response of HEPA Filters to Shock Waves," Shock and Vibration Bulletin 52, Part 3, 43-50 (May 1982).

Printed in the United States of America
Available from
National Technical Information Service
US Department of Commerce
5285 Port Royal Road
Springfield, VA 22161
Microfiche (A01)

| Page Range | NTIS Price Code | Page Range | NTIS Price Code | Page Range | NTIS Price Code | Page Range | NTIS Price Code |
|---|---|---|---|---|---|---|---|
| 001-025 | A02 | 151-175 | A08 | 301-325 | A14 | 451-475 | A20 |
| 026-050 | A03 | 176-200 | A09 | 326-350 | A15 | 476-500 | A21 |
| 051-075 | A04 | 201-225 | A10 | 351-375 | A16 | 501-525 | A22 |
| 076-100 | A05 | 226-250 | A11 | 376-400 | A17 | 526-550 | A23 |
| 101-125 | A06 | 251-275 | A12 | 401-425 | A18 | 551-575 | A24 |
| 126-150 | A07 | 276-300 | A13 | 426-450 | A19 | 576-600 | A25 |
| | | | | | | 601 up* | A99 |

*Contact NTIS for a price quote.

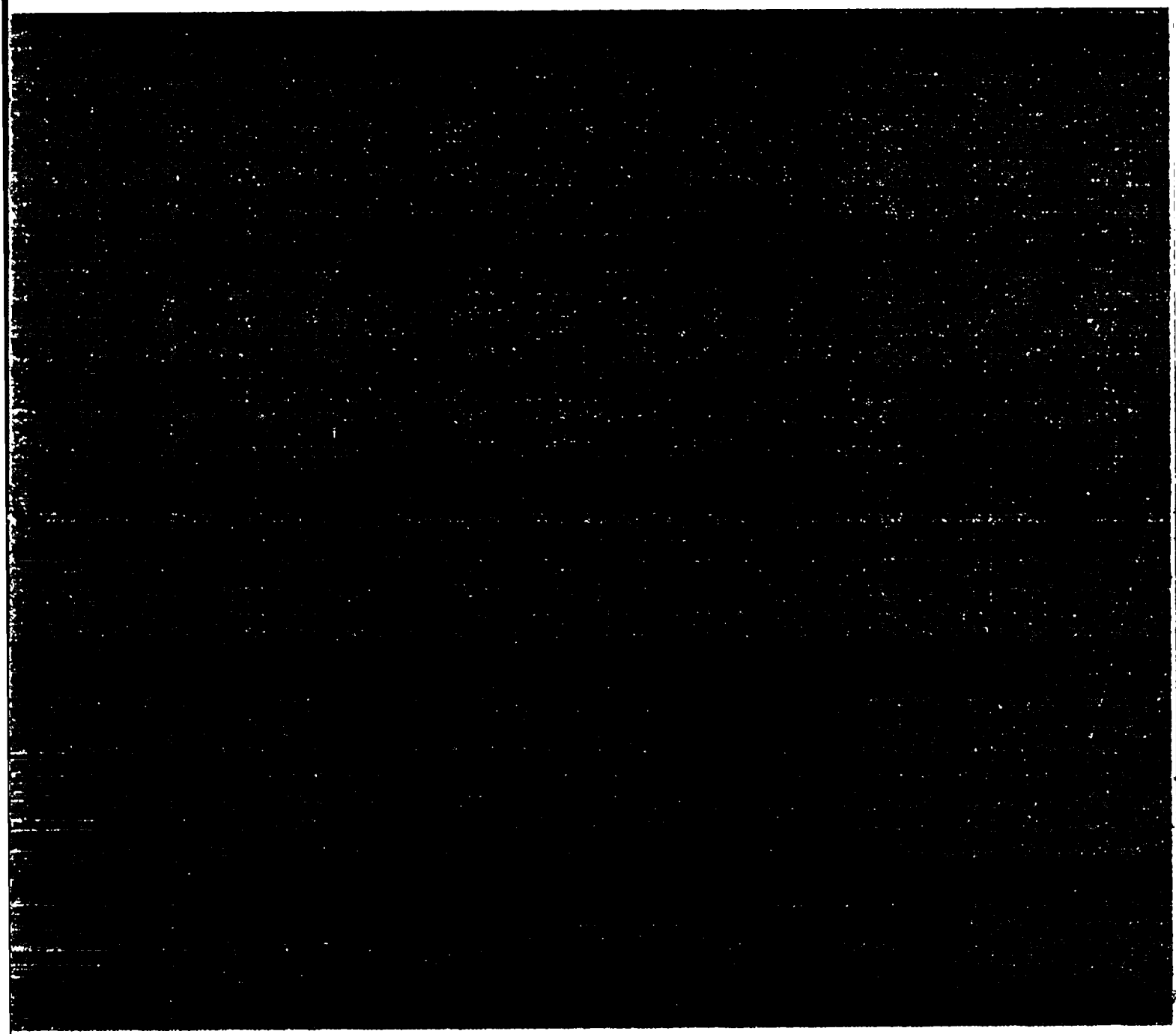

Los Alamos